THE UNIVERSITY OF CALGARY

Sulfated β-Cyclodextrins in Enantiomeric Separations and Mobility Conservation Model in Cyclodextrin-mediated Capillary Electrophoresis

by

Jinglan Yan

A THESIS

SUBMITTED TO THE FACULTY OF GRADUATE STUDIES

IN PARTIAL FULFILMENT OF THE REQUIREMENTS FOR THE

DEGREE OF MASTER OF SCIENCE

DEPARTMENT OF CHEMISTRY

CALGARY, ALBERTA

AUGUST, 1998

© Jinglan Yan 1998

National Library of Canada
Acquisitions and Bibliographic Services
395 Wellington Street
Ottawa ON K1A 0N4
Canada

Bibliothèque nationale du Canada
Acquisitions et services bibliographiques
395, rue Wellington
Ottawa ON K1A 0N4
Canada

Your file Votre référence

Our file Notre référence

The author has granted a non-exclusive licence allowing the National Library of Canada to reproduce, loan, distribute or sell copies of this thesis in microform, paper or electronic formats.

The author retains ownership of the copyright in this thesis. Neither the thesis nor substantial extracts from it may be printed or otherwise reproduced without the author's permission.

L'auteur a accordé une licence non exclusive permettant à la Bibliothèque nationale du Canada de reproduire, prêter, distribuer ou vendre des copies de cette thèse sous la forme de microfiche/film, de reproduction sur papier ou sur format électronique.

L'auteur conserve la propriété du droit d'auteur qui protège cette thèse. Ni la thèse ni des extraits substantiels de celle-ci ne doivent être imprimés ou autrement reproduits sans son autorisation.

0-612-35009-6

Canada

ABSTRACT

Over the last decade capillary electrophoresis has rapidly become popular for the separation of enantiomers. Native cyclodextrins and their derivatives are the most extensively used chiral additives in capillary electrophoresis. Despite their popularity, however, the basic mechanisms of electrophoretic separations using cyclodextrins are poorly understood.

This thesis work seeks a fundamental understanding of enantiomeric separations using charged cyclodextrins. Exceptional resolutions were obtained herein with β-cyclodextrins derviatized with four and thirteen sulfates. The complex stability and complex mobility were both found to contribute to the separations. Electrodispersion was found to be the key determinant of efficiency.

Experimental observations also suggested a surprising correlation between the mobility of the solute and the mobility of the solute-cyclodextrin complex. The mobility of the solute-cyclodextrin was found to be a function of the intrinsic mobilities of the solute and the cyclodextrin, rather than by the overall charge-to-mass of the complex.

ACKNOWLEDGEMENTS

Sincere thanks are expressed to my supervisor Dr. Charles Lucy for his guidance and support throughout this research project. His encouragement for free thinking and prompt feedback on my thesis writing are very much appreciated.

I would also like to thank my fellow students in Dr. Lucy's group Ken Yeung, Shilin Fu, Dongmei Li, Yusuf Muombwa, Jeremy Melanson, Kathleen Tremblay, and Jojo Tsang for their cooperation. Special thanks are given to Ken and Shilin, who helped me start at the beginning of this research and who have given me many invaluable advices.

The Department of Chemistry, the University of Calgary, and the Natural Sciences and Engineering Research Council of Canada are acknowledged for their financial support in this research. Their funds have also enabled me to attend the HPCE'98 and 81st CSC (1998) conferences.

TABLE OF CONTENTS

CHAPTER 4 FUTURE WORK

LIST OF TABLES

LIST OF FIGURES

LIST OF ABBREVIATIONS

μ	Mobility
μ_a	Observed (Apparent) Mobility of a Solute (Equation 1.7 and 1.8)
μ_c	Observed Mobility Corrected for Viscosity
μ_e	Electrophoretic Mobility of a Solute (Equation 1.5)
13-SCD	13-Sulfated β-Cyclodextrin
4-SCD	Tetra-sulfated β-Cyclodextrin
AB	4-(Aminomethyl)benzene Sulfonamide
BA	Benzylamine
BCD	β-Cyclodextrin
BI	Butylimidazole
BT	Benzyltrimethylammonium
CD	Cyclodextrin
CE	Capillary Electrophoresis
CEKC	Capillary Electrokinetic Chromatography
CZE	Capillary Zone Electrophoresis
DP	Diphenhydramine
EI	Ethylimidazole
EOF	Electroosmotic Flow
GC	Gas Chromatography
HA	Homatropine
HI	Histidine

HPLC	High Performance Liquid Chromatography
ICD	Ionized Cyclodextrin
IM	Imidazole
MA	Methyl Mandelate
MES	Morpholino-ethanesulfonic acid monohydrate
MI	Methylimidazole
φ	Mole Fraction
NCD	Neutral Cyclodextrin
NDS	Naphthalene Disulfonic Acid
PI	Propylimidazole
PR	Propranolol
SCD	Sulfated Cyclodextrin
t_v	Elution Time in Viscosity Measurements (Section 2.2.4)
UV	Ultraviolet

CHAPTER 1 INTRODUCTION

1.1 OBJECTIVE OF THESIS

Over the last decade capillary electrophoresis (CE) has rapidly become popular among separation scientists for the separation of enantiomers. Cyclodextrins (CDs) and their derivatives are the most frequently used chiral selectors in CE. The size, charge, and substitution can greatly affect the performance and resolving power of cyclodextrins. Choosing the right type of cyclodextrin for a specific application is often done by trial and error. It can be time-consuming and costly. Therefore, it is of fundamental importance and practical interest to gain a better understanding of cyclodextrin-solute complexing mechanisms. The aim of this research project is first to characterize the mobility behavior of charged cyclodextrins in enantiomeric separations. A mobility-conservation model is then proposed based on this initial data and more extensive studies with achiral compounds. Finally, preliminary studies on a rapid and high-efficiency partial filling technique for chiral separations with negatively charged cyclodextrins are reported.

1.2 INTRODUCTION TO CAPILLARY ELECTROPHORESIS

1.2.1 INSTRUMENTATION

Capillary electrophoresis (CE) is the hybrid technique of high performance liquid chromatography and electrophoresis. The separation of analytes is achieved by differential migration of solutes in an electric field.

Figure 1.1 is a schematic diagram of a CE instrument. The electrophoresis is performed in narrow-bore fused silica capillaries with inner diameters ranging from 25 to

75 μm. A very high electric field strength (100-500 V/cm) is applied across the capillary for high

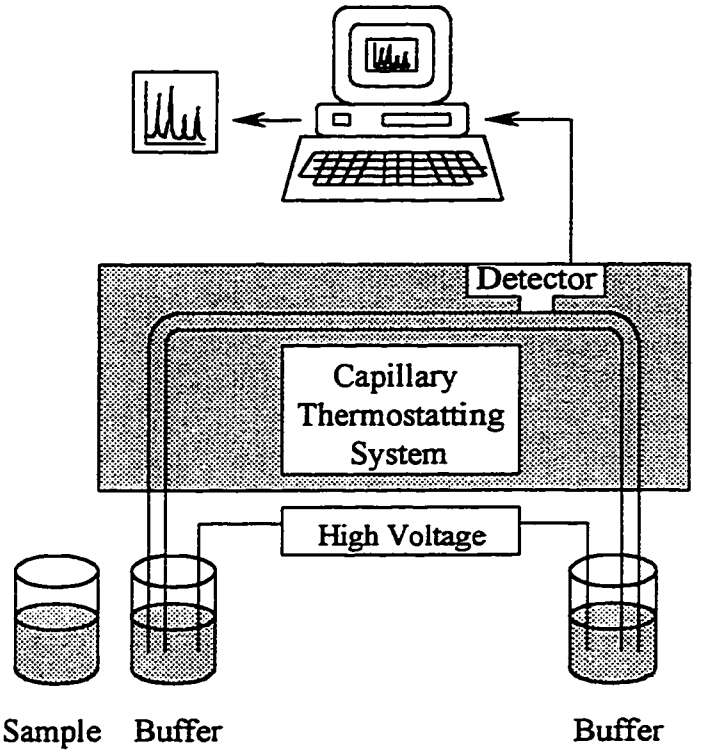

Figure 1.1 Schematic of a CE instrument.

efficiency separations. Buffer vials containing background electrolyte are placed at either end of the capillary when the electrophoretic separation takes place. An extremely small volume of sample is needed for injection (only 1-50 nl injected). An on-line detector is located at one end of the capillary. Detection signals are transferred to a PC computer to be monitored and processed. The computer is also capable of programming and automatically controlling sample runs. The capillary is thermostatted to ensure run to run reproducibility and efficient heat dissipation.

1.2.2 BASIC PRINCIPLES

1.2.2.1 ELECTROPHORESIS PROCESS

Electrophoresis is the differential movement of charged species (ions) by attraction or repulsion in an electric field. Separation by electrophoresis is based on differences in solute velocity in an electric field.

The velocity of an ion is given by

$$v = \mu_e E \qquad (1\text{-}1)$$

where v is the ion velocity (cm/s), μ_e is the electrophoretic mobility ($cm^2/(Vs)$), and E is the applied electric field (V/cm).

The ion experiences two opposing forces in the buffer solution. One is the electrostatic force which drives the ion towards an electrode (F_E). This driving force is given by

$$F_E = qE \qquad (1\text{-}2)$$

where q is the charge on the solute.

The other opposing force is the frictional force caused by the medium opposing the ion's motion (F_F). The frictional force for a spherical ion is given by

$$F_F = -6\pi\eta r v \qquad (1\text{-}3)$$

where η is the solution viscosity, r is the ion radius, and v is the ion velocity.

During electrophoresis, a steady state is attained, wherein the two forces are equal, but in opposite directions.

$$qE = 6\pi\eta r v \qquad (1\text{-}4)$$

Solving for velocity and substituting equation (1-4) into equation (1-1), and rearranging for μ_e, we obtain

$$\mu_e = \frac{q}{6\pi\eta r} \qquad (1\text{-}5)$$

From this equation, it is evident that the mobility of the analyte is a function of both the charge and size. Small, highly charged species have high mobilities, whereas large minimally charged species have low mobilities.

In our studies of cyclodextrin mediated capillary electrophoresis, we will alter the mobility of the solutes by changing both their sizes and charges by complexing the solutes with cyclodextrins.

1.2.2.2 ELECTROOSMOTIC FLOW

Under aqueous conditions, the silanol groups (SiOH) on the surface of fused silica capillaries can ionize and exist in an anionic form (SiO^-). This makes the capillary wall negatively charged (see Figure 1.2). The ionized silanol groups on the capillary wall attract cationic species from the buffer. The ionic layer that is formed has a positive charge density that decreases exponentially as the distance from the wall increases. The double layer formed closest to the surface is called "Stern layer" and is essentially static. A more diffuse layer formed distal to the Stern layer is called the "Outer Helmholtz Plane" (OHP). Under an applied field, cations in the Outer Helmholtz Plane migrate in the direction of the cathode, carrying their waters of hydration with them. Due to the cohesive nature of the hydrogen bonding of the waters of hydration to the water molecules of the bulk solution, the entire buffer solution is pulled toward the cathode. This bulk flow of liquid in the capillary under an applied voltage is called electroosmotic flow (EOF).

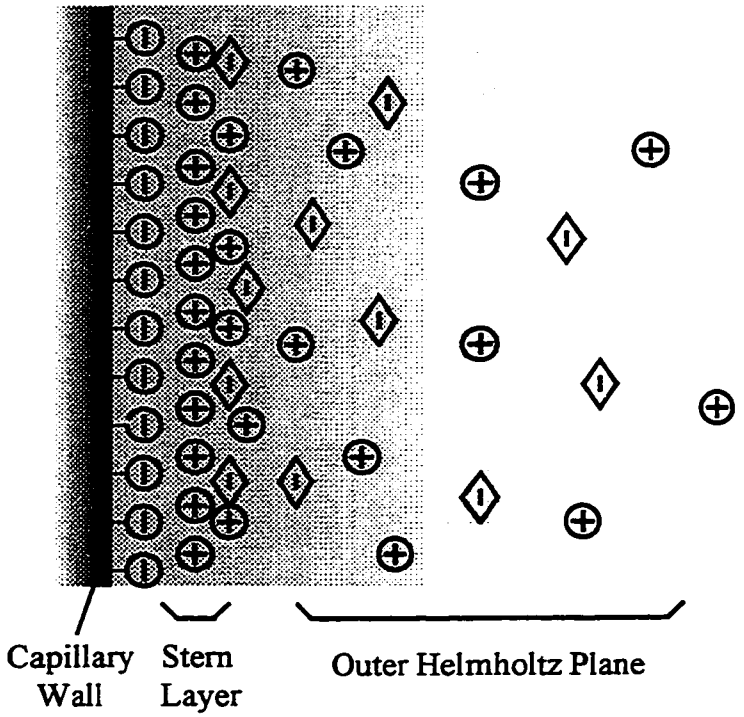

Figure 1.2 Diagram of the ionic layers at the capillary wall.

The magnitude of the EOF is given by

$$\mu_{EOF} = \varepsilon\zeta/\eta \qquad (1\text{-}6)$$

where μ_{EOF} is the EOF "mobility", ζ is the zeta potential, and ε is the dielectric constant.

EOF is dependent on the pH and ionic strength of the buffer solution in the capillary. EOF carries all solutes in the buffer solution toward cathode. With the existence of EOF, the apparent mobility of an ion (μ_a) is the sum of two terms.

$$\mu_a = \mu_e + \mu_{EOF} \qquad (1\text{-}7)$$

where μ_a is the apparent mobility of a solute, and μ_e is the electrophoretic mobility of a solute dictated by Equation 1-5.

1.2.2.3 EOF SUPPRESSION BY COATING CAPILLARY WALLS

The magnitude of EOF is generally greater than the mobilities of all organic solutes and large inorganic solutes. Thus almost all solutes end up being flushed out of the capillary in the cathodic direction, regardless of their individual charges. This coelution is sometimes beneficial in fast analysis. However, when closely eluting compounds are being separated as in enantiomeric analysis, this strong EOF does not allow enough time for sufficient resolution to be achieved. Under such conditions the EOF must be suppressed.

There are many different ways to suppress EOF in capillary electrophoresis. Examples include the use of very low pH buffers, of high concentration of salts, and to add cationic or zwitterionic surfactants in the buffer [1]. However, these attempts suffer from a number of problems: i) the applicable pH range is limited; ii) high salt concentration may cause band broadening due to Joule heat; and iii) surfactants may interact with samples or other additives thus making the optimization of a separation too complicated. To overcome these restrictions people have covalently bonded hydrophilic polymers onto the inner capillary wall to act as an inert permanent coating.

Polyacrylamide coated capillaries are now commercially available. This type of coating is stable over a buffer pH range of about 2.3-8, up to a temperature of 60°C, and has good long term stability [2][3]. A neutral polyacrylamide coated capillary is used throughout this research.

1.2.2.4 DETECTION OF EXCESSIVE HEAT GENERATION BY AN OHM'S LAW PLOT

In CE, the application of high voltage and the passage of electric current through the buffer generates so-called Joule heating. Joule heat causes a temperature gradient within the capillary with the temperature being highest in the center of the capillary and the lowest along the capillary walls. Since a one degree change in temperature results in a 2 to 3% change in viscosity [4], the temperature gradient results in a viscosity gradient in the capillary with the highest viscosity along the capillary wall and the lowest in the center. The solutes that are closer to the center of the capillary will have higher mobilities than the solutes that are closer to the wall of the capillary. This inequality in mobility across the capillary is a source of bandbroadening and peak deformation. Thus it is detrimental in CE separations. While the theoretical equations predict [4] that the higher the voltage applied, the higher the efficiency achieved, Joule heating ultimately limits the application of very high voltages. Therefore special care must be taken to avoid excessive heat generation.

An Ohm's law plot is a simple and effective way to monitor Joule heating. As shown in Figure 1.3, an Ohm's law plot plots the current observed to pass through the capillary versus the voltage used. When the heat is efficiently dissipated, this plot is linear with an intercept at the origin. A disproportional increase in current with voltage indicates a temperature increase. That is, the rate of heat generation is greater than the rate of heat dissipation. In Figure 1.3, the positive deviation of the data points from the straight line at high voltages indicates excessive heat generation under these conditions.

The separation voltage should be chosen as the highest voltage in the linear region of the Ohm's law plot.

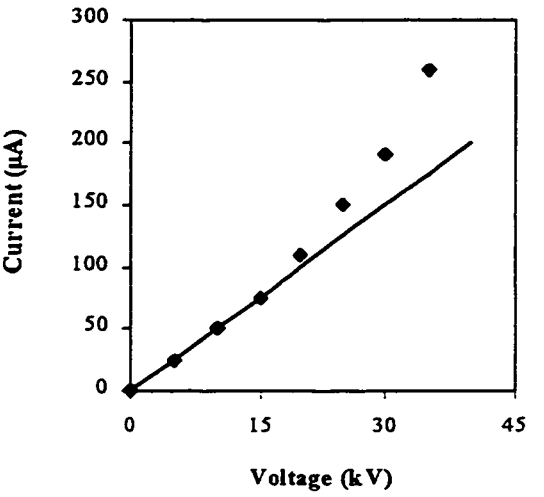

Figure 1.3 Ohm's law plot.

The conductivity of the buffer, and thus the heat generation, will vary with the buffer composition. Similarly, the heat dissipation will depend on the capillary diameter. Therefore, an Ohm's Law plot should be generated for each new experiment.

1.3 CHIRAL SEPARATIONS IN CE

1.3.1 INTRODUCTION

Chiral compounds are a group of molecules that have at least one chiral center in them. The importance of separating racemates into their stereoisomeric compositions arises from the fact that optical isomers often have drastically different therapeutic, pharmacological, and toxicologic properties. It is usually the case that one isomer is

much different than the other one therapeutically. The other one sometimes can be less potent in some cases, can cause undesired side effects, or can even be toxic in some other cases. Even if the other isomer does not have any side effect, it will still take the body extra effort to metabolize it and get it out of the body, and thus be an unnecessary burden to the metabolic system. Nowadays, most prescribed drugs contain at least one chiral center, and 75-90% are marketed as racemates [5]. Similarly pesticides, herbicides, agrochemicals, and halogenated hydrocarbons may also possess chiral centers. Therefore there has been a strong push toward better and higher efficiency chiral separation techniques.

Among the various techniques developed for chiral recognition and separation of enantiomeric compounds, gas chromatography (GC) and high performance liquid chromatography (HPLC) have been the most successful [6]. Since optical isomers possess identical physical properties, they usually can not be resolved in an achiral environment. Therefore some kind of chiral selector is required. Typically the chiral selector is fixed onto the stationary phase in chromatographic techniques. Many useful chiral stationary phases were designed for use in GC or HPLC and have become commercially available.

CE is a relatively new technique in this field. The first enantiomeric separation using CE was reported in 1985 [7]. Ever since then, CE has become more and more popular for the separation of enantiomers. In CE, the chiral recognizing agents are added to the buffer solution instead of being fixed to the column supporting material as in chromatographic techniques. The main strength of CE in this area is the high efficiency and the ease of changing buffer composition. With the extremely high efficiencies

achievable (100,000 ω 1,000,000 theoretical plates) CE is capable of resolving compounds with very low separation factors (α), which is often the case with enantiomers. The type and concentration of chiral selector can be easily changed in the background electrolyte in order to find the optimal condition. In chromatographic separations where the efficiencies are lower, satisfactory resolutions are very difficult to achieve without a suitable stationary phase.

Other advantages of using CE for chiral separations include extremely small injection volume (nanoliters or less), fully automated instrumentation, flexibility, environmental friendliness and relatively low costs.

A variety of selecting agents such as cyclodextrins, crown ethers, chiral ergot alkaloids, surfactants, antibiotics [8], proteins, and so on, are available for enantiomeric separations in CE. Among them, CDs are by far the most frequently used chiral additives.

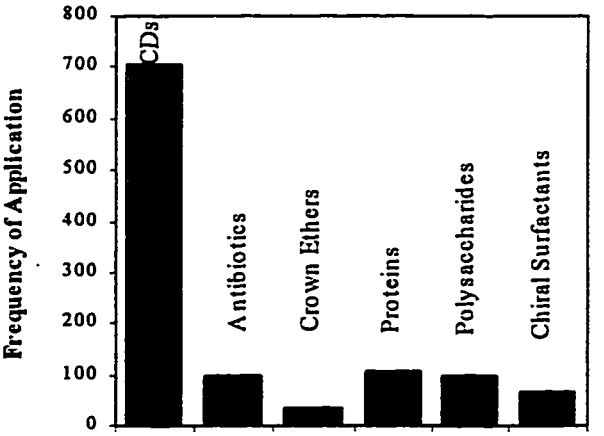

Figure 1.4 Frequency of the application of the different chiral selectors (adapted from reference [9]).

1.3.2 CYCLODEXTRINS AND THEIR DERIVATIVES IN ENANTIOMERIC SEPARATIONS

Cyclodextrins (CDs) are cyclic oligosaccharides consisting of 6, 7, or 8 D(+)-glucopyranose units and are named α, β, or γ -cyclodextrin, respectively. Figure 1.4(a)

(a)

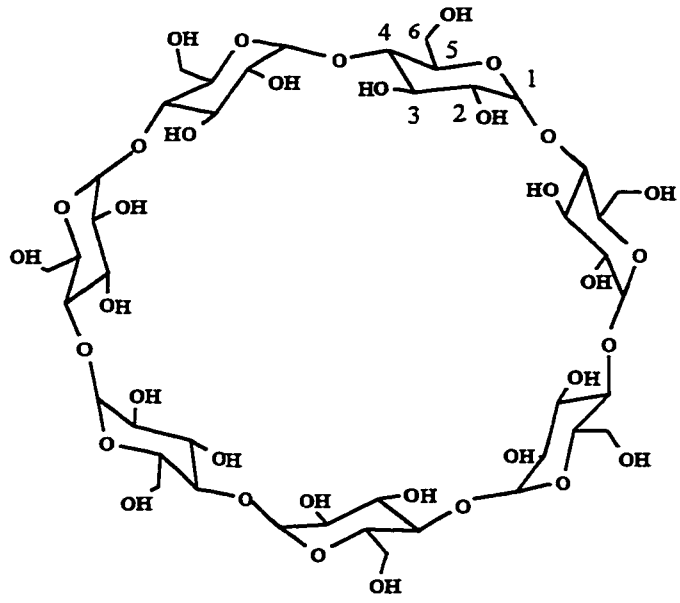

(b)

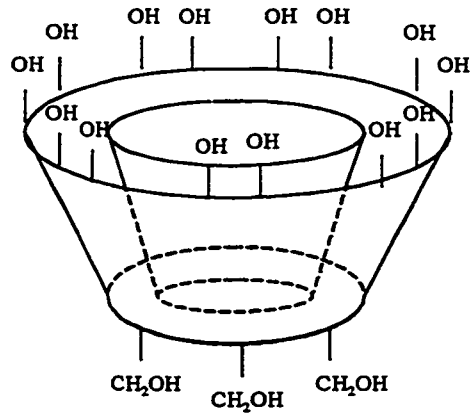

Figure 1.5 (a) Chemical structure of β-CD; (b) Truncated cone shape of a β-cyclodextrin.

shows the chemical structure of a β-cyclodextrin, which contains 7 glucopyranose units. As shown in Figure 1.4(b) cyclodextrins have the shape of a truncated cone. The cavity of CDs is hydrophobic, whereas the hydroxyl groups on the rims make the surface hydrophilic. As can be seen in Table 1.1, α, β, and γ CDs have about the same cavity depth. Their inner diameters differ as a result of different numbers of giucopyranose units.

Table 1.1 Physical properties of the cyclodextrins [10]

Cyclodextrin	Number of glucose residues	Molecular weight	Water solubility (g/100ml)	Cavity dimensions (Å)	
				Internal diameter	Depth
α-	6	972	14.5	4.5	6.7
β-	7	1,135	1.85	~7.0	~7.0
γ-	8	1,297	23.2	~8.5	~7.0

Enantiomeric separations with CDs are generally attributed to two main interactions between CDs and chiral solutes. One interaction is the inclusion of a bulky moiety of the solute molecule into the CD cavities through hydrophobic interactions. The other interaction involves secondary polar interactions such as dipole-dipole interactions or hydrogen bonds between the CD hydroxyl groups at position 2 or 3 and solute polar

moieties that are close to the solute's chiral center. Many experimental techniques have provided proofs for those interactions [11].

Cyclodextrins are often derivatized to improve their water solubility, to alter the depth of the cavity, and to control the secondary interactions between the cyclodextrins and the solutes. The hydroxyl groups in positions 2, 3, and 6 are readily derivatized. Many derivatives have been used successfully in CE and they were found to have drastically different enantiomeric selectivities from their parent native cyclodextrins [12]. Some examples of the most frequently used neutral derivatives are heptakis-O-methyl cyclodextrin (M-CD), heptakis (2,6-di-O-methyl) cyclodextrin (DM-CD), heptakis (2,3,6-tri-methyl) cyclodextrin (TM-CD), hydroxyethyl cyclodextrin (HE-CD) and hydroxypropyl cyclodextrin (HP-CD)[13]. Charged cyclodextrin derivatives such as amino-substituted cyclodextrins [14][15], carboxylated cyclodextrins [16], sulfobutylether-β-cyclodextrin [17][18], and sulfated CDs, have also found wide applications by themselves or in a mixture with neutral cyclodextrins [19].

Negatively charged CDs have been found to be more efficient chiral selectors than neutral CDs [16]. Tait et al. [20] proposed that when the charge on the cyclodextrin is opposite that of the solute, this will magnify the difference between the solute mobility and that of the complex, which is called "separation window". Also, the introduction of charges onto the chiral selectors makes possible additional interactions such as Coulombic interactions between the selector and the analyte, which may improve the chiral recognition. Finally, if the cyclodextrin has a characteristic mobility, it is possible to separate neutral enantiomers.

In the present CE terminology, the separation of enantiomers with neutral chiral selectors is ascribed to capillary zone electrophoresis (CZE) and charged chiral selectors to capillary electrokinetic chromatography (CEKC or EKC). Therefore, the enantiomeric separations with CDs are divided into two operation modes. Despite that, the chiral separation mechanisms are largely the same in the two cases. In the next section some of the theoretical models for enantiomeric separations with CDs will be discussed.

1.4 THEORETICAL MODELS FOR CD MEDIATED SEPARATIONS

1.4.1 WREN-ROWE MODEL

In 1992, Stephen A. Wren and Raymond C. Rowe proposed the first theoretical model for enantiomeric separations in capillary zone electrophoresis buffers containing cyclodextrins [21][22][23].

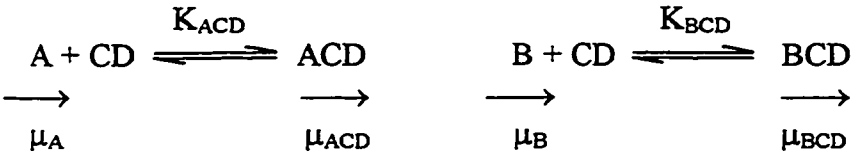

A and B represent the two enantiomers of a chiral compound. They have the same electrophoretic mobility in free solution ($\mu_A = \mu_B = \mu_1$). The electrophoretic mobilities of the analyte-cyclodextrin complexes are also assumed to be the same ($\mu_{ACD} = \mu_{BCD} = \mu_2$). However the two enantiomers have different affinities for the chiral selector, that is, $K_{ACD} \neq K_{BCD}$. If the exchange of A between the free and bound forms is very rapid, then the apparent electrophoretic mobility of A ($\mu_{a,A}$) will be a function of the proportion of the time that A is free (φ_A) and the proportion that it is complexed (φ_{ACD}), i.e.,

$$\mu_{a,A} = \varphi_A\mu_A + \varphi_{ACD}\mu_{ACD} = \varphi_A\mu_1 + \varphi_{ACD}\mu_2 \quad (1\text{-}8)$$

$$\text{Since } \varphi_A = \frac{[A]}{[A]+[ACD]} \quad (1\text{-}9)$$

$$\text{and } \varphi_{ACD} = \frac{[ACD]}{[A]+[ACD]} \quad (1\text{-}10)$$

Substituting Equation 1-9 and 1-10 into Equation 1-8 yields,

$$\mu_{a,A} = \left(\frac{[A]}{[A]+[ACD]}\right)\mu_1 + \left(\frac{[ACD]}{[A]+[ACD]}\right)\mu_2 \quad (1\text{-}11)$$

$$K_{ACD} = \frac{[ACD]}{[A][CD]} \quad (1\text{-}12)$$

rearranging Equation 1-12,

$$[ACD] = K_1[A][CD] \quad (1\text{-}13)$$

substituting 1-13 into 1-11 and rearranging,

$$\mu_{a,A} = \frac{\mu_1 + \mu_2 K_{ACD}[CD]}{1 + K_{ACD}[CD]} \quad (1\text{-}14)$$

For enantiomer B the same derivation applies and we can get a similar equation

$$\mu_{a,B} = \frac{\mu_1 + \mu_2 K_{BCD}[CD]}{1 + K_{BCD}[CD]} \quad (1\text{-}15)$$

Two extremes can be obtained from Equations 1-14 and 1-15.

1. When [CD] = 0, $\mu_{a,A} = \mu_{a,B} = \mu_1$. That is, the apparent mobilities of both enantiomers in cyclodextrin free buffer are equal to the free solute mobility. The enantiomers are not separated without the addition of cyclodextrins.
2. When [CD] is very large, both enantiomers are fully complexed. The first terms of both the denominator and numerator can be ignored compared to the

second terms, and so $\mu_{a,A} = \mu_{a,B} = \mu_2$. That is, the observed mobility of the enantiomers will plateau out at a constant mobility μ_2 at high CD concentrations.

The difference in the apparent electrophoretic mobility of A and B ($\Delta\mu_{AB}$) then is:

$$\Delta\mu_{AB} = \frac{\mu_1 + \mu_2 K_{ACD}[CD]}{1 + K_{ACD}[CD]} - \frac{\mu_1 + \mu_2 K_{BCD}[CD]}{1 + K_{BCD}[CD]} \qquad (1\text{-}16)$$

This rearranges to

$$\Delta\mu = \frac{(\mu_1 - \mu_2)(K_{BCD} - K_{ACD})[CD]}{1 + [CD](K_{ACD} + K_{BCD}) + K_{ACD}K_{BCD}[CD]^2} \qquad (1\text{-}17)$$

The optimum concentration of chiral selector can be found from Equation 1-17 by using differential calculus. It occurs when $d(\Delta\mu)/d[CD] = 0$. The solution was found to be

$$[CD] = \frac{1}{\sqrt{K_{ACD}K_{BCD}}} \qquad (1\text{-}18)$$

The Wren-Rowe model has been well-accepted because of its simplicity and its reasonable agreement with experimental data. However, the Wren-Rowe model only takes into account the effect of the chiral selector concentration, ignoring another important controlling factor, pH. It is not the most complete model. Also it assumes that the mobility of both cyclodextrin-analyte complexes for the two enantiomers are the same, which is not always true [24]. Nevertheless, it is still a very important and basic mathematical model for chiral separations in capillary electrophoresis.

1.4.2 SURAPANENI MODEL

This model was developed to model the separation of enantiomers of neutral species by a combination of an ionizable cyclodextrin (ICD) and a neutral cyclodextrin (NCD)[25]. It is assumed that the electroosmotic flow is negligible at the working conditions. Thus, neither the neutral solute nor the NCD has any mobility. It is also assumed that the ICD is in its fully charged form. The neutral analyte can form inclusion complexes with both the ICD and the NCD. The two enantiomers of the neutral analyte (A and B) interact with either selector to different extents. The neutral solute only has mobility when it is in the complexed form with ICD. The analyte-ICD complex will then assume the charge of the ICD.

Therefore two sets of equilibrium processes can be written in this dual-selector system:

$$\underset{\mu_A=0}{A} + \underset{}{ICD} \overset{K_{AICD}}{\rightleftharpoons} \underset{\mu_{AICD}}{AICD} \qquad \underset{\mu_B=0}{B} + \underset{}{ICD} \overset{K_{BICD}}{\rightleftharpoons} \underset{\mu_{BICD}}{BICD}$$

$$K_{AICD} = \frac{[AICD]}{[A][ICD]} \quad (1\text{-}19) \qquad K_{BICD} = \frac{[BICD]}{[B][ICD]} \quad (1\text{-}20)$$

$$\underset{\mu_A=0}{A} + \underset{}{NCD} \overset{K_{ANCD}}{\rightleftharpoons} \underset{\mu_{ANCD}=0}{ANCD} \qquad \underset{\mu_B=0}{B} + \underset{}{NCD} \overset{K_{BNCD}}{\rightleftharpoons} \underset{\mu_{BNCD}=0}{BNCD}$$

$$K_{ANCD} = \frac{[ANCD]}{[A][NCD]} \quad (1\text{-}21) \qquad K_{BNCD} = \frac{[BNCD]}{[B][NCD]} \quad (1\text{-}22)$$

Since the neutral analyte is mobile only when it is complexed with the charged cyclodextrin (ICD), the apparent mobility of an enantiomer A (μ_A), is a function the analyte-ICD complex mobility (μ_{AICD}) and the mole fraction of the analyte complexed (φ_{AICD}):

$$\mu_A = \mu_{AICD}\varphi_{AICD} \tag{1-23}$$

The mole fraction of the analyte complexed is:

$$\varphi_{AICD} = \frac{[AICD]}{[A]+[AICD]+[ANCD]} \tag{1-24}$$

Substituting Equation 1-19 and Equation 1-21 into Equation 1-24 and rearranging gives:

$$\varphi_{AICD} = \frac{K_{AICD}[ICD]}{1+K_{AICD}[ICD]+K_{ANCD}[NCD]} \tag{1-25}$$

Substituting Equation 1-25 into Equation 1-23, we get the expression of the apparent electrophoretic mobility of the enantiomer A:

$$\mu_A = \frac{\mu_{AICD}K_{AICD}[ICD]}{1+K_{AICD}[ICD]+K_{ANCD}[NCD]} \tag{1-26}$$

The apparent mobility expression for the other enantiomer can be obtained by analogy:

$$\mu_B = \frac{\mu_{BICD}K_{BICD}[ICD]}{1+K_{BICD}[ICD]+K_{BNCD}[NCD]} \tag{1-27}$$

The selectivity for enantiomers A and B is:

$$\alpha = \frac{\mu_A}{\mu_B} = \frac{\mu_{AICD}}{\mu_{BICD}}\left(\frac{K_{AICD}[ICD]}{K_{BICD}[ICD]}\right)\left(\frac{1+K_{BICD}[ICD]+K_{BNCD}[NCD]}{1+K_{AICD}[ICD]+K_{ANCD}[NCD]}\right) \tag{1-28}$$

An interesting feature about Equation 1-28 is that the A enantiomer complexation constant is in the numerator in the second term while it is in the denominator in the third term. The converse is true for the enantiomer B. So if the second term differs from 1 the

third term will bring it back closer to 1, offsetting the effect of the second term. The selectivity can be improved when a neutral selector that has opposite selectivity from the ionized selector is used, which can magnify the deviation from 1. When a neutral selector that has the same selectivity is used, the gain in selectivity will only be marginal.

When the analyte-NCD and analyte-ICD complexation stability constants and the analyte-ICD complex mobilities are known, the Surapaneni model can be used to predict the optimum resolution condition in chiral separation of neutral species in a dual-selector system.

1.4.3 MULTIPLE EQUILIBRIA MODEL

Rawjee et al. proposed a multiple equilibria model for the enantiomeric separations of weak acids and weak bases with β-cyclodextrin [26][27]. This model examines the effects of both pH and CD concentration on the chiral separation.

A weak acid or weak base solute enantiomers will undergo three pairs of equilibrium processes in a buffer solution: (1) acid-base equilibrium of the solutes in aqueous buffer; (2) the inclusion complexation equilibrium between cyclodextrins and the protonated form of the solutes; and (3) inclusion complexation between cyclodextrins and the deprotonated form of the solutes. The equilibrium expressions for the R enantiomer of a weak acid solute (HR) are shown below:

a. Acid dissociation :

$$HR + H_2O \rightleftharpoons H_3O^+ + R^-$$

$$K_{HR} = \frac{[R^-][H_3O^+]}{[HR]} \qquad (1\text{-}26)$$

b. Complexation between CD and protonated form

$$HR + CD \rightleftharpoons HRCD$$

$$K_{HRCD} = \frac{[HRCD]}{[HR][CD]} \qquad (1\text{-}27)$$

c. Complexation between CD and deprotonated form

$$R^- + CD \rightleftharpoons RCD^-$$

$$K_{RCD^-} = \frac{[RCD^-]}{[R^-][CD]} \qquad (1\text{-}28)$$

The mass balance equation of the HR related species is:

$$c_{HR} = [HR] + [R^-] + [HRCD] + [RCD^-] \qquad (1\text{-}29)$$

Since the neutral forms of the solute and the complex do not contribute to the effective mobility, the effective mobility can be expressed as the sum of mole-fraction-weighted ionic mobility of the charged species:

$$\mu_R^{eff} = \mu_{R^-}\varphi_{R^-} + \mu_{RCD^-}\varphi_{RCD^-} \qquad (1\text{-}30)$$

Substituting all the equilibrium expressions and the mass balance equation into Equation 1-30 and rearranging yields:

$$\mu_R^{eff} = \frac{\mu_{R^-} + \mu_{RCD^-}K_{RCD^-}[CD]}{1 + K_{RCD^-}[CD] + \frac{[H_3O^+]}{K_{HR}}(1 + K_{HRCD}[CD])} \qquad (1\text{-}31)$$

Similar expressions can be obtained for the S enantiomer. After the effective mobility expressions of both R and S enantiomers are obtained, the separation selectivity, α, is given by [26]:

$$\alpha = \frac{1+\frac{\mu_{RCD^-}}{\mu_-^0}K_{RCD^-}[CD]}{1+\frac{\mu_{SCD^-}}{\mu_-^0}K_{SCD^-}[CD]} \times \frac{1+K_{SCD^-}[CD]+\frac{[H_3O^+]}{K_a}(1+K_{HSCD}[CD])}{1+K_{RCD^-}[CD]+\frac{[H_3O^+]}{K_a}(1+K_{HRCD}[CD])}$$

(1-32)

where $\mu_{R^-} = \mu_{S^-} = \mu_-$.

By analogous argument, the separation selectivity for basic solutes can be obtained as [27]:

$$\alpha = \frac{1+\frac{\mu_{HRCD^+}}{\mu_+^0}K_{HRCD^+}[CD]}{1+\frac{\mu_{HSCD^+}}{\mu_+}K_{HSCD^+}[CD]} \times \frac{1+K_{HSCD^+}[CD]+\frac{[H_3O^+]}{K_b}(1+K_{SCD}[CD])}{1+K_{HRCD^+}[CD]+\frac{[H_3O^+]}{K_b}(1+K_{RCD}[CD])}$$

(1-33)

where $\mu_{HR^+} = \mu_{HS^+} = \mu_+$.

These two equations are the general expressions for the chiral separation of weak acids and bases. It is apparent that the chiral selectivity in a CD-based separation system depends on a number of parameters such as the pH of the buffer, the concentration of cyclodextrin, the acid-base dissociation constant of the analyte, the complex stability constants, and the free and complex mobilities of the analytes. To simplify these equations, the authors have identified three limiting situations. These are when: (i) only the non-ionic forms of the two enantiomers; (ii) only the ionic forms of the two enantiomers; and (iii) both forms of the two enantiomers interact differently with CD. The effects of varying pH or CD concentration on the chiral separation were then discussed for these individual situations [28].

In this research, the pH of the buffer was adjusted to ensure full ionization of the analytes. Thus the last two models mentioned above do not apply to our situation. Therefore, the more general Wren-Rowe model was used throughout this thesis.

1.4.4 HIGHER ORDER EQUILIBRIA

The models discussed in Sections 1.4.1-1.4.3 all assume 1:1 stoichiometry for the solute-CD complex. While this assumption is true in the majority of the interactions encountered in CE, there are situations where some large molecules may have more than one possible binding site and so higher order equilibrium can become significant. Bowser and Chen [29] have pointed out that determining the correct stoichiometry of an interaction is a crucial step in quantitatively describing the analyte migration behavior. If the wrong model is chosen, the calculated constants will reflect neither the real interactions between the analyte and the additive, nor their real effects on the net mobility of the analyte. They therefore derived a model which accounts for the effect of both first- and second-order equilibria.

This model deals with the equilibria between an analyte (A) that possesses two binding sites and an additive (C) with one binding site. The analyte A and additive C interact in the ways illustrated below (the numbers in parentheses represent the binding site on the analyte):

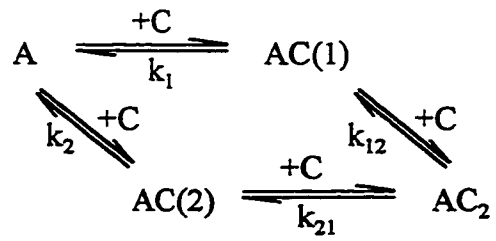

There are two pathways for the first-order binding with the equilibrium constants of k_1 and k_2, and for the second-order binding with equilibrium constants of k_{12} and k_{21}. However, since the observed equilibrium constants are always the sum of the equilibrium constants that have the same stoichiometry, it is impossible to obtain the individual constants. Therefore the equilibrium constants that have the same stoichiometries are grouped together to give a total first-order binding equilibrium constant, K_1, and total second-order binding equilibrium constant, K_2. Thus the equilibrium can be simplified to

$$A + 2C \overset{K_1}{\rightleftharpoons} AC + C \overset{K_2}{\rightleftharpoons} AC_2$$

The associated equilibrium constants are

$$K_1 = \frac{[AC(1)]+[AC(2)]}{[A][C]} = \frac{[AC]}{[A][C]} \tag{1-34}$$

$$K_2 = \frac{[AC_2]}{([AC(1)]+[AC(2)])[C]} = \frac{[AC_2]}{[AC][C]} \tag{1-35}$$

$$K_1K_2 = \frac{[AC_2]}{[A][C]^2} \tag{1-36}$$

The observed mobility μ_{obs} of the analyte will be a mole-fraction weighted linear combination of the free analyte mobility and the complex mobilities, i.e.,

$$\mu_{obs} = \varphi_A\mu_A + \varphi_{AC}\mu_{AC} + \varphi_{AC_2}\mu_{AC_2} \tag{1-37}$$

Substituting the equilibrium expressions into Equation 1-37 and rearranging yields

$$\mu_{obs} - \mu_A = \frac{(\mu_{AC} - \mu_A)K_1[C] + (\mu_{AC_2} - \mu_A)K_1K_2[C]^2}{1 + K_1[C] + K_1K_2[C]^2} \tag{1-38}$$

Equation 1-38 describes the effect of analyte-additive interactions with both 1:1 and 1:2 stoichiometries on the net mobility of an analyte. This equation is used to fit our experimental data as a check for the existence of higher order equilibrium.

1.5 OUTLINE OF THESIS

Chapter 1 is an introduction to enantiomeric separations in CE technique. The background and theories related to cyclodextrin mediated capillary electrophoresis were discussed.

Chapter 2 will characterize enantiomeric separations for two model cationic solutes using negatively charged sulfated β-cyclodextrins. Their complexation behaviors, high resolving power, and mobility matching effect were studied.

Chapter 3 will focus on the study of the relationship between the free solute mobility and the solute-charged cyclodextrin complex mobility. A mobility conservation model is proposed based on the data collected in our lab as well as literature data.

Chapter 4 discusses some areas requiring further study as well as presents preliminary results from a partial filling technique designed to avoid the UV-absorbance disturbance caused by the 13-sulfated cyclodextrin. Some enantiomeric separations were performed using this technique.

1.6 REFERENCES

1. Yeung, K. K.-C.; Lucy, C. A. *Anal. Chem.* 1997, 69, 3435-3441.

2. Nakatani, M.; Shibukawa, A.; Nakagawa, T. *Electrophoresis* 1995, 16, 1451-1456.

3. Ahmadzadeh, H.; Arriaga, E.; Stathakis, C.; Dovichi, N. J.; Righetti, P. G., Poster Presentation, HPCE'98, 1998, Orlando, Florida, USA.

4. Heiger, D. N. *"High Performance Capillary Electrophoresis – An Introduction"*, , Hewlett-Packard Company, Germany, 1992.

5. Ward, T. J. *Anal. Chem.* 1994, 66, 633A.

6. Terabe, S. *J. Chromatogr. A*, 1994, 666, 295-319.

7. Gassmann, E.; Kuo, J. E.; Zare, R. N. *Science*, 1985, 230, 813-814.

8. Gasper, M. P.; Berthod, A.; Nair, U. B.; Armstrong, D. W. *Anal. Chem.* 1996, 68, 2501.

9. Gübitz, G.; Schmid, M. G. *J. Chromatogr. A*, 1997, 792, 179-225.

10. Bender, M. L.; Komiyama, M. *"Cyclodextrin Chemistry"*, Springer-Verlag, New York, 1978.

11. Li, S.; Purdy, W. C. *Anal. Chem.* 1992, 64, 1405.

12. Miura, M.; Funazo, K.; Tanaka, M. *Anal. Chim. Acta* 1997, 357, 177.

13. Lin, B.; Zhu, X.; Epperlein, U.; Schwierskott, M.; Schlunk, R.; Koppenhoefer, B. *J. High. Resol. Chromatogr.* 1998, 21, 215.

14. O'Keeffe, F.; Shamsi, S. A.; Darcy, R.; Schwinté, P.; Warner, I. M. *Anal. Chem.* 1997, 69, 4773.

15. Bunke, A.; Jira, T. *J. Chromatogr. A*, 1998, 798, 275.

16. Tanaka, Y.; Yanagawa, M.; Terabe, S. *J. High Resol. Chromatogr.* 1996, 19, 421.

17. Groom, C. A.; Luong, J. H. T. *Electrophoresis* 1997, 18, 1166.

18. Luna, E. A.; Bornancini, E. R. N.; Tait, R. J.; Thompson, D. O.; Stobaugh, J. F.; Rajewski, R. A.; Stella, V. J. *J. Pharm. Biomed. Anal.* 1996, 15, 63.

19. Lurie, I. S.; Klein, R. F. X. *Anal. Chem.* 1994, 66, 4019.

20. Tait, R. J.; Thompson, D. O.; Stella, V. J.; Stobaugh, J. F. *Anal. Chem.* 1994, 66, 4013.

21. Wren, S. A.; Rowe, R. C. *J. Chromatogr.* 1992, 603, 235-241.

22. Wren, S. A.; Rowe, R. C *J. Chromatogr.* 1993, 635, 113-118.

23. Wren, S. A. *J. Chromatogr.* 1993, 636, 57-62.

24. Copper, C. L.; Davis, J. B.; Cole, R. O.; Sepaniak, M. J. *Electrophoresis* 1994, 15, 785.

25. Surapaneni, S.; Ruterbories, K.; Lindstrom, T. *J. Chromatogr. A*, 1997, 761, 249-257.

26. Rawjee, Y. Y.; Staerk, D. U.; Vigh, Gy. *J. Chromatogr.* 1993, 635, 291-306.

27. Rawjee, Y. Y.; Williams, R. L.; Vigh, Gy. *J. Chromatogr. A*, 1993, 652, 233-245.

28. Rawjee, Y. Y.; Williams, R. L.; Vigh, Gy. *J. Chromatogr. A*, 1994, 680, 599-607.

29. Bowser, M. T.; Chen, D. D. Y. *Anal. Chem.*, 1998, 70, 3261.

CHAPTER 2 CHARACTERIZATION OF CYCLODEXTRIN MEDIATED CHIRAL SEPARATIONS WITH SULFATED β-CYCLODEXTRINS

2.1 INTRODUCTION

Sulfated β-cyclodextrin is one of the negatively charged cyclodextrins that are commercially available. There are three possible sulfating sites in each glucopyranose

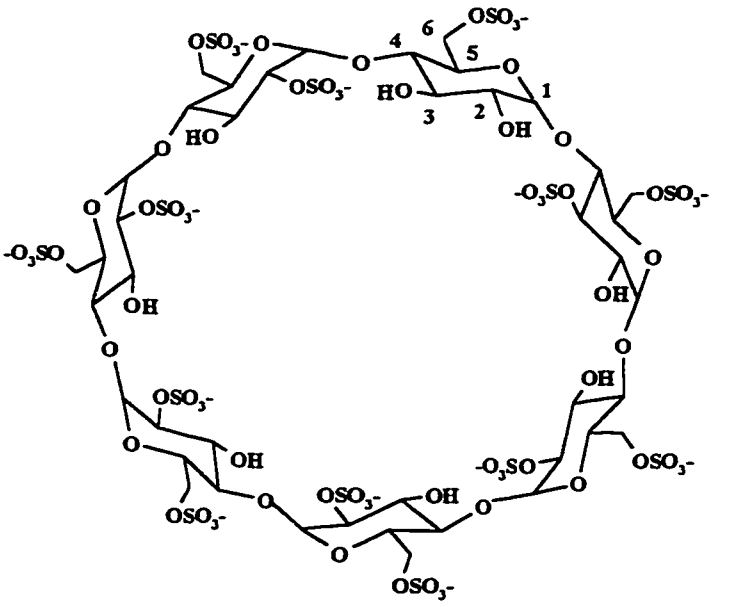

Figure 2.1 Hypothetical structure of a 13-sulfated β-cyclodextrin.

unit, C2, C3, and C6 (see Figure 2.1). Therefore there are a total of 21 possible sulfation sites in a β-cyclodextrin. Shown in Figure 2.1 is a hypothetical chemical structure of a 13-sulfated β-cyclodextrin. The substitution sites are postulated. For tetra-sulfated β-cyclodextrin, only 4 out of 21 possible sites are substituted with sulfate groups. In reality, however, all commercially available negatively charged cyclodextrins are

mixtures [1], constituted of a series of derivatives with different degrees of substitution and different substitution patterns. The reported degree of substitution is the average number estimated by mass analysis.

Theoretically, negatively charged CDs broaden the separation window [2], so that higher resolutions can be achieved at lower CD concentrations. It is also desirable to introduce more charges into the chiral selector in order to improve the resolution [3]. Practically, many researchers have observed extremely high resolving power in separations with negatively charged CDs [1][2][4][5]. However the mechanism by which such separations are achieved with charged cyclodextrins is not fully clear. Deviations from the Wren-Rowe model (Section 1.4.1) have been noted in the literature. That is, separations may not depend on the difference in stability constants alone.

The aim of this chapter is to provide a systematic study of the complexation behavior of negatively charged CDs. Model enantiomeric separations are performed using β-cyclodextrin and two types of sulfated β-cyclodextrin. The solutes chosen have been used extensively in past studies of cyclodextrin mediated chiral separations [6][7] [21].

2.2 EXPERIMENTAL

2.2.1 APPARATUS

All the experiments were carried out on a Beckman P/ACE 2100 capillary electrophoresis instrument (Fullerton, CA, USA). The capillary was a polyacrylamide coated neutral capillary (eCap, Beckman) with an internal diameter of 50 μm and total length of 37 cm. The detection window was 7 cm from the end of capillary.

Absorbance of solutes was measured at 214 nm. A voltage of 10 kV was used for all the mobility measurements. This voltage was chosen to be the highest voltage within the linear range of the Ohm's law plot (Section 1.2.2.4). This minimized the separation time without distorting the sample peak with Joule heating. The capillary cartridge was temperature contralled at 20 °C.

2.2.2 REAGENTS

Sulfated β-cyclodextrins (SCD) with the degree of substitution (D.S.) of 4 and 13 were purchased from Cerestar (Hammond, IN, USA). Buffer components MES (morpholino-ethanesulfonic acid monohydrate) and Jeffamine 900 (poly(propylene glycol-*b*-ethylene glycol-*b*-propylene glycol) bis(2-aminopropyl ether)) were obtained from Sigma-Aldrich Canada Ltd. (Oakville, Ontario). Mesityl oxide (Aldrich, 98%) was used as a neutral EOF marker. 1,5-Naphthalenedisulfonic acid disodium salt (NDS) (95%), homatropine (±), propranolol (DL) (99%) and (R, +) (98%), and methyl mandelate S-(+)- (99%) and R-(-)- (99%), were obtained from Sigma-Aldrich Canada. The structures of these analytes are as shown in Figure 2.2. All chemicals were used as received.

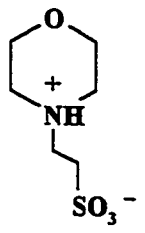

MES (morpholino-ethanesulfonic acid), pKa = 6.1[8]

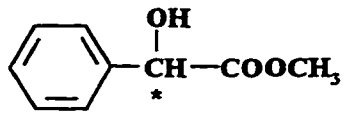

Methyl Mandelate (neutral)

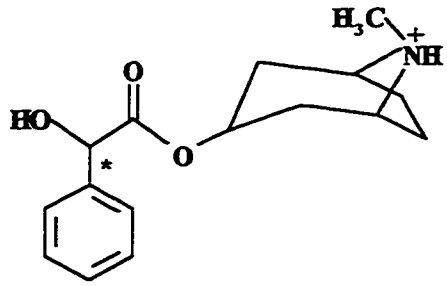

Homatropine, pKa = 9.9 [9]

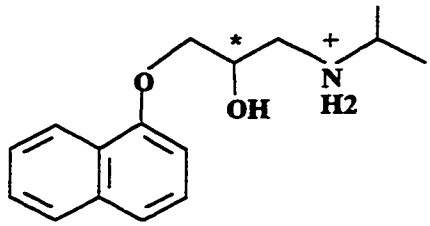

Propranolol, pKa = 9.5 [10]

Figure 2.2 Structure of the MES buffer and the analytes. The stars indicate the position of the chiral carbon.

2.2.3 PROCEDURES

A 400 mM MES stock solution was first made. The background electrolyte solution was made as follows: first, the appropriate amount of sulfated β-cyclodextrin (SCD) was weighed out and transferred into a 100 ml volumetric flask; then 50 ml of the 400 ml MES stock solution was added to this volumetric flask, and the volume was brought up to mark with distilled deionized water (Barnstead type D4700 NANOpure deionization system); finally, the pH of all solutions was adjusted to 4.6 with Jeffamine

900 or 6 M sulfuric acid and filtered through 0.45 μm syringe filters (Nalge Company, NY, USA).

Homatropine, methyl mandelate, and propranolol solutions were made up in 200 mM MES buffer solution and adjusted to pH 4.6 using Jeffamine 900. A voltage of 10 kV was applied for all separations. A 3 s hydrodynamic injection (0.5 p.s.i.; 1 p.s.i. = 6894.76 Pa) was used to introduce samples onto the capillary. The capillary cartridge was maintained at 20 °C all the time. At the start of each day the capillary was flushed with deionized water for 10 min under high pressure (20 p.s.i.). The EOF in this neutral capillary was monitored using the 3-injection method (see section 2.2.5) to ensure that the polyacrylamide coating was intact. After each run, the capillary was rinsed (20 p.s.i.) with deionized water for 1.5 min and with running buffer for 1.5 minutes. At the end of a day, the capillary was rinsed with 0.1 M HCl for 5 min, followed by deionized water for 10 min. Then the capillary was placed in a cassette box with both ends dipped in vials of deionized water and stored in a refrigerator in an upright position. Alternatively when this capillary was to be used again within 18 hours, the capillary was kept in the instrument with both ends immersed in vials of deionized water.

2.2.4 VISCOSITY MEASUREMENT

Solutions containing high concentrations of cyclodextrins are very viscous. Since mobility is inversely related to viscosity, failure to recognize this results in misinterpretation of the data [11]. Therefore the apparent mobility measured for a solute needs to be corrected by a relative viscosity factor η/η_0, where η is the viscosity of the buffer containing cyclodextrin and η_0 is the viscosity of the buffer without cyclodextrin.

This corrects mobilities in any cyclodextrin containing buffer to that in the cyclodextrin free buffer.

According to Poiseuille's Law [12]:

$$\overline{U} = \frac{\Delta P r^2}{8\eta L} \qquad (2\text{-}1)$$

where $\overline{U}$ is the average linear velocity of the liquid, ΔP is the pressure difference along a tube of length L, r is the radius of the tube, and η is the viscosity of the liquid. In our capillary, the linear velocity, $\overline{U}$, can be measured by pushing a neutral marker (mesityl oxide in our case) through the capillary under low pressure (0.5 p.s.i.; 1 p.s.i. = 6894.76 Pa). The velocity is then calculated as below:

$$\overline{U} = l/t_V \qquad (2\text{-}2)$$

where l is the capillary length between injection end and the detection window, and t_V is the time needed for the neutral marker to travel this length under low pressure.

Substitution of Equation 2-2 into 2-1 and rearrangement yields:

$$\eta = \left(\frac{\Delta P r^2}{8lL}\right) t_V \qquad (2\text{-}3)$$

Equation 2-3 shows that the viscosity of a buffer is determined by the time (t_V) needed to push the buffer through a certain length (l). That is:

$$\eta/\eta_0 = t_V/t_{V,0} \qquad (2\text{-}4)$$

where $t_{V,0}$ is the pushing time in cyclodextrin free buffer.

In this work, all apparent mobilities (μ_a) are multiplied by this relative mobility ratio ($t_V/t_{V,0}$) to get corrected mobilities (μ_c) [13]:

$$\mu_c = \mu_a(t_V/t_{V,0}) \qquad (2\text{-}5)$$

2.2.5 MEASUREMENT OF EOF MOBILITY BY 3-INJECTION METHOD

From Equation 1-7 we know that the observed mobility of a solute is composed of its effective mobility and the electroosmotic flow (EOF) mobility. However all equations referring to mobility in cyclodextrin mediated capillary electrophoresis actually refer to the effective mobility. Therefore, it is very important to measure accurately the EOF mobility to get a precise value of the solute effective mobility.

In an untreated fused silica capillary the magnitude of EOF is in the order of 10^{-4} $cm^2/(Vs)$. Under such conditions we can simply inject a neutral marker into the capillary and wait for it to migrate to the detection window. The neutral marker does not have any intrinsic mobility. It moves only with EOF. Thus the observed mobility of the neutral marker will be equal to the EOF mobility. The whole measurement usually takes less than ten minutes.

However, in coated neutral capillaries, such as the polyacrylamide coated eCap capillary used herein, the EOF is reduced to the order of 10^{-6} $cm^2/(Vs)$. It would take hours for a neutral marker to come out if the above mentioned simple method were used. The long migration time also would cause severe bandbroadening of the neutral marker peak, making detection difficult. Therefore, a three-injection mobility determination method proposed by Williams and Vigh [14] was adapted to determine the small EOF in our neutral capillary.

With reference to Figure 2.3, the procedure for this method is as follows:

A. The capillary is rinsed and filled with background electrolyte (BGE). Then a neutral marker band (N1) is loaded into the capillary by hydrodynamic injection under low pressure.

B. The same pressure is applied again to transfer N1 a distance into the capillary. Another injection of the neutral marker then introduces a second marker band (N2) onto the capillary.

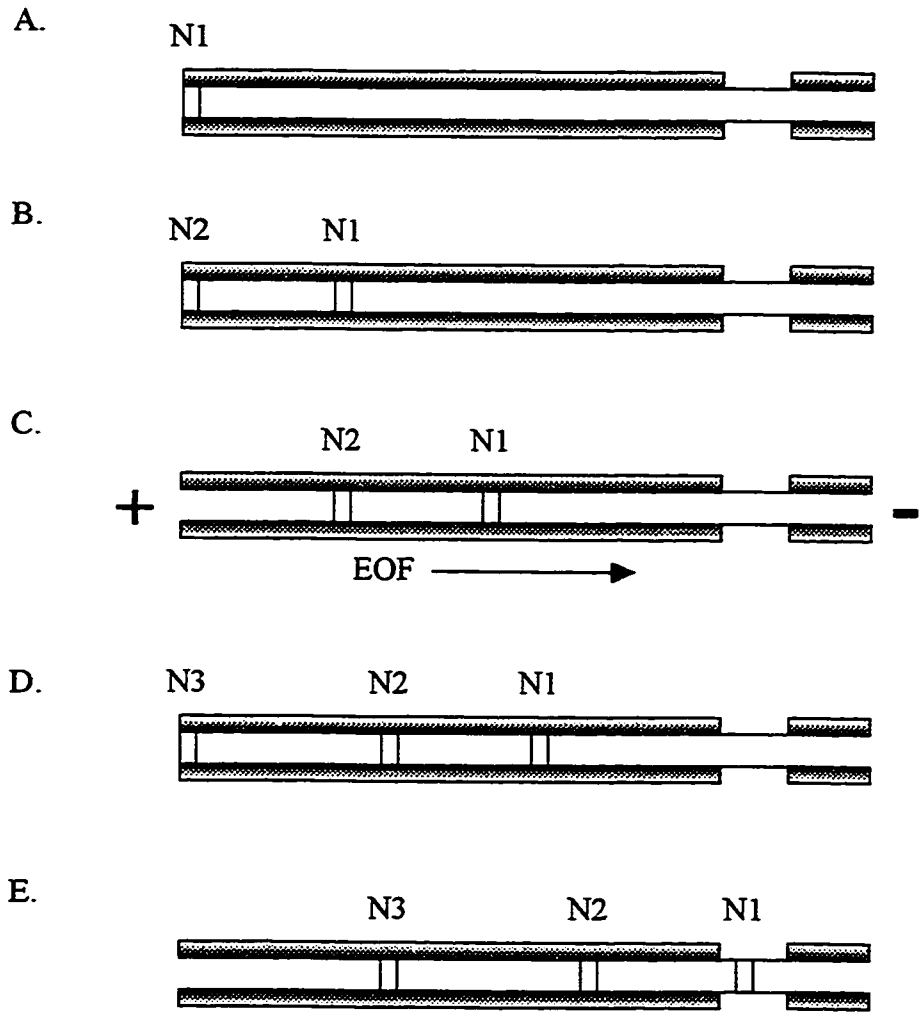

Figure 2.3 Schematics of 3-injection mobility measurement [13].

C. Both N2 and N1 are transferred again into the capillary for the same period of time as in B. Now a separation voltage (V_{sep}) is turned on for a certain period of time (t_{migr}). During this time both N1 and N2 move with mobilities equal to the EOF mobility (μ_{EOF}).

D. After the voltage is withdrawn, a third band of the neutral marker solution is injected.

E. Low pressure is applied again and data acquisition is initiated simultaneously to record the passage of all three bands. An example of the resultant signal is shown in Figure 2.4.

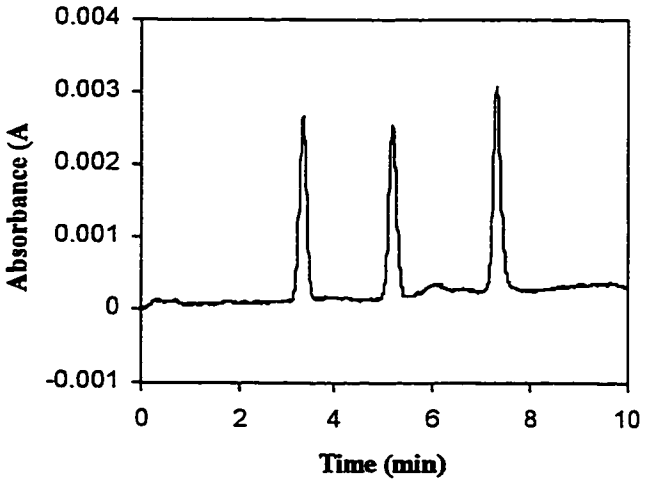

Figure 2.4 The signal obtained from step E of the 3-Injection method for determining EOF (step E in Figure 2.3).

The pressure mobilization mobility in step E with which all three bands move by the detector, is calculated by:

$$U_m = L_d/t_{N3} \qquad (2\text{-}6)$$

The distance between N1 and N2 is the distance caused by pressure pushing alone. It would be the distance between N2 and N3 if there were no EOF present. It is calculated by:

$$L_{init} = (t_{N2} - t_{N1})\, U_m \qquad (2\text{-}7)$$

However, the existence of EOF will make the distance between N3 and N2 differ from L_{init}. It is calculated by:

$$L_{final} = (t_{N3} - t_{N2})\, U_m \qquad (2\text{-}8)$$

The difference between L_{init} and L_{final} is the distance traveled by the neutral marker during electrophoresis, and is calculated by:

$$\Delta L = L_{final} - L_{init} = [(t_{N3} - t_{N2}) - (t_{N2} - t_{N1})]\, U_m \qquad (2\text{-}9)$$

Then EOF mobility can be calculated as:

$$\mu_{EOF} = \frac{\Delta L \cdot L}{V \cdot t_{migr}} \qquad (2\text{-}10)$$

where V is the voltage applied during step C and L is the total length of the capillary.

In our experiments, this 3-injection method was used to test the EOF in neutral capillary from day to day with a 200 mM MES buffer (pH = 4.6) as background electrolyte. Mesityl oxide was used as the neutral EOF marker. All neutral capillaries have inner diameters of 50 μm and a total length of 37 cm or 27 cm. The separation voltage was set to 18.5 kV for 37 cm capillary and 13.5 kV for 27 cm capillary for 5 min. The low pressure push in step B and C in Figure 2.4 lasts for 2 min. The EOF measured

in this way for a new eCap neutral capillary (Beckman) was about 4-7 $\times 10^{-6}$ $cm^2/(Vs)$. As the capillary aged over 3 months under intense use, the EOF mobility gradually increased to about 1×10^{-5} $cm^2/(Vs)$. Any sudden change in the EOF mobility indicated damage to the polyacrylamide coating, and the capillary was replaced.

However with charged cyclodextrins in the background electrolyte, organic compounds such as mesityl oxide may interact with the cyclodextrins. Thus the mobility of these compounds does not only depend on the EOF alone, but also on the concentration of cyclodextrin. As a matter of fact, mesityl oxide has given us "negative" (anodic) EOF mobility in tetra-sulfated β-cyclodextrin mediated buffers when the EOF would be expected to be "positive" (cathodic). To solve this problem, 200 mM MES in D_2O solution was used as the neutral marker. D_2O has a different refractive index (1.3280 [15]) than H_2O (1.3330 [16]). Thus a strong refractive index peak is obtained when the D_2O solution band passes by the detector. Unfortunately, the precision of EOF measurements made with D_2O in cyclodextrin containing buffers was $\pm 5 \times 10^{-6}$ $cm^2/(Vs)$. This prevented direct observation of the subtle EOF changes that are believed to have occurred when the charged cyclodextrin concentration was increased (see Section 3.3).

2.3 DATA HANDLING

2.3.1 CURVE FITTING

2.3.1.1 DETERMINATION OF FREE CD CONCENTRATION

For a complexation equilibrium between solute A and a cyclodextrin:

$$A + CD \rightleftharpoons ACD$$

the equilibrium constant is:

$$K_{ACD} = \frac{[ACD]}{[A][CD]} \qquad (2\text{-}11)$$

and thus:

$$[ACD] = [A][CD]K_{ACD} \qquad (2\text{-}12)$$

Penn and Goodall [17] have pointed that it is the free cyclodextrin concentration, [CD], not the total analytical concentration of cyclodextrin, C_{CD}, that should be used in all curve fittings. When neutral cyclodextrins are used, it has often been assumed that [CD] is equal to the total analytical concentration of the cyclodextrin (C_{CD}). With neutral cyclodextrins typically a few millimolar to 100 mM cyclodextrin is required to achieve separation. Compared with typical sample concentrations of 10^{-4} M or less, the assumption is valid in most cases for neutral cyclodextrins. However with sulfated β-cyclodextrins, baseline resolution can often be achieved with less than 1 mM cyclodextrin. Under such conditions the sample concentration is comparable to the cyclodextrin concentration. Now the assumption is not reasonable. Under such conditions we must determine the free cyclodextrin concentration to get reliable results. The following procedure for calculating free cyclodextrin concentrations is based on the appendix of reference [17].

Using C_A and C_{CD} for the analytical concentrations of the analyte and cyclodextrin, respectively, the concentration of free analyte ([A]) and free cyclodextrin ([CD]) can be expressed from the concentration of the complex ([ACD]) as follows:

$$[A] = C_A - [ACD] \qquad (2\text{-}13)$$

$$[CD] = C_{CD} - [ACD] \qquad (2\text{-}14)$$

Substituting (2-13) and (2-14) into (2-12) yields:

$$[ACD] = (C_A - [ACD])(C_{CD} - [ACD])K_{ACD} \qquad (2\text{-}15)$$

Rearranging (2-15) gives,

$$K[ACD]^2 - [(C_A + C_{CD})K + 1][ACD] + C_A C_{CD} K = 0 \qquad (2\text{-}16)$$

Finally, making: $a = K$; $b = (C_A + C_{CD})K + 1$; and $c = C_A C_{CD}$, and solving the quadratic in Equation (2-16) and discarding the one unreasonable solution, the concentration of the complex ACD is:

$$[ACD] = \frac{-b - \sqrt{b^2 - 4ac}}{2a} \qquad (2\text{-}17)$$

The free CD concentration ([CD]) can then be determined using Equation 2-13.

2.3.1.2 CURVE FITTING

The complex mobilities (μ_{ACD}) and the stability constants (K) for solute-cyclodextrin complexes were obtained by non-linear curve fitting according to Equation 1-14. The free solute mobility was obtained directly from the solute migration time in the absence of cyclodextrin. The curve fitting was performed using both the Solver function of Microsoft Excel and the Curve Fitter function of SlideWrite Plus (version 2.0 for Windows, Advanced Graphics Software, Inc., Carlsbad, CA). Solver iteratively alters the parameters to minimize the sum of the squares of the residuals. Curve Fitter uses the iterative Levenberg-Marquardt algorithm, which yields parameters based on the minimization of the sum of the squared deviations. The two methods were in very good agreement for all the curve fits we have done. The statistical results listed in Section 2.4.1 are obtained using Curve Fitter, since Solver does not give standard deviations.

2.3.2 DATA CORRECTIONS IN SULFATED CYCLODEXTRIN MEDIATED SYSTEMS

An abnormal mobility behavior was observed when negatively charged cyclodextrins were used as a buffer component. Instead of seeing the theoretical mobility

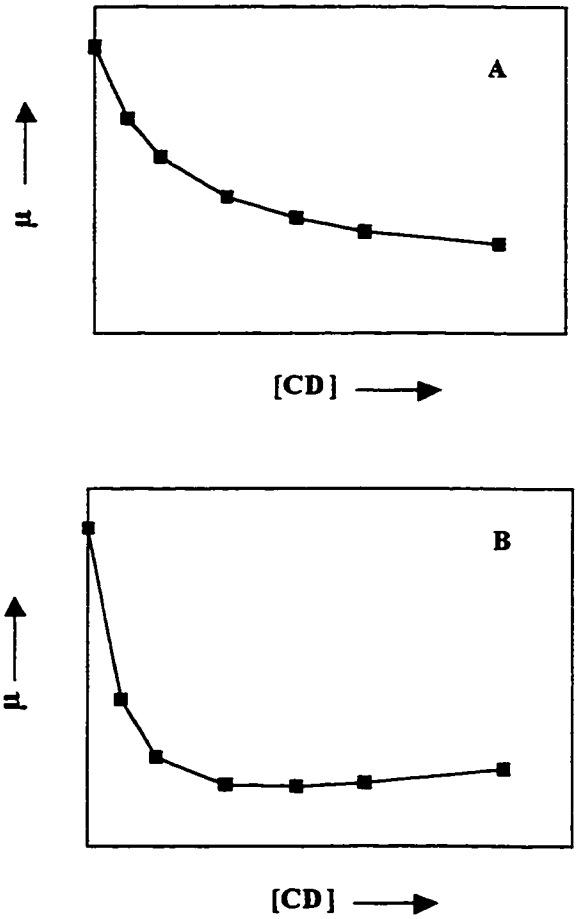

Figure 2.5 A theoretical μ-[CD] plot (A) and an actual μ-[CD] plot with 13-sulfated β-CD (B).

behavior as shown in Figure 2.5(A), we were seeing a positive drift of observed mobility at high charged cyclodextrin concentrations as shown in Figure 2.5(B).

We postulate two possible causes for this deviation from the Wren-Rowe model. The first possible cause is an adsorption of negatively charged cyclodextrins onto the capillary wall. This adsorption will introduce a negative charge on the inner capillary wall and consequently cause a cathodic EOF. Such an EOF would increase the apparent cationic mobility (or decrease the apparent anionic mobility) of the solutes. Cai and Vigh have observed an adsorption of negatively charged cyclodextrins on an uncoated capillary wall at pH 2.5 [18]. At this pH, the negative charge density on the capillary is very low and consequently the EOF is very small. The adsorption of negatively charged cyclodextrins increased EOF mobility in that capillary. The sulfated cyclodextrins used in our experiments may adsorb onto the polyacrylamide coated capillary wall in a similar manner. It is expected that adsorption would become more severe as the cyclodextrin concentration increases, causing a stronger EOF at higher cyclodextrin concentrations.

The second possible cause for the drifting mobility is an ionic strength effect caused by the addition of high concentrations of the multiple-charged cyclodextrins. This effect would diminish the absolute value of solute mobilities, regardless of whether the complex mobility was cathodic or anodic. Figure 2.6 is a hypothetical graph showing the effects of these two possible causes. The corrected mobility versus cyclodextrin concentration plot of two hypothetical solutes with positive and negative mobilities, respectively, are shown here.

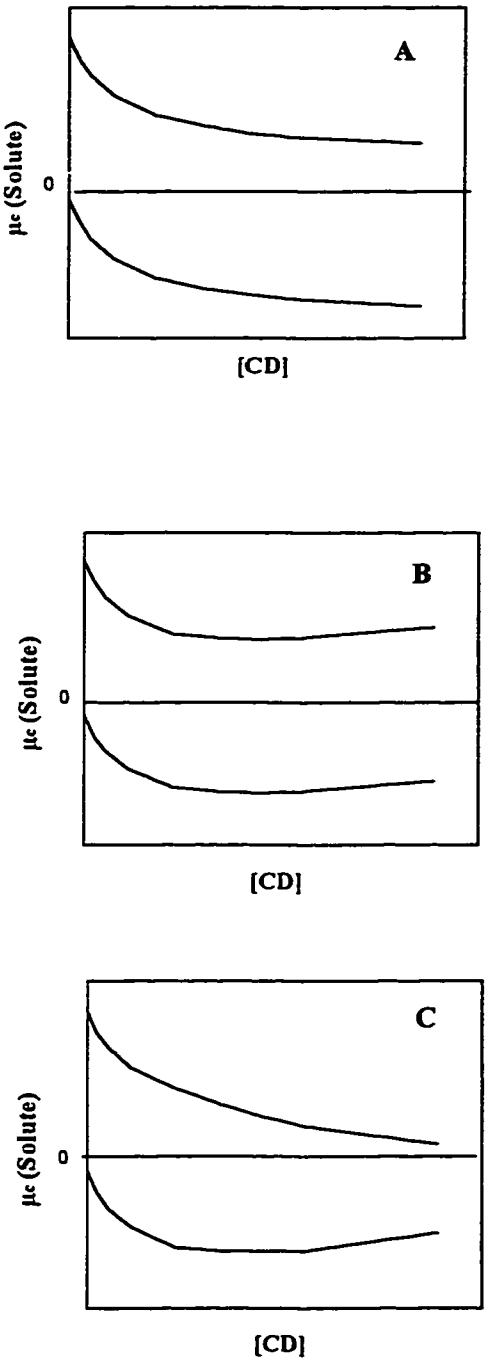

Figure 2.6 Hypothetical graphs of the effects expected from EOF or ionic strength effect. A. without adsorption or ionic effect; B. adsorption effect; C. ionic strength effect. See text for explanation.

The solute mobilities observed at high cyclodextrin concentrations in Figure 2.5(B) and in Chapter 3 drift upward, even when the mobilities are positive. That is, the solutes show increasing cathodic mobility at high cyclodextrin concentrations. This increasing cathodic mobility is not consistent with the ionic strength hypothesis. Therefore, it is unlikely that the ionic strength effect dominates. On the other hand, this trend (an increase in cathodic mobility as cyclodextrin concentration increases) agrees well with what we would expect for an adsorption effect (see Figure 2.6). Thus we think an EOF effect is the main reason behind this drifting mobility.

Due to the small magnitude of the EOF in the neutral capillary, however, we could not accurately measure the EOF mobility directly, as described in Section 2.2.5. Also, there may be other effects that are introduced by the addition of high charge cyclodextrins, which can not be corrected by EOF mobility alone. Therefore, two approaches were used to treat this matter.

The first approach is Limited Range approach. Since the EOF effect should become more severe at high cyclodextrin concentrations and negligible at low concentrations the last two data points were omitted when curve fitting was performed. We think that in this way by putting more emphasis on the early points where the existence of EOF is not significant we can get more accurate complex mobility values.

An alternative approach is NDS Correction approach. Naphthalene disulfonic acid (NDS) was used as a model solute to examine the effect of the addition of cyclodextrins. Naphthalene disulfonic acid is a naphthalene based di-anionic compound. It has been reported that electrostatic repulsion prevents negatively charged phenol derivatives from forming complexes with tetra-negatively charged sulfobutylether-β-

cyclodextrins [19]. Naphthalene disulfonic acid has a bigger size (two aromatic rings versus one in phenols), which is expected to cause more steric hindrance, and one more negative charge, which should induce stronger electrostatic repulsion by the negative charges of the cyclodextrins. Therefore we would expect no complexation of the NDS by sulfated cyclodextrins. Thus any variation in NDS mobility should reflect the non-complexation effects caused by the addition of cyclodextrins.

To use NDS to correct the effects caused by charged cyclodextrins, the mobility of NDS is first measured in the same series of cyclodextrin buffers as used for all the other solutes and under identical experimental conditions. Shown in Figure 2.7 and Table 2.1 are the experimental results for NDS in 13-sulfated CD buffers.

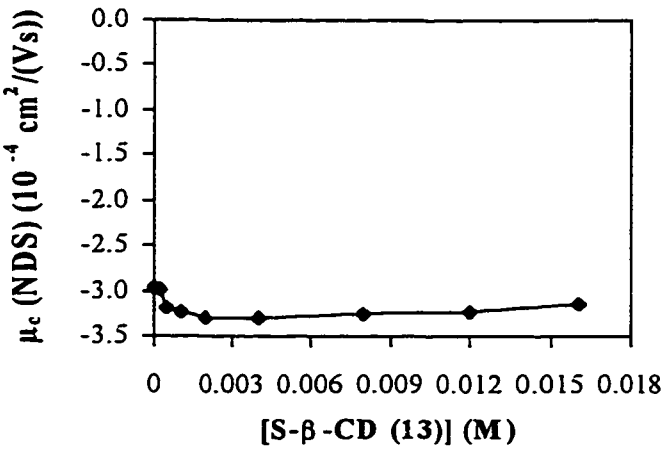

Figure 2.7 Naphthalene disulfonic acid mobility as a function of 13-sulfated β-cyclodextrin concentration. The line is simply connecting all data points. Conditions: 1.0×10^{-3} M naphthalene disulfonic acid solution prepared in 200 mM MES buffer, pH = 4.6, V = 10 kV, T = 20 °C, λ =214, capillary 37/30 cm.

Table 2.1 Mobility measurements of naphthalene disulfonic acid with 13-sulfated CD[a].

[CD] (M)	t (min)	$\mu_a \times 10^4$ ($cm^2/(Vs)$)	t_v (min)	$\mu_c \times 10^4$ ($cm^2/(Vs)$)	$\Delta\mu \times 10^4$ ($cm^2/(Vs)$)
0	6.25	-2.960	7.97	-2.960	0
0.00025	6.27	-2.951	8.04	-2.978	-0.018
0.0005	5.86	-3.157	8.04	-3.186	-0.226
0.001	5.79	-3.195	8.06	-3.231	-0.271
0.002	5.74	-3.223	8.18	-3.308	-0.348
0.004	5.82	-3.179	8.26	-3.294	-0.334
0.008	5.94	-3.114	8.34	-3.259	-0.299
0.012	6.15	-3.008	8.54	-3.223	-0.263
0.016	6.39	-2.895	8.63	-3.135	-0.175

a. Experimental conditions are as in Figure 2.7. "t" is the migration time; "μ_a" is the apparent mobility (mobility without viscosity correction); "t_v" is the time observed for the viscosity measurement as described in section 2.2.5; and "μ_c" is the corrected mobility (mobility with viscosity correction). $\Delta\mu$ is calculated by subtracting the respective mobility value by the free mobility of NDS.

An upward drifting was observed in Figure 2.7 for NDS as observed for positive solutes. The difference between the observed mobilities at different cyclodextrin concentrations and the free NDS mobility ($\Delta\mu$) should then reflect the influence of the addition of cyclodextrin on the mobility of ions. The reason for the initial decrease in mobility (increase in negative mobility) when cyclodextrin was first added is unknown. Regardless, to correct this influence for all the positive solutes, the $\Delta\mu$ values were subtracted from the respective solute mobility values to get NDS corrected mobilities

(μ_{NDS}). The NDS corrected mobilities were then fit to Equation 1-14 (NDS Correction approach).

The same procedure was applied to NDS when tetra-sulfated CD was used. The mobility results of NDS with tetra-sulfated CD are shown in Figure 2.8 and Table 2.2 below.

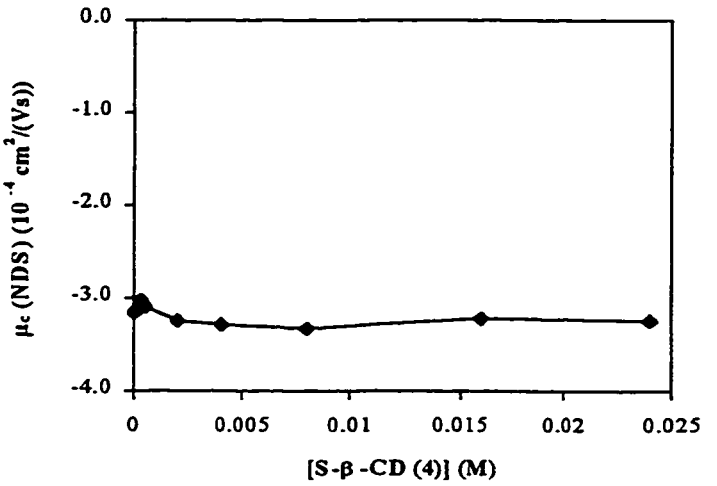

Figure 2.8 Naphthalene disulfonic acid (NDS) mobility as a function of the tetra-sulfated β-cyclodextrin concentration. The line is simply connecting all data points. Conditions: 1.0×10^{-3} M naphthalene disulfonic acid solution prepared in 200 mM MES buffer, pH = 4.6, V = 10 kV, T = 20 °C, λ =214, capillary 37/30 cm.

Table 2.2 Mobility measurements of naphthalene disulfonic acid with tetra-sulfated β-cyclodextrin[a].

[CD] (M)	t (min)	$\mu_a \times 10^4$ ($cm^2/(Vs)$)	t_V (min)	$\mu_c \times 10^4$ ($cm^2/(Vs)$)	$\Delta\mu \times 10^4$ ($cm^2/(Vs)$)
0	5.86	-3.154	7.16	-3.154	0
0.00025	6.20	-2.986	7.26	-3.032	0.122
0.0005	6.08	-3.043	7.25	-3.083	0.071
0.002	5.82	-3.179	7.30	-3.241	-0.087
0.004	5.80	-3.192	7.36	-3.282	-0.127
0.008	5.80	-3.192	7.46	-3.328	-0.174
0.016	6.18	-2.996	7.68	-3.218	-0.064
0.024	6.32	-2.925	7.92	-3.236	-0.081

a. Experimental conditions are as in Figure 2.8. The meanings of the symbols are as in Table 2.1. $\Delta\mu$ is calculated by subtracting the respective mobility value by the free mobility of NDS.

Naphthalene disulfonic acid (NDS) showed similar mobility behavior in tetra-sulfated cyclodextrin to that in 13-sulfated cyclodextrin (Figure 2.7) only with a smaller magnitude. This smaller magnitude is to be expected since the charge on a tetra-sulfated cyclodextrin (-4) is much less than that on a 13-sulfated cyclodextrin (-13). As a result the addition of tetra-sulfated cyclodextrin has less influence on the ions. The $\Delta\mu$ obtained in Table 2.2 is then used to correct solute mobility data with tetra-sulfated CD.

The advantage of Limited Range approach is its simplicity. Obviously it is not capable of correcting any effect that happens at low cyclodextrin concentrations. NDS Correction, on the other hand, can correct over the whole concentration range thus is a

superior method as compared to Limited Range approach. However, there also are concerns about this approach: first, NDS is negatively charged while all the analytes are positively charged; second, NDS is di-charged while the analytes are monocharged. Therefore using NDS approach we may correct some effects that are specific to negative ions but not apply to positive ions. Or we may exaggerate the ionic strength effects or reverse the direction of this effect. Regardless we believe that the real value can be bracketed by the values obtained from these two approaches. The difference between these two approaches will reflect the uncertainty in determining the true complex mobility.

2.4 RESULTS AND DISCUSSION

2.4.2 SULFATED β-CYCLODEXTRIN COMPLEX MOBILITY BEHAVIOR

Capillary electrophoresis is a technique that separates analytes based on the difference in their effective mobilities. Mobilities in turn depend on the charge to volume ratio (Equation 1-5). Enantiomers have identical physical properties. Thus, they exhibit exactly the same free mobilities ($\mu_A = \mu_B$) in their uncomplexed forms. When a chiral complexing additive is added into the buffer system, it can form a complex with the analytes. Both the charge and the volume of the molecules may be altered in this way. Therefore the complex has a different mobility (μ_{AC} or μ_{BC}) than the free solute mobility. Since the CD complexation process is a facile equilibrium, solutes spend part of their time in and part out of the chiral additive. As a result the observed mobility of a solute is between μ_A and μ_{AC}, and is a linear combination of μ_A and μ_{AC} (Equation 1-8 and 1-9). The difference in the observed mobilities of the two enantiomers will depend on their

different affinities toward CD, dictated by their stability constants K (Equation 1-17). In addition, if the complex mobilities differ ($\mu_{AC} \neq \mu_{BC}$) then the selectivity also depends on μ_{AC} and μ_{BC}. Therefore, stability constants (K) of this binding process and the complex mobility (μ_{AC} and μ_{BC}) play important roles in the separation of solutes, and will be examined in this section.

The usual way of studying solute-cyclodextrin complexation in CE is to run the solute in a series of buffers containing increasing concentrations of the cyclodextrin. The observed mobilities in the different cyclodextrin buffers are then corrected for viscosity as described in Section 2.2.4. Next, the corrected mobilities are plotted against cyclodextrin concentration and non-linear curve fitting is performed according to the Wren-Rowe model (Equation 1-14). As Bowser and Chen pointed out (Section 1.4.4 and reference [20], ignoring higher order complexation can lead to misinterpretation of experimental data. Therefore, non-linear curve fitting according to Equation 1-38 (1:2 binding) was also performed to determine if 1:2 binding was occurring.

In the following experiments, the buffer pH was chosen to ensure that homatropine and propranolol are completely monocharged.

2.4.1.1 NEUTRAL β-CYCLODEXTRIN

2.4.1.1.1 HOMATROPINE

Results for homatropine and propranolol with neutral β-cyclodextrin are included here for comparison with the sulfated β-cyclodextrins. Figure 2.9 is a plot of the corrected mobilities of racemic homatropine in β-cyclodextrin containing buffers.

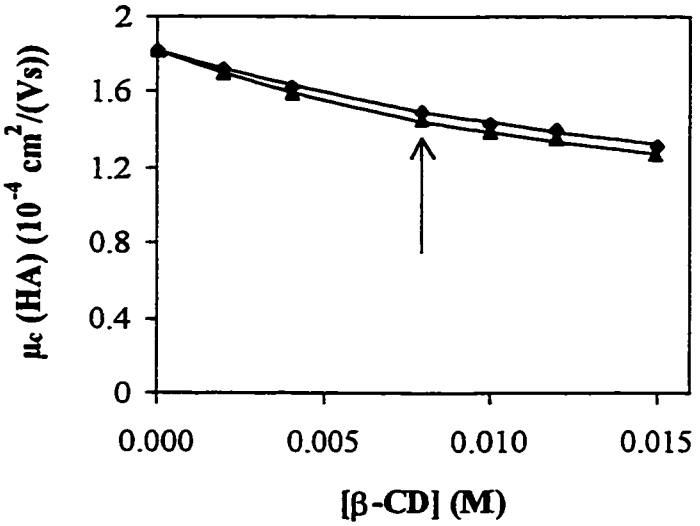

Figure 2.9 Corrected homatropine mobility as a function of β-cyclodextrin concentration. (◆) — first peak; (▲) — second peak. Solid line is constructed using equation 1-14 and curve fitting results for 1:1 binding from Table 2.4. Conditions: 200 mM MES buffer, pH = 4.6, V = 10 kV, T = 20 °C, λ =214 nm, capillary 37/30 cm. The arrow indicates where near baseline resolution was achieved (≈ 8 mM).

Table 2.3 Homatropine mobility measurement with β-CD[a].

[CD] (M)	t_1 (min)	t_2 (min)	$\mu_{a1} \times 10^4$ ($cm^2/(Vs)$)	$\mu_{a2} \times 10^4$ ($cm^2/(Vs)$)	t_V (min)	$\mu_{c1} \times 10^4$ ($cm^2/(Vs)$)	$\mu_{c2} \times 10^4$ ($cm^2/(Vs)$)
0	10.17	10.17	1.819	1.819	7.04	1.819	1.819
0.00025	10.46	10.46	1.769	1.769	7.05	1.771	1.771
0.002	10.86	11.01	1.703	1.680	7.11	1.721	1.697
0.004	11.63	11.88	1.591	1.557	7.18	1.623	1.589
0.008	12.84	13.25	1.441	1.396	7.33	1.500	1.453
0.01	13.56	14.01	1.364	1.320	7.40	1.434	1.388
0.012	14.03	14.51	1.319	1.275	7.47	1.400	1.353
0.015	15.12	15.67	1.224	1.181	7.58	1.317	1.271

a. Experimental conditions are as in Figure 2.9. Enantiomerically pure homatropine was not available. Therefore subscript 1 indicates the first peak observed (i.e., the faster enantiomer) and 2 indicates the second peak. Meanings of other symbols are as in Table 2.1.

The only effect the neutral cyclodextrin brings to the buffer system is an increased viscosity. There are no ionic effects involved. The EOF mobility in this system is negligible (below 5×10^{-6} $cm^2/(Vs)$) compared with the magnitude of the mobilities of the enantiomers. Therefore only corrections for viscosity are needed for this system. The corrected mobilities are used for non-linear curve fitting and the results are listed in Table 2.4.

Table 2.4 Curve fitting statistics for homatropine with β-cyclodextrin.

1:1 binding		
	Peak 1	Peak 2
μ_A*	1.819	1.819
μ_{ACD}*	0.6 ± 0.1	0.69 ± 0.07
K (M^{-1})	45± 6	62 ± 6
R^2	0.9985	0.9987
Fitting Equation	$y = (1.819 + \mu_{ACD}K[CD])/ (1 + K[CD])$	
1:1 +1:2 binding		
	Peak 1	Peak 2
μ_A*	1.819	1.819
μ_{ACD}*	0.59 ± 0. 15	0. 69 ± 0. 09
K_1 (M^{-1})	45 ± 8	61 ± 8
$\mu_{A(CD)2}$*	0 ± 9E-9	0 ± 1
K_2 (M^{-1})	0 ± 0.5	0 ± 0.5
R^2	0.9985	0.9987
Fitting Equation	$y = 1.819 + \frac{(\mu_{ACD} - 1.819)K_1[CD] + (\mu_{A(CD)_2} - 1.819)K_1K_2[CD]}{1 + K_1[CD] + K_1K_2[CD]^2}$	

*unit: 10^{-4} $cm^2/(Vs)$.

The observed mobility for homatropine in 200 mM MES (pH 4.6) was 1.819 x 10^{-4} $cm^2/(Vs)$ in the absence of cyclodextrin. This value was taken as the mobility of the free solute (μ_{free}). As can be seen in Figure 2.9, equation 1-14 (1:1 binding) fits the observed data points. This is also indicated by the excellent correlation coefficient for the 1:1 binding (R^2>0.998). The correlation coefficient for 1:2 binding is also very good. However the values of zero for the K for secondary complexation shows that 1:2 binding is negligible in this system. Therefore only 1:1 binding for this complexation process

will be considered throughout this chapter. The complex mobility of the two enantiomers are statistically equal at 95% confidence interval. On the other hand, the stability constants are small but are statistically different.

2.4.1.1.2 PROPRANOLOL

The same treatment was applied to propranolol in neutral β-cyclodextrin mediated buffers. No resolution was observed within the β-cyclodextrin concentration range used (0 - 15 mM). The concentration range for β-cyclodextrin is limited by its solubility (~ 16 mM). Thus there is only single mobility curve shown in Figure 2.10.

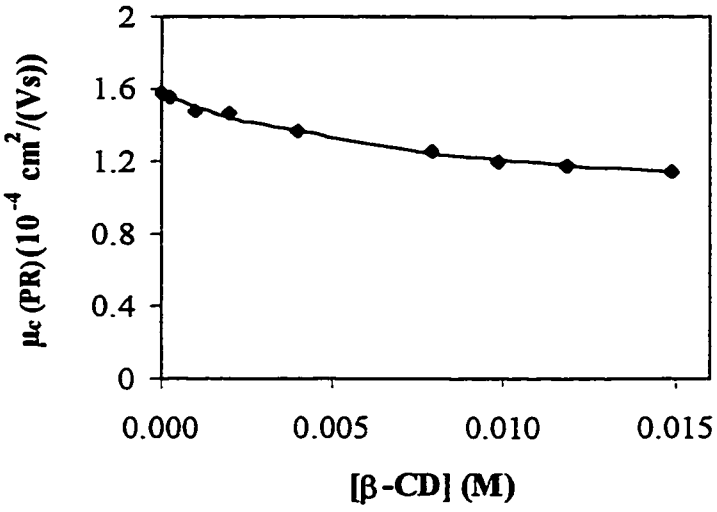

Figure 2.10 Corrected mobility of propranolol vs. [β-CD]. Solid line is constructed using equation 1-14 and curve fitting results for 1:1 binding from Table 2.4. Experimental conditions: 200 mM MES buffer, pH = 4.6, V = 10 kV, T = 20 °C, λ =214 nm, capillary 37/30 cm.

Table 2.5 Propranolol mobility measurements with β-CD[a].

[CD] (M)	t (min)	$\mu_a \times 10^4$ ($cm^2/(Vs)$)	t_v (min)	$\mu_c \times 10^4$ ($cm^2/(Vs)$)
0	11.76	1.573	7.02	1.573
0.25	11.91	1.553	7.07	1.555
1	12.56	1.473	7.15	1.480
2	12.78	1.448	7.15	1.462
4	13.82	1.339	7.2	1.365
8	15.28	1.211	7.17	1.258
10	16.17	1.144	7.46	1.200
12	16.63	1.112	7.5	1.178
15	17.4	1.063	7.59	1.141

a. Experimental conditions are as in Figure 2.10. Enantiomeric separation of propranolol was not achieved. Subscript "a" indicates the apparent mobility while subscript "c" indicates the mobility corrected for viscosity effect. Subscript "v" indicates viscosity measurement as described in section 2.2.5.

Table 2.6 Curve fitting statistics for propranolol with β-cyclodextrin.

1:1 binding	
μ_A*	1.573
μ_{ACD}*	0.87 ± 0.05
K (M^{-1})	$(1.1 \pm 0.2) \times 10^2$
R^2	0.9958
Fitting Equation	$y = (1.573 + \mu_{ACD}K[CD])/ (1 + K[CD])$
1:1 +1:2 binding	

μ_A*	1.573
μ_{ACD}*	1 ± 6
K_1 (M^{-1})	$(1 \pm 13) \times 10^2$
$\mu_{A(CD)2}$*	-0.1 ± 633
K_2 (M^{-1})	2 ± 900
R^2	0.9959
Fitting Equation	$y = 1.573 + \frac{(\mu_{ACD} - 1.573)K_1[CD] + (\mu_{A(CD)_2} - 1.573)K_1K_2[CD]^2}{1 + K_1[CD] + K_1K_2[CD]^2}$

* unit: 10^{-4} $cm^2/(Vs)$.

The secondary stability constant ($K_2 = 2$) is negligible compared with the 1:1 binding stability constant ($K_1 = 132$). Also, negative complex mobility is not possible for this positively charged solute complexed by a neutral cyclodextrin. Finally, very high uncertainties are associated with each parameter in the 1:2 binding result. Therefore, the 1:2 binding results are not reasonable, and so the statistical results again favor 1:1 binding.

The stability constant for propranolol-β-CD complex (K ~100) is higher than that for homatropine-β-CD complex (K ~ 40-60). However homatropine was baseline resolved whereas no resolution was observed for propranolol. Thus strong stability constants do not necessarily ensure chiral recognition. The inability of neutral β-cyclodextrin to resolve propranolol is consistent with observations by other groups. For instance, Wren and Rowe [21] only achieved slight separation of propranolol enantiomers under optimum β-CD conditions in the presence of 4 M urea.

2.4.1.2 TETRA-SULFATED β-CYCLODEXTRIN

2.4.1.2.1 HOMATROPINE

As discussed in Section 2.2.5 mesityl oxide partitioned into sulfated β-cyclodextrin. Therefore it could not be used to measure the EOF mobility. Instead D_2O was used for the 3-injection method to measure the EOF mobility in the neutral capillary at different sulfated β-cyclodextrin buffer concentrations (Section 2.2.5). Unfortunately, the measured EOF mobility fluctuated around and very close to zero. Both positive and negative values were observed. The longer the voltage was applied during Step C (Section 2.2.5 and Figure 2.3), the smaller was the absolute value of the measured EOF mobility. Therefore we concluded that the EOF is so small in this system that even the 3-injection method can hardly detect it.

Unfortunately for the systems that contain charged cyclodextrins, the addition of charged cyclodextrins introduced complicate effects within the buffer system as discussed in Section 2.3.2. Ignoring these effects can lead to misinterpretation of experimental results as we will show in Table 2.8. Cai and Vigh have also noticed similar problems and pointed out that the effective mobility of enantiomers can not be used directly to obtain meaningful complexation constant values [18]. Therefore these effects are corrected using two approaches: Limited Range and NDS Correction as described in detail in Section 2.3.2. Both correction methods are used because of the complexity of the system. By using both we are able to estimate the uncertainty of the statistical results. We will use the results obtained by these correction methods when charged cyclodextrins are used for complexation.

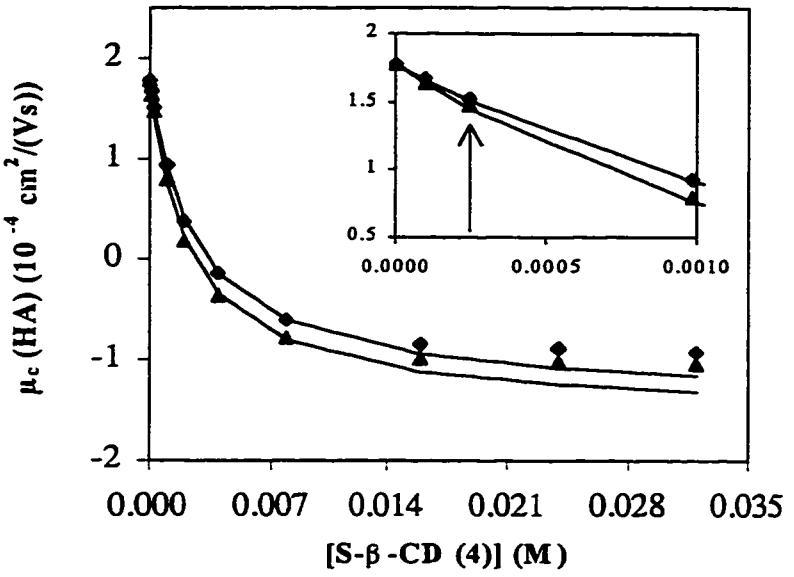

Figure 2.11 Homatropine-tetra-sulfated β-cyclodextrin complex mobility versus SCD concentration. (◆) — first eluting enantiomer; (▲) — second eluting enantiomer. Solid line is constructed using equation 1-14 and curve fitting results for 1:1 binding from Table 2.7 (Limited Range). Conditions: 200 mM MES buffer, pH = 4.6, V = 10 kV, T = 20 °C, λ =214 nm, capillary 37/30 cm. The arrow indicates where baseline resolution was achieved (≈ 0.25 mM).

Homatropine was much better separated with tetra-sulfated β-cyclodextrin than with the neutral β-cyclodextrin. Only 0.25 mM was needed to achieve baseline resolution. In contrast, ~ 8 mM neutral β-CD was needed. This is consistent with the general observation that negatively charged CDs provide higher resolution at lower CD concentrations [1][2].

Table 2.7 Homatropine (±) mobility measurements with tetra-sulfated β-CD[a].

[CD] (M)	t_1 (min)	t_2 (min)	$\mu_{a1} \times 10^4$ ($cm^2/(Vs)$)	$\mu_{a2} \times 10^4$ ($cm^2/(Vs)$)	t_V (min)	$\mu_{c1} \times 10^4$ ($cm^2/(Vs)$)	$\mu_{c2} \times 10^4$ ($cm^2/(Vs)$)
0	10.4	10.4	1.779	1.779	7.18	1.779	1.779
0.00005	10.67	10.69	1.734	1.731	7.1	1.715	1.711
0.0001	10.94	11.11	1.691	1.665	7.1	1.672	1.647
0.00025	12.1	12.53	1.529	1.476	7.17	1.527	1.474
0.001	19.82	23.4	0.933	0.791	7.21	0.937	0.794
0.002	48.48	98.71	0.382	0.187	7.23	0.384	0.189
0.004	133.15	51.29	-0.139	-0.361	7.18	-0.139	-0.361
0.008	31.6	24.01	-0.585	-0.771	7.34	-0.598	-0.788
0.016	23.44	19.87	-0.789	-0.931	7.62	-0.838	-0.988
0.024	22.33	19.55	-0.828	-0.946	7.71	-0.890	-1.016
0.032	22.57	20.09	-0.820	-0.921	8.1	-0.925	-1.039

a. Conditions are as in Figure 2.11. Meanings of symbols are as in Table 2.1.

The introduction of charged cyclodextrins into the buffer system brings up complex effects such as increased EOF caused by adsorption of cyclodextrin, and other ionic strength effects. As described in Section 2.3.2, these effects are corrected by Limited Range approach and NDS Correction approach. The Limited Range approach is aimed at diminishing the EOF effect on the determination of the complex mobility. Since the EOF becomes more severe at high cyclodextrin concentrations, the last two mobility data points were omitted when doing curve fitting. The NDS Correction approach uses a model solute, naphthalene disulfonic acid (NDS), to probe the total influence of the addition of the charged cyclodextrins on ionic mobilities. The anionic NDS is believed to not complex with negatively charged cyclodextrins (see Section 2.3.2). Thus, any change in its mobility reflects non-complexing effects in the separation system. All the solute

mobilities are corrected by the changes in the NDS mobility. The NDS corrected mobilities (μ_{NDS}) are then used for nonlinear curve fitting to obtain the NDS corrected statistical results.

The corrected results are presented in Table 2.9 and 2.10. The results of fitting the data in Table 2.7 directly to Equation 1-14 without correction are listed in Table 2.8 for comparison.

Table 2.8 Curve fitting statistics for homatropine with tetra-sulfated β-CD (without corrections).

1:1 binding		
	Peak 1	Peak 2
μ_A*	1.779	1.779
μ_{ACD} *	-1.17 ± 0.04	-1.28 ± 0.04
K (M^{-1})	$(4.5 \pm 0.2) \times 10^2$	$(5.4 \pm 0.3) \times 10^2$
R^2	0.9985	0.9977
Fitting Equation	$y = (1.779 + \mu_{ACD}K[CD])/ (1 + K[CD])$	
1:1 +1:2 binding		
	Peak 1	Peak 2
μ_A*	1.779	1.779
μ_{AC}*	-1.0 ± 0. 3	-1.3 ± 0.2
K_1 (M^{-1})	$(4.0 \pm 0.3) \times 10^2$	$(4.5 \pm 0.2) \times 10^2$
μ_{AC2}*	-1.0 ± 0.1	-1.03 ± 0.05
K_2 (M^{-1})	$(1.1 \pm 0.5) \times 10^2$	$(1.2 \pm 0.4) \times 10^2$
R^2	0.9999	0.9999
Fitting Equation	$y = 1.779 + \frac{(\mu_{AC} - 1.779)K_1[CD] + (\mu_{AC_2} - 1.779)K_1K_2[CD]^2}{1 + K_1[CD] + K_1K_2[CD]^2}$	

*unit: 10^{-4} $cm^2/(Vs)$.

In Table 2.8 both Equation 1-14 and 1-38 fit the data very well (R^2>0.997). The interesting feature is that the stability constants for the secondary complexation look very reasonable. Both of the secondary complexation stability constants (K_2) are about one quarter of the respective 1:1 binding constants (K_1). Thus they are not negligible. The two complex mobilities for 1:2 binding (-1.0 and –1.03) are statistically about the same as the 1:1 binding complex mobilities (-1.0 and –1.3). This is a bit surprising since the charge of the complex should have doubled. However considering the volume of the 1:2 complex is also about double that of the 1:1 complex, this result is not completely impossible. Thus, based on Table 2.8 there seems to be a good chance that homatropine undergoes 1:2 binding with tetra-sulfated β-cyclodextrin. However, as will be seen in Table 2.9 and 2.10, the correction for the sulfated cyclodextrin induced effects completely excludes the possibility of 1:2 binding.

The results corrected using Limited Range and NDS Correction are listed in Table 2.9 and 2.10 (see Section 2.3.2 for these correction procedures), respectively.

Table 2.9 Curve fitting statistics for homatropine with tetra-sulfated β-cyclodextrin (Limited Range approach).

1:1 BINDING		
	First Peak	Second Peak
μ_A*	1.779	1.779
μ_{AC}*	-1.39 ± 0.05	-1.53 ± 0.06
K (M^{-1})	$(3.8 \pm 0.2) \times 10^2$	$(4.5 \pm 0.2) \times 10^2$
R^2	0.9996	0.9994
Fitting Equation	$y = (1.779 + \mu_{AC}K[CD])/ (1 + K[CD])$	
1:1 +1:2 BINDING		
	First Peak	Second Peak
μ_A*	1.779	1.779
μ_{AC}*	-2 ± 5	-0.2 ± 1
K_1 (M^{-1})	$(3 \pm 4) \times 10^2$	$(6 \pm 4) \times 10^2$
μ_{AC2}*	$(-2 \pm 786) \times 10^1$	-1.3 ± 0.2
K_2 (M^{-1})	-2 ± 600	$(3 \pm 2) \times 10^2$
R^2	0.9998	0.9999
Fitting Equation	$y = 1.779 + \frac{(\mu_{AC} - 1.779)K_1[CD] + (\mu_{AC_2} - 1.779)K_1K_2[CD]^2}{1 + K_1[CD] + K_1K_2[CD]^2}$	

*unit: 10^{-4} $cm^2/(Vs)$.

Table 2.10 Curve fitting statistics for homatropine with tetra-sulfated β-cyclodextrin (NDS Correction approach).

1:1 BINDING		
	First Peak	Second Peak
μ_A*	1.779	1.779
μ_{AC}*	-1.08 ± 0.06	-1.17 ± 0.05
K (M^{-1})	$(4.4 \pm 0.4) \times 10^2$	$(5.6 \pm 0.4) \times 10^2$
R^2	0.9978	0.9984
Fitting Equation	$y = (1.779 + \mu_{AC}K[CD])/ (1 + K[CD])$	
1:1 +1:2 BINDING		
	First Peak	Second Peak
μ_A*	1.779	1.779
μ_{AC}*	-1 ± 5	-1.2 ± 0.2
K_1 (M^{-1})	$(5 \pm 9) \times 10^2$	$(5.4 \pm 1.0) \times 10^2$
μ_{AC2}*	0.3 ± 600	0 ± 2
K_2 (M^{-1})	-2 ± 700	1 ± 8
R^2	0.9979	0.9984
Fitting Equation	$y = 1.779 + \frac{(\mu_{AC}1.779)K_1[CD] + (\mu_{AC_2} - 1.779)K_1K_2[CD]^2}{1 + K_1[CD] + K_1K_2[CD]^2}$	

*unit: 10^{-4} $cm^2/(Vs)$.

In Table 2.9 and 2.10, both 1:1 and 1:2 binding fit the observed mobility behavior (R^2>0.997). The correlation coefficients (R^2) for 1:2 binding are even slightly better than those for 1:1 binding. However, the negative or very small secondary complexation stability constants (K_2) as well as the large uncertainties in K_2 excluded the possibility of 1:2 binding. The one exception is the K_2 for the second enantiomer when Limited Range

is used (Table 2.9). This binding constant has a reasonable value (300 M^{-1}). However, there is large error associated with all the parameters for this particular fit. In addition, the two enantiomers must have the same complexation behavior, and the statistical results for the first peak clearly exclude the possibility of 1:2 binding. The results from NDS Correction favor 1:1 binding as well. Therefore, it can be concluded that the apparent 1:2 binding from the results without correction (Table 2.8) is caused by artifacts. Thus, false results could be obtained without correcting for the effects of the addition of charged cyclodextrins. For this reason, all the statistical results quoted later are EOF or NDS corrected results for 1:1 binding only.

Limited Range only partly corrects the artifacts at high cyclodextrin concentrations. This correction approach can not compensate for any effects at low cyclodextrin concentrations. On the other hand, NDS Correction corrects over the whole cyclodextrin concentration range used. Thus, we believe that NDS Correction is a superior correction method. However, Limited Range results are also shown since we think that the difference between these two approaches is the maximum error of the determination of stability constants and complex mobilities. For example, the maximum error associated with stability constant determination for homatropine is estimated from the results in Table 2.9 and 2.10 as about 100 M^{-1}.

2.4.1.2.2 PROPRANOLOL

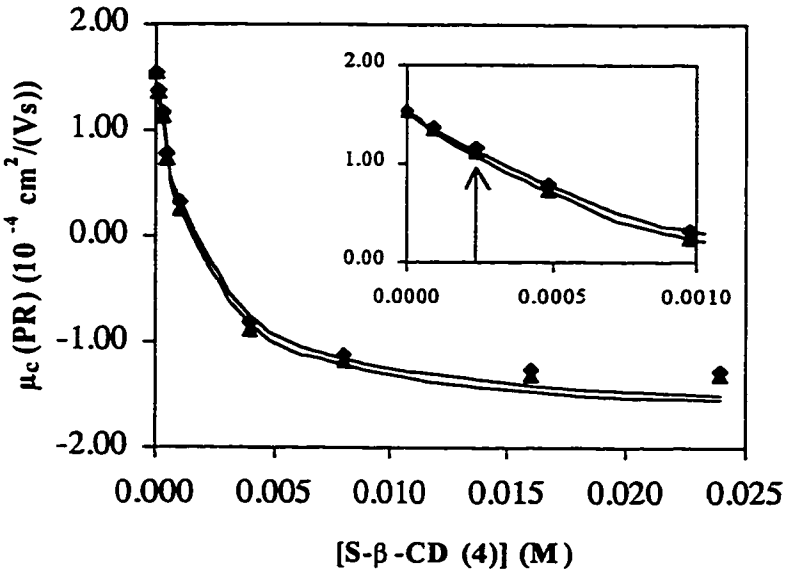

Figure 2.12 Corrected propranolol mobility as a function of tetra-sulfated β-CD concentration. (◆) — (S) enantiomer; (▲) — (R) enantiomer. Solid line is constructed using equation 1-14 and curve fitting results for 1:1 binding from Table 2.12. Conditions: 200 mM MES buffer, pH = 4.6, V = 10 kV, T = 20 °C, λ =214 nm, capillary 37/30 cm. The arrow indicates where baseline resolution was achieved (≈ 0.25 mM).

Baseline resolution for propranolol enantiomers was achieved with only 0.25 mM tetra-sulfated β-CD. Recall that in Section 2.4.1.1.2 no resolution was obtained when neutral β-CD was used.

Table 2.11 Propranolol mobility measurements with tetra-sulfated β-CD[a].

[CD] (M)	t_1 (min)	t_2 (min)	$\mu_{a1} \times 10^4$ ($cm^2/(Vs)$)	$\mu_{a2} \times 10^4$ ($cm^2/(Vs)$)	t_V (min)	$\mu_{c1} \times 10^4$ ($cm^2/(Vs)$)	$\mu_{c2} \times 10^4$ ($cm^2/(Vs)$)
0	12.05	12.05	1.535	1.535	7.35	1.535	1.535
0.0001	13.60	13.79	1.360	1.342	7.38	1.366	1.347
0.00025	15.98	16.49	1.158	1.122	7.40	1.166	1.130
0.0005	23.54	25.5	0.786	0.725	7.35	0.786	0.725
0.001	57.14	77.19	0.324	0.240	7.36	0.324	0.240
0.004	22.66	20.70	-0.816	-0.894	7.43	-0.825	-0.903
0.008	16.68	15.83	-1.109	-1.169	7.40	-1.117	-1.177
0.016	15.17	14.57	-1.220	-1.270	7.63	-1.266	-1.318
0.024	15.60	15.15	-1.186	-1.221	7.92	-1.278	-1.316

a. Conditions are as in Figure 2.12. Meanings of symbols are as in Table 2.1.

Table 2.12 Curve fitting statistics for propranolol with tetra-sulfated β-cyclodextrin (Limited Range).

1:1 BINDING		
	S-Propranolol	**R-Propranolol**
μ_A*	1.535	1.535
μ_{ACD}*	-1.72 ± 0.07	-1.74 ± 0.06
K (M^{-1})	(6.1 ± 0.4) × 10^2	(6.7 ± 0.4) × 10^2
R^2	0.9987	0.9988
Fitting Equation	$y = (1.535 + \mu_{ACD}K[CD])/ (1 + K[CD])$	
1:1 +1:2 BINDING		
	S-Propranolol	**R-Propranolol**

μ_A*	1.535	1.535
μ_{ACD}*	-2 ± 1	-2 ± 1
K_1 (M^{-1})	$(5 \pm 1) \times 10^2$	$(5 \pm 1) \times 10^2$
$\mu_{A(CD)2}$*	$(-0.2 \pm 2) \times 10^2$	5 ± 200
K_2 (M^{-1})	-4 ± 400	9 ± 300
R^2	0.9998	0.9998
Fitting Equation	$y = 1.535 + \frac{(\mu_{ACD} - 1.535)K_1[CD] + (\mu_{A(CD)_2} - 1.535)K_1K_2[CD]}{1 + K_1[CD] + K_1K_2[CD]^2}$	

*unit: 10^{-4} $cm^2/(Vs)$.

Table 2.13 Curve fitting statistics for the propranolol with tetra-sulfated β-CD (NDS Correction).

1:1 BINDING		
	S-Propranolol	**R-Propranolol**
μ_A*	1.535	1.535
μ_{ACD}*	-1.36 ± 0.02	-1.39 ± 0.02
K (M^{-1})	$(8.3 \pm 0.4) \times 10^2$	$(9.3 \pm 0.4) \times 10^2$
R^2	0.9995	0.9994
Fitting Equation	$y = (1.535 + \mu_{ACD}K[CD])/(1 + K[CD])$	
1:1 +1:2 BINDING		
	S-Propranolol	**R-Propranolol**
μ_A*	1.535	1.535
μ_{ACD}*	-1 ± 4	-1 ± 2
K_1 (M^{-1})	$(0.8 \pm 1) \times 10^3$	$(9 \pm 8) \times 10^2$
$\mu_{A(CD)2}$*	-0.001 ± 3000	1 ± 6000
K_2 (M^{-1})	-0.4 ± 1000	0.3 ± 800
R^2	0.9995	0.9994

Fitting Equation	$y = 1.535 + \frac{(\mu_{ACD} - 1.535)K_1[CD] + (\mu_{A(CD)_2} - 1.535)K_1K_2[CD]^2}{1 + K_1[CD] + K_1K_2[CD]^2}$

*unit: $10^{-4}\,cm^2/(Vs)$.

Again all approaches to fitting the mobility to Equations 1-14 (1:1 binding) or 1-38 (1:2 binding) fit very well (R^2>0.998). Therefore quality of R^2 cannot be used to validate or invalidate any of the models. Rather, we must look at the physical meanings of the parameters generated. The very small or even negative stability of 1:2 binding constants in Table 2.12 and 2.13 argue against the existence of 1:2 binding in the complexation of propranolol with tetra-sulfated β-cyclodextrin.

Note that there is a large increase in the stability constants from propranolol-β-cyclodextrin complexation to the same solute with tetra-sulfated β-cyclodextrin complexation (from ~ 100 M^{-1} in Table 2.6 to ~ 900 M^{-1} in Table 2.13). Even considering the relatively large uncertainty in determination of propranolol-tetra-sulfated β-cyclodextrin stability constant (about ± 300 M^{-1}), the increase is still significant. We found the same increase with homatropine (from ~ 60 M^{-1} in Table 2.4 to ~ 500 M^{-1} in Table 2.10 at an uncertainty of ± 100 M^{-1}). The neutral β-cyclodextrin interacts with solutes mainly through hydrophobic and secondary hydrogen bond interactions. In tetra-sulfated β-cyclodextrin only 4 out of 21 possible substitution sites are sulfated. As a result they would not alter the properties of the cyclodextrin cavity very much, and so the non-Coulombic interactions should remain the same. Thus this increase in stability

constant, i.e., the affinity toward the cyclodextrin, may be attributed to the attraction between the negative charges on the CD and the positive charge on the solute.

2.4.1.2.3 METHYL MANDELATE

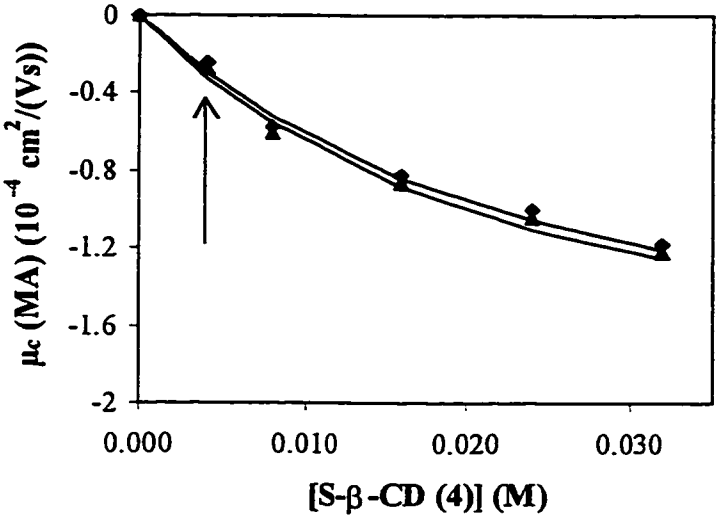

Figure 2.13 Corrected mobility of methyl mandelate as a function of tetra-sulfated β-CD concentration. (◆) — S-enantiomer; (▲) — R-enantiomer. Solid line is constructed using equation 1-14 and curve fitting results for 1:1 binding from Table 2.15. Conditions: 200 mM MES buffer, pH = 4.6, V = 7.3 kV, T = 20 °C, λ =214 nm, capillary 27/20 cm. The arrow indicates where baseline resolution was achieved (≈ 4 mM).

Table 2.14 Methyl mandelate mobility measurements with tetra-sulfated β-CD[a].

[CD] (M)	t_1 (min)	t_2 (min)	$\mu_{a1} \times 10^4$ ($cm^2/(Vs)$)	$\mu_{a2} \times 10^4$ ($cm^2/(Vs)$)	t_V (min)	$\mu_{c1} \times 10^4$ ($cm^2/(Vs)$)	$\mu_{c2} \times 10^4$ ($cm^2/(Vs)$)
0	—	—	0	0	2.9	0	0
0.004	53.19	48.27	-0.2318	-0.2554	3.04	-0.2430	-0.2677
0.008	23.64	22.23	-0.5215	-0.5546	3.16	-0.5683	-0.6043
0.016	16.62	15.79	-0.7418	-0.7808	3.23	-0.8262	-0.8696
0.024	14.23	13.62	-0.8664	-0.9052	3.34	-0.9978	-1.0425
0.032	12.42	11.98	-0.9927	-1.0291	3.44	-1.1775	-1.2207

a. Conditions are as in Figure 2.13. Meanings of symbols are as in Table 2.1.

Table 2.15 Curve fitting statistics for methyl mandelate with tetra-sulfated β-cyclodextrin (Limited Range).

1:1 binding		
	Peak 1 (S)	Peak 2 (R)
μ_A*	0	0
μ_{ACD}*	-2.2 ± 0.9	-2.2 ± 0.7
K (M^{-1})	(4 ± 2) × 10^1	(4 ± 2) × 10^1
R^2	0.9863	0.9878
Fitting Equation	$y = (0 + \mu_{ACD}K[CD])/ (1 + K[CD])$	
1:1 +1:2 BINDING		
	Peak 1 (S)	Peak 2 (R)
μ_A*	0	0
μ_{ACD}*	-1.25 ± 1 × 10^{-6}	1 ± 5
K_1 (M^{-1})	35 ± 4 × 10^{-6}	33 ± 0.0004
$\mu_{A(CD)2}$*	-1 ± 1	-1 ± 5
K_2 (M^{-1})	1017 ± 0.0007	1005 ± 0.0004
R^2	1	1

Fitting Equation	$y = 0 + \frac{(\mu_{ACD} - 0)K_1[CD] + (\mu_{A(CD)_2} - 0)K_1K_2[CD]^2}{1 + K_1[CD] + K_1K_2[CD]^2}$

*unit: 10^{-4} $cm^2/(Vs)$

Table 2.16 Curve fitting statistics for methyl mandelate with tetra-sulfated β-CD (NDS Correction).

1:1 binding		
	Peak 1 (S)	Peak 2 (R)
μ_A*	0	0
μ_{ACD} *	-3.5 ± 0.2	-3.1 ± 2
K (M^{-1})	(2 ± 1) × 10^1	(2 ± 1) × 10^1
R^2	0.9772	0.9804
Fitting Equation	$y = (0 + \mu_{ACD}K[CD])/(1 + K[CD])$	
1:1 +1:2 binding		
	Peak 1 (S)	Peak 2 (R)
μ_A*	0	0
μ_{ACD}*	1.6 ± 1	1.0 ± 0.4
K_1 (M^{-1})	(1 ± 1) × 10^1	(1 ± 1) × 10^1
$\mu_{A(CD)2}$*	-1.16 ± 0.03	-1.19 ± 0.03
K_2 (M^{-1})	(9 ± 7) × 10^2	(9 ± 5) × 10^2
R^2	0.99999	0.99999
Fitting Equation	$y = 0 + \frac{(\mu_{ACD} - 0)K_1[CD] + (\mu_{A(CD)_2} - 0)K_1K_2[CD]^2}{1 + K_1[CD] + K_1K_2[CD]^2}$	

*unit: 10^{-4} $cm^2/(Vs)$

Methyl mandelate is a neutral solute, and so it does not have any intrinsic mobility. Methyl mandelate acquires negative (anionic) mobility when it forms complexes with negatively charged cyclodextrins. Therefore, it can not have positive mobilities. The positive complex mobilities (μ_{ACD}) in Tables 2.15 and 2.16 exclude the possibility of 1:2 binding since methyl mandelate is neutral and the CD is negative . The complex mobilities for the S-enantiomer are negative in Table 2.13, but their magnitude is about the same as our experimental data with 0.032 M tetra-sulfated β-CD. However, from Figure 2.15 we know that the mobility curve has not plateaued out yet at that mobility, so this mobility can not be the complex mobility and 1:2 binding was excluded.

Since methyl mandelate is neutral, it would only be affected by the EOF effect but not by ionic effects introduced by charged cyclodextrin. Thus using a charged solute, such as NDS, to correct its mobilities may not be the best approach. This may be the reason why big errors are associated with the parameters obtained using NDS Correction.

No matter which correction method was used, the stability constants for methyl mandelate are much smaller than those for homatropine and propranolol when tetra-sulfated β-CD is used. The magnitude of the mandelate-tetra-sulfated β-CD complex stability constant is in the same order as those for homatropine and propranolol with neutral β-CD. In both cases there is no charge-to-charge interaction between the solutes and the cyclodextrin. Cai and Vigh also observed that negatively charged cyclodextrins complexes neutral analytes very weakly [18]. This confirmed the postulation in Section 2.4.1.2.2 that electrostatic attraction is responsible for the increase in the stability constants (K_1) for homatropine and propranolol complexation with tetra-sulfated β-CD.

2.4.1.3 THIRTEEN-SULFATED β-CYCLODEXTRIN

2.4.1.3.1 HOMATROPINE

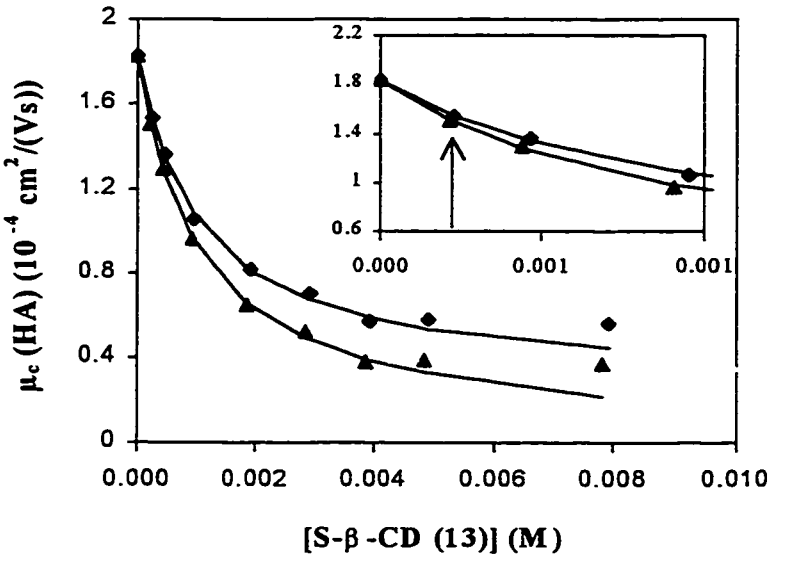

Figure 2.14 Corrected mobility of homatropine as a function of 13-sulfated β-CD concentration. (◆) — first eluting enantiomer; (▲) — second eluting enantiomer. Solid line is constructed using equation 1-14 and curve fitting results from Table 2.18. Conditions: 200 mM MES buffer, pH = 4.6, V = 7.3 kV, T = 20 °C, λ =214 nm, capillary 27/20 cm. The arrow indicates where baseline resolution was achieved (≈ 0.5mM).

The 13-sulfated β-CD also showed a higher chiral resolving ability than neutral β-CD. Homatropine enantiomers were baseline resolved at a 13-sulfated β-CD concentration of 0.5 mM in contrast to 8 mM with neutral β-CD. However more 13-

sulfated β-CD is needed (0.5 mM) to baseline resolve homatropine than tetra-sulfated β-CD (0.25 mM). This observation is contrary to the expectation that the higher the charge on the chiral selector, the better the resolution.

Table 2.17 Homatropine mobility measurements with 13-sulfated β-CD[a].

[CD] (M)	t_1 (min)	t_2 (min)	$\mu_{a1} \times 10^4$ ($cm^2/(Vs)$)	$\mu_{a2} \times 10^4$ ($cm^2/(Vs)$)	t_V (min)	$\mu_{c1} \times 10^4$ ($cm^2/(Vs)$)	$\mu_{c2} \times 10^4$ ($cm^2/(Vs)$)
0	6.74	6.74	1.829	1.829	2.87	1.829	1.829
0.00025	8.10	8.26	1.522	1.493	2.90	1.538	1.508
0.0005	9.27	9.72	1.330	1.268	2.93	1.358	1.295
0.001	12.15	13.38	1.015	0.921	3.00	1.061	0.963
0.002	15.74	19.98	0.783	0.617	3.00	0.819	0.645
0.003	18.5	24.87	0.666	0.496	3.02	0.701	0.522
0.004	22.69	34.37	0.543	0.359	3.01	0.570	0.376
0.005	21.76	32.13	0.567	0.384	2.92	0.576	0.390
0.006	20.16	29.06	0.612	0.424	2.94	0.626	0.435
0.008	22.75	34.5	0.542	0.357	3.00	0.566	0.374

a. Conditions are as in Figure 2.14. Meanings of symbols are as in Table 2.1.

Table 2.18 Curve fitting statistics for homatropine with 13-sulfated β-CD (Limited Range).

1:1 BINDING		
	1st Peak	2nd Peak
μ_A*	1.829	1.829
μ_{ACD}*	0.26 ± 0.03	0.01 ± 0.03
K (M^{-1})	$(9.6 \pm 0.6) \times 10^2$	$(9.8 \pm 0.5) \times 10^2$
R^2	0.9985	0.9991

Fitting Equation	$y = (1.829 + \mu_{ACD}K[CD])/(1 + K[CD])$	
1:1 +1:2 BINDING		
	1st Peak	**2nd Peak**
μ_A*	1.829	1.829
μ_{ACD}*	0.26 ± 0.04	0.01 ± 0.04
K_1 (M^{-1})	$(9.6 \pm 0.8) \times 10^2$	$(9.8 \pm 0.6) \times 10^2$
$\mu_{A(CD)2}$*	0 ± 0.8	0 ± 70
K_2 (M^{-1})	0 ± 0.8	0 ± 70
R^2	0.9985	0.9991
Fitting Equation	$y = 1.829 + \frac{(\mu_{ACD} - 1.829)K_1[CD] + (\mu_{A(CD)_2} - 1.829)K_1K_2[CD]^2}{1 + K_1[CD] + K_1K_2[CD]^2}$	

*unit: 10^{-4} $cm^2/(Vs)$.

Table 2.19 Curve fitting statistics for homatropine with 13-sulfated β-cyclodextrin (NDS Correction).

1:1 BINDING		
	1st Peak	**2nd Peak**
μ_A*	1.829	1.829
μ_{AC}*	0.68 ± 0.08	0.44 ± 0.08
K (M^{-1})	$(8 \pm 2) \times 10^2$	$(8 \pm 2) \times 10^2$
R^2	0.9776	0.9844
Fitting Equation	$y = (1.829 + \mu_{ACD}K[CD])/(1 + K[CD])$	
1:1 +1:2 BINDING		
	1st Peak	**2nd Peak**

μ_A*	1.829	1.829
μ_{AC}*	0.3 ± 1	-0.05 ± 0.4
K_1 (M^{-1})	$(5 \pm 3) \times 10^2$	$(5 \pm 2) \times 10^2$
μ_{AC2}*	-0.6 ± 1	0.2 ± 1.8
K_2 (M^{-1})	$(-2 \pm 11) \times 10^2$	$(-1 \pm 6) \times 10^2$
R^2	0.9806	0.9887
Fitting Equation	$y = 1.829 + \frac{(\mu_{ACD} - 1.829)K_1[CD] + (\mu_{A(CD)_2} - 1.829)K_1K_2[CD]^2}{1 + K_1[CD] + K_1K_2[CD]^2}$	

*unit: 10^{-4} $cm^2/(Vs)$.

Again, the zero and even negative stability constants (K_2) for 1:2 binding in Table 2.18 and 2.19 indicate that the 1:1 binding is dominant in the complexation of homatropine with 13-sulfated β-cyclodextrin. The correlation coefficient (R^2) is lower with the NDS Correction approach than with the Limited Range approach, indicating a poorer fitting. The stability constants obtained with NDS Correction are associated with large errors and are statistically equal. The complex mobilities (μ_{AC}) are statistically different regardless of whether the EOF or NDS Correction approach is used.

The stability constants increased from ~ 500 M^{-1} (Table 2.10) to ~ 800 M^{-1} (Table 2.19) when the substitution number of cyclodextrin changed from 4 to 13. Thirteen-sulfated cyclodextrin possesses more negative charges and so stronger electrostatic attraction can be expected. This may be the reason for the higher stability constants. Surprisingly the difference in free solute mobility and the complex mobility (the separation window) is smaller with 13-sulfated β-CD (~ 1.3 x 10^{-4} $cm^2/(Vs)$) than that

with tetra-sulfated β-CD (~ 2.8 x 10^{-4} $cm^2/(Vs)$) even though 13-sulfated β-CD is supposed to have a higher negative intrinsic mobility due to its higher charge.

The positive complex mobility (μ_{AC}) obtained for homatropine from non-linear curve fitting is surprising since the net charge of this complex is –12! However, similar phenomena were also observed by other laboratories. Cai et al. [22] found that the migration of some weak bases remains cathodic in low pH buffer at a –7-charged cyclodextrin concentration as high as 50 mM. Bunke and Jira [23] found no reversal of charge of negatively charged weak acids at high concentrations of a positively charged cyclodextrin. Tanaka et al have identified a group of positive solutes that keep cationic migration direction at high negatively charged cyclodextrin concentrations [5].

2.4.1.3.2 PROPRANOLOL

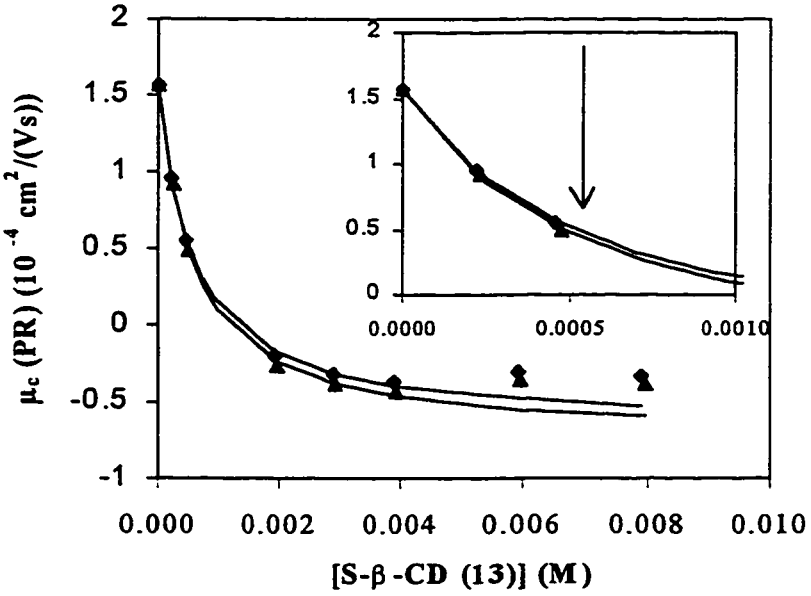

Figure 2.15 Corrected propranolol mobility as a function of 13-Sulfated β-CD concentration. (◆) — R-enantiomer; (▲) — S-enantiomer. Solid line is

constructed using equation 1-14 and curve fitting results from Table 2.21. Conditions: 200 mM MES buffer, pH = 4.6, V = 10 kV, T = 20 °C, λ =214 nm, capillary 37/30 cm. The arrow indicates where baseline resolution was achieved (≈ 0.5mM).

In contrast to homatropine, the observed mobility of propranolol reversed at high 13-sulfated β-CD concentrations. Baseline resolution of propranolol enantiomers was achieved at 0.5 mM 13-sulfated β-CD. This is comparable, but not superior, to tetra-sulfated β-CD (0.25 mM) and is much better than neutral β-CD where no separation was achieved.

Table 2.20 Propranolol (±) mobility measurements with 13-sulfated β-CD[a].

[CD] (M)	t_1 (min)	t_2 (min)	$\mu_{a1} \times 10^4$ ($cm^2/(Vs)$)	$\mu_{a2} \times 10^4$ ($cm^2/(Vs)$)	t_v (min)	$\mu_{c1} \times 10^4$ ($cm^2/(Vs)$)	$\mu_{c2} \times 10^4$ ($cm^2/(Vs)$)
0	11.77	11.77	1.572	1.572	6.92	1.572	1.572
0.00025	19.29	20.21	0.959	0.915	6.93	0.960	0.916
0.0005	33.67	37.9	0.549	0.488	6.94	0.550	0.489
0.002	97.03	70.69	-0.191	-0.262	6.98	-0.192	-0.264
0.003	59.41	48.55	-0.311	-0.381	7.00	-0.315	-0.385
0.004	51.66	43.44	-0.358	-0.426	7.03	-0.364	-0.432
0.006	63.73	53.06	-0.290	-0.349	7.08	-0.297	-0.357
0.008	58.8	50.45	-0.315	-0.367	7.13	-0.324	-0.378

a. Conditions are as in Figure 2.15. Meanings of symbols are as in Table 2.1.

Table 2.21 Curve fitting statistics for R-propranolol with 13-sulfated β-CD (Limited Range).

1:1 BINDING		
	R-Propranolol	**S-Propranolol**
μ_A*	1.572	1.572
μ_{ACD}*	-0.67 ± 0.03	-0.75 ± 0.03
K (M^{-1})	$(18.0 \pm 0.8) \times 10^2$	$(17.9 \pm 0.9) \times 10^2$
R^2	0.9993	0.9991
Fitting Equation	$y = (1.572 + \mu_{ACD}K[CD])/ (1 + K[CD])$	
1:1 +1:2 BINDING		
	R-Propranolol	**NDS Correction**
μ_A*	1.572	1.572
μ_{ACD}*	-0.67 ± 0.04	-0.75 ± 0.04
K_1 (M^{-1})	$(1.8 \pm 0.1) \times 10^3$	$(1.8 \pm 0.1) \times 10^3$
$\mu_{A(CD)2}$*	0 ± 100	0 ± 100
K_2 (M^{-1})	0 ± 100	0 ± 100
R^2	0.9993	0.9991
Fitting Equation	$y = 1.572 + \frac{(\mu_{ACD} - 1.572)K_1[CD] + (\mu_{A(CD)_2} - 1.572)K_1K_2[CD]^2}{1 + K_1[CD] + K_1K_2[CD]^2}$	

*unit: 10^{-4} $cm^2/(Vs)$.

Table 2.22 Curve fitting statistics for propranolol with 13-sulfated β-CD (NDS Correction).

1:1 BINDING		
	R-Propranolol	**S-Propranolol**
μ_A*	1.572	1.572
μ_{ACD}*	-0.17 ± 0.04	-0.23 ± 0.05
K (M^{-1})	(2.1 ± 0.2) × 10^3	(2.1 ± 0.2) × 10^3
R^2	0.9954	0.9951
Fitting Equation	$y = (1.572 + \mu_{ACD}K[CD])/ (1 + K[CD])$	
1:1 +1:2 BINDING		
	R-Propranolol	**S-Propranolol**
μ_A*	1.572	1.572
μ_{ACD}*	-0.3 ± 0.4	-0.4 ± 0.2
K_1 (M^{-1})	(1.8 ± 0.4) × 10^3	(1.8 ± 0.3) × 10^3
$\mu_{A(CD)2}$*	3 ± 400	3 ± 200
K_2 (M^{-1})	6 ± 800	8 ± 600
R^2	0.9968	0.9972
Fitting Equation	$y = 1.572 + \frac{(\mu_{ACD} - 1.572)K_1[CD] + (\mu_{A(CD)_2} - 1.572)K_1K_2[CD]^2}{1 + K_1[CD] + K_1K_2[CD]^2}$	

*unit: 10^{-4} $cm^2/(Vs)$.

The very small to zero 1:2 binding stability constants (K_2) in Table 2.21 and 2.22 again indicate that 1:1 binding is dominant in this case. Both Limited Range and NDS Correction fit the experimental data very well (R^2>0.995). However, the stability constants (K_1) are statistically equal using both approaches. Also there is not a big

difference between the complex mobilities (μ_{AC}) of individual enantiomers. So, no strong driving force for chiral separation can be seen here.

We observed very high stability constants for the complexes with 13-sulfated cyclodextrin, about 2000 M^{-1}. The stability constant (K_1) of 2000 M^{-1} is much higher than those observed with neutral cyclodextrin complexation or tetra-sulfated β-CD. Comparable high stability constant for complexation between neutral analyte and a negatively charged cyclodextrin, sulfobutylether-cyclodextrin was also observed by Surapaneni et al [24].

The separation window, defined as the difference between the free solute mobility (μ_A) and the complex mobility μ_{ACD}, is ~1.8×10^{-4} $cm^2/(Vs)$ with 13-sulfated β-CD, smaller than what obtained in propranolol-tetra-sulfated β-CD complexation (~ 3.3×10^{-4} $cm^2/(Vs)$). The same trend, i.e., a decrease in separation window, was also observed with homatropine (see Section 2.4.1.3.1).

Attempts were made to separate methyl mandelate using 13-sulfated β-CD. However, methyl mandelate was never observed at the detector located near the anode, even when high concentrations of 13-sulfated β-CD were used.

2.4.1.4 DIFFERENT BINDING BEHAVIOR OF β-CYCLODEXTRIN, TETRA-SULFATED β-CYCLODEXTRIN AND THIRTEEN-SULFATED β-CYCLODEXTRIN

A few points can be drawn from the mobility studies and statistical results described in Section 2.4.1:

1. The mobility behavior of all individual enantiomers in complexation processes follow Wren-Rowe model (Equation 1-14) as evidenced by the good correlation coefficients (R^2 is generally greater than 0.97).
2. The magnitude of the stability constants of homatropine and propranolol increases as the cyclodextrin changes from neutral β-CD to tetra-sulfated β-CD to 13-sulfated β-CD. With the same tetra-sulfated β-CD, higher complex stability constants are obtained with the positive solutes than with the neutral methyl mandelate. This indicates an involvement of charge-charge interaction in the complexation, as also pointed out by Tanaka et al [5]. It seems that the stronger the electrostatic attraction is between the solute and the cyclodextrin, the more stable is the complex formed.
3. Higher charge does not ensure greater resolving power of the chiral selector. For instance, tetra-sulfated cyclodextrin resolves enantiomers at a lower concentration (0.25 mM) than 13-sulfated cyclodextrin (0.5 mM). The separation window, defined as the difference between the free solute mobility and the complex mobility, is smaller with 13-sulfated β-CD than with tetra-sulfated β-CD. This yields the surprising observation that the tetra-sulfated β-CD provides superior separations to the 13-sulfated β-CD.

4. There may be different chiral recognition mechanisms operating with the tetra-sulfated cyclodextrin than the 13-sulfated cyclodextrin. In tetra-sulfated β-CD, the cavity of the β-CD has not been altered significantly, so solutes can still enter the cavity and have hydrophobic interaction with the cyclodextrin. But in 13-sulfated β-CD there can be 6 or even more sulfate groups substituted on the larger rim of the cyclodextrin, forming steric hindrance. Solutes may not be able to enter the cavity of 13-sulfated β-CD anymore. Charged solutes can still interact with the cyclodextrin through electrostatic attractions, but neutral solutes will not interact. This is supported by the fact methyl mandelate was resolved by tetra-sulfated cyclodextrin but was never observed in 13-sulfated cyclodextrin-containing buffers.

2.4.2 Δμ DEVIATION FROM WREN-ROWE OPTIMUM

As described in Section 1.4.1 the Wren-Rowe model predicts that the optimum separation can be achieved at a CD concentration given by

$$[CD] = \frac{1}{\sqrt{K_{ACD} K_{BCD}}} \qquad (1\text{-}18)$$

The accuracy of this prediction was tested using the data and fit parameters discussed in Section 2.4.1. In the following figures experimental data are shown as discrete points, the theoretical predictions based on 1:1 binding are shown as smooth solid lines, and the optimum cyclodextrin concentrations are indicated by an arrow.

2.4.2.1 HOMATROPINE

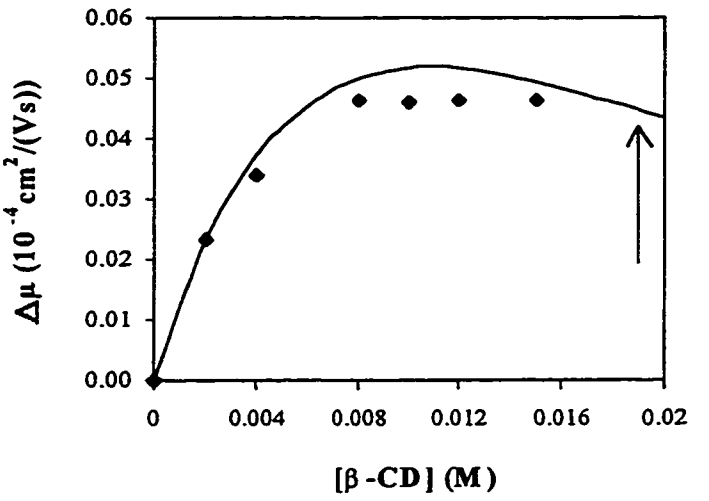

Figure 2.16 Homatropine- β-cyclodextrin complex mobility difference ($\Delta\mu$) versus CD concentration. Solid line is constructed using equation 1-16 and curve fitting results from Table 2-4. Conditions: 200 mM MES buffer, pH = 4.6, V = 10 kV, T = 20 °C, λ=214 nm, capillary 37/30 cm. The arrow indicates the optimum predicted by Wren-Rowe model.

From Table 2.4 we see that the two complex mobilities (μ_{ACD} and μ_{BCD}) of homatropine enantiomers are statistically equal, but there is small difference in the stability constants. Thus, this case agrees with Wren-Rowe model, which predicts that only the difference in stability constants determines the chiral resolution. According to this model, the difference in the apparent mobility of the two enantiomers ($\Delta\mu$) first increases as cyclodextrins are added. The separation then reaches a maximum at the cyclodextrin concentration predicted by Equation 1-18. After the maximum the separation decreases until it disappears at very high cyclodextrin concentrations.

However the optimum CD concentration predicted by the Wren-Rowe model is ≈ 19 mM. This concentration has exceeded the solubility of β-CD (≈ 15-16 mM). Thus could not be tested. On the other hand, the predicted $\Delta\mu$ line (the solid line) was obtained by substituting the statistical results in Table 2.4 into Equation 1-16. The predicted line agrees with experimental data well, but it shows an optimum at ~ 11 mM, lower than the concentration predicted by Wren-Rowe model. This discrepancy arises from the fact that when we plot the predicted line, we used different values for the two enantiomer complex mobilities (0.6 and 0.69 $cm^2/(Vs)$ in Table 2.4) whereas the complex mobilities are statistically equal. Thus the apparent difference in the complex mobilities makes the optimum come earlier than it should have.

An observation can be made from Figure 2.16 that the last few data points are almost plateaued, no significant increase in separation would be expected even if 19 mM were achievable. This is in agreement with Wren-Rowe prediction that the smaller is the stability constant, the higher is the concentration required to achieve optimum separation, and the broader is the optimum concentration range [21].

The statistical results for homatropine-tetra-sulfated β-CD (Table 2.10) show that the complex mobilities are statistically equal (-1.08 ± 0.06 vs. -1.17 ± 0.05) $\times 10^{-4}$ $cm^2/(Vs)$) but there is a slight difference in their stability constants (440 ± 40 vs. 560 ± 40) M^{-1}). The difference in stability constants is the main driving force in this enantiomeric separation. Therefore there is a good agreement between the Wren-Rowe prediction and experimental data (Figure 2.17). Again the predicted $\Delta\mu$ line (the solid line) agrees with experimental data very well, indicating the fit was accurate.

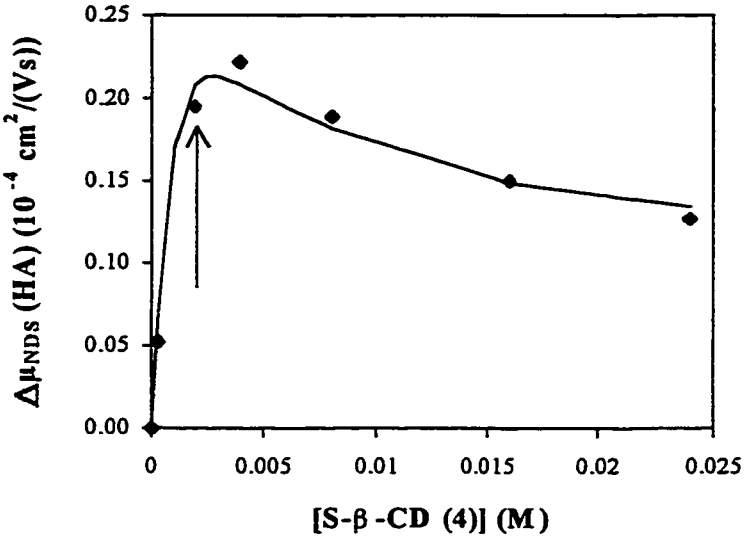

Figure 2.17 The difference in NDS corrected homatropine mobility as a function of tetra-sulfated β-cyclodextrin concentration. Solid line is constructed using equation 1-16 and curve fitting results from Table 2.10 (NDS Correction). Conditions: 200 mM MES buffer, pH = 4.6, V = 10 kV, T = 20 °C, λ = 214 nm, capillary 37/30 cm. The arrow indicates the optimum CD concentration predicted by Wren-Rowe model (≈ 2 mM).

In contrast to the case with tetra-sulfated β-CD the statistical results for homatropine with the 13-sulfated β-CD (Table 2.19) show that the stability constants for homatropine-13-sulfated β-CD complexes are statistically equal (both are 800 ± 200 M^{-1}) and the complex mobilities are different (0.68 ± 0.08 vs. 0.44 ± 0.08) × 10^{-4} cm^2/(Vs).) Now the difference in complex mobilities is the only driving force for the chiral separation, the stability constants play only a minor role, if any. Thus the Wren-Rowe

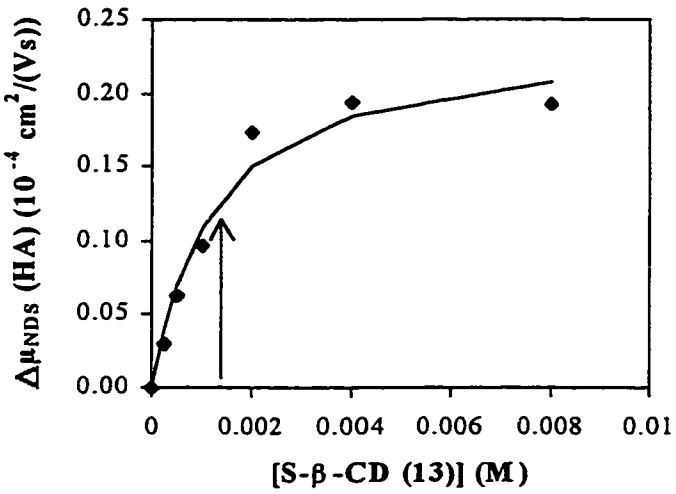

Figure 2.18 Homatropine- Sulfated β-cyclodextrin (S.D.= 13) complex mobility difference (Δμ) versus CD concentration. Solid line is constructed using equation 1-16 and curve fitting results from Table 2.17 (NDS Correction). Conditions: 200 mM MES buffer, pH = 4.6, V = 10 kV, T = 20 °C, λ = 214 nm, capillary 37/30 cm. The arrow indicates the optimum CD concentration predicted by Wren-Rowe model (≈ 1.3 mM).

prediction is far off in this case (Figure 2.18). The predicted line does not agree with experimental data very well at middle to high cyclodextrin concentrations. This may be due to the large uncertainty in determining the stability constants of the homatropine-13-sulfated β-CD complexes (Table 2.19).

2.4.2.2 PROPRANOLOL

No resolution of propranolol enantiomers were observed with neutral β-CD so discussion of the separation behavior of propranolol will be limited to that with charged cyclodextrins.

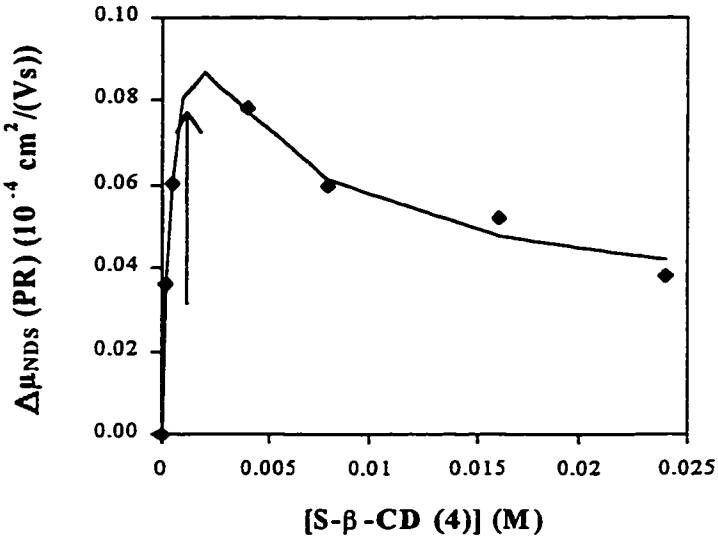

Figure 2.19 Propranolol- Sulfated β-cyclodextrin (S.D.= 4) complex mobility difference (Δμ) versus tetra-sulfated β-CD concentration. Solid line is constructed using equation 1-14 and curve fitting results from Table 2.13 (NDS Correction). Conditions: 200 mM MES buffer, pH = 4.6, V = 10 kV, T = 20 °C, λ = 214 nm, capillary 37/30 cm. The arrow indicates the optimum CD concentration predicted by Wren-Rowe model (≈1 mM).

Very similar to case of homatropine-tetra-sulfated β-CD complexation, the statistical results for propranolol-tetra--sulfated β-CD complexation clearly show that the

complex mobilities are equal (-1.36 ± 0.02 vs. –1.39 ± 0.02) × 10^{-4} $cm^2/(Vs)$) whereas the stability constants are different (830 ± 40 vs. 930 ± 40) M^{-1}). Therefore a very good agreement is seen between experimental data and Wren-Rowe prediction in Figure 2.19. There is also an excellent agreement between experimental data and the predicted line. This is an indication of the accuracy of the curve fitting.

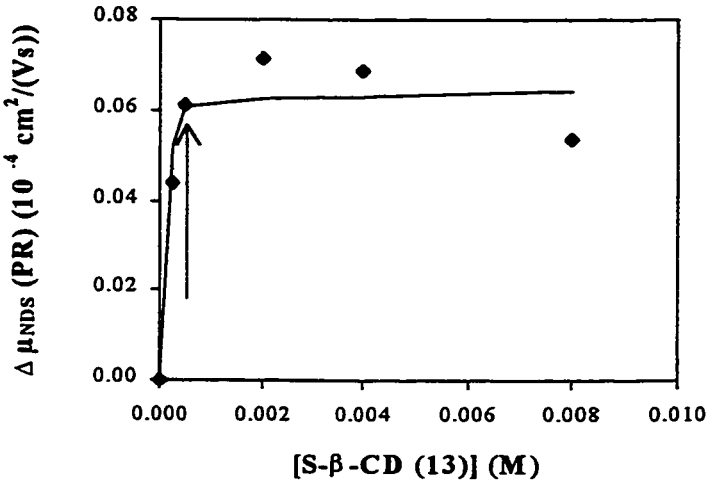

Figure 2.20 Propranolol-Sulfated β-cyclodextrin (S.D.= 13) complex mobility difference (Δμ) versus CD concentration. Solid line is constructed using equation 1-16 and curve fitting results from Table 2.22 (NDS Correction). Conditions: 200 mM MES buffer, pH = 4.6, V = 10 kV, T = 20 °C, λ = 214 nm, capillary 37/30 cm. The arrow indicates the optimum CD concentration predicted by Wren-Rowe model (≈ 0.5 mM).

Comparing the statistics in Table 2.22, neither stability constants (2100 ± 200 vs. 2200 ± 200 M^{-1}) nor complex mobilities (-0.17 ± 0.04 vs. –0.23 ± 0.05) × 10^{-4} $cm^2/(Vs)$)

are statistically different from each other for propranolol with 13-sulfated β-cyclodextrin. This makes it difficult to accurately predict optimum separation conditions by Equation 1-16. As a result the predicted mobility difference (solid line) does not agree very well with experimental data. On the other hand, Wren-Rowe prediction is not too bad in this case, $\Delta\mu$ at the predicted condition is only 20% less than the true optimum.

2.4.2.3 METHYL MANDELATE

Methyl mandelate was only separated by tetra-sulfated β-CD. Neutral β-CD can not be used to separate neutral compounds since neither of the solute or the chiral selector has any mobility. The complex of neutral solute with β-CD has zero mobility as well. So there is no separation window at all. Attempts were also made to separate methyl mandelate with 13-sulfated β-CD. However methyl mandelate was never detected in 13-sulfated β-CD buffer. Therefore, only the data with tetra-sulfated β-CD is shown here.

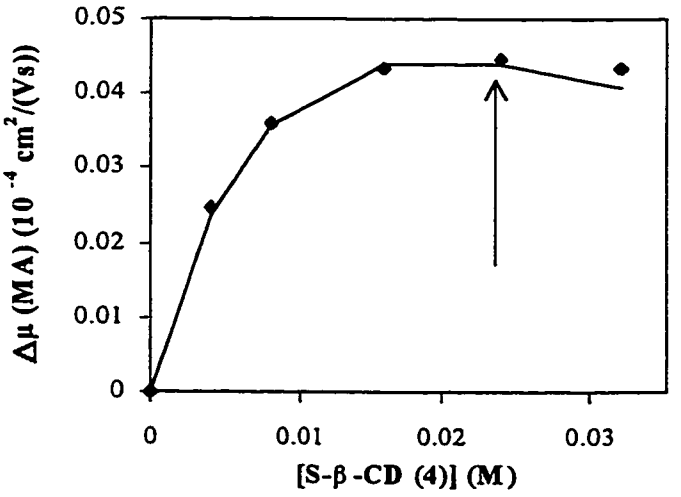

Figure 2.21 The difference in EOF corrected methyl mandelate mobility as a function of tetra-sulfated β-cyclodextrin concentration. Solid line is constructed

using equation 1-16 and curve fitting results from Table 2.15 (Limited Range). Conditions: 200 mM MES buffer, pH = 4.6, V = 10 kV, T = 20 °C, λ = 214, capillary 37/30 cm. The arrow indicates the optimum CD concentration predicted by Wren-Rowe model ($\approx$ 23 mM).

Since NDS Correction is a method that more suitable for charged solutes, Limited Range is used here for methyl mandelate.

Methyl mandelate enantiomers have equal complex mobility (-2.2 $\pm$ 0.9 vs. –2.2 $\pm$ 0.7) $\times$ 10^{-4} $cm^2/(Vs)$) and slightly different stability constants (39 $\pm$ 23 vs. 43 $\pm$ 23) M^{-1}. The large errors in stability constants and complex mobilities may arise from a lack of data points. Since Limited Range approach omits the last two data points, there were only four mobility data points available for curve fitting, this introduced large uncertainty in the fitting results. In this case Wren-Rowe model works very well again because the driving force for the enantiomeric separation is the difference in stability constants alone.

2.4.2.4 SUMMARY OF DELTA MOBILITY BEHAVIORS WITH DIFFERENT CYCLODEXTRINS

1. Charged cyclodextrins have higher resolving power than native cyclodextrin. For instance, propranolol was not resolved by β-cyclodextrin, but was resolved by both type of sulfated β-cyclodextrins. The separation $\Delta\mu$ achieved with charged cyclodextrins is higher than that with neutral cyclodextrin. For instance the separation between homatropine enantiomers

with charged cyclodextrins was over 0.2×10^{-4} $cm^2/(Vs)$ whereas it was less than 0.05×10^{-4} $cm^2/(Vs)$ with neutral β-cyclodextrin.

2. The separation behavior of solutes in neutral and tetra-sulfated β-cyclodextrins follow the Wren-Rowe predictions. That is, the separation mainly depends on differences in the stability constants. However with 13-sulfated β-cyclodextrin the separation depends on the difference in complex mobilities. As a result the Wren-Rowe model does not work very well in 13-sulfated β-cyclodextrin systems.
3. Separation does not only depend on the cyclodextrin type, but is also solute dependent. For example, the optimum separation achieved for homatropine was over 0.2×10^{-4} $cm^2/(Vs)$ whereas for propranolol the best separation was less than 0.1×10^{-4} $cm^2/(Vs)$.
4. For the same solute, 13-sulfated β-cyclodextrin achieves comparable but slightly less separation than tetra-sulfated β-cyclodextrin. They both give 0.2 x 10^{-4} $cm^2/(Vs)$ for homatropine and about 0.09 x 10^{-4} $cm^2/(Vs)$ for propranolol. So the higher negative charge on 13-sulfated β-cyclodextrin does not ensure better resolving power.

2.4.3 HIGH CONCENTRATION MOBILITY MATCHING EFFECT OF SULFATED-β-CYCLODEXTRIN

The Wren–Rowe model only refers to the separation ($\Delta\mu$), i.e., the separation of the peak centers, not to resolution (R). In reality electrodispersion severely broadens

peaks at the Wren–Rowe optimum, lowering the resolution of enantiomer peaks. Taking homatropine-tetra-sulfated β-cyclodextrin complexation as model system, it is shown in Figure 2.18 that the Wren-Rowe optimum (~ 2 mM) is not the point that has the highest resolution. In addition, in this case at Wren-Rowe optimum the net mobility of the enantiomers is close to zero. That is, very long separation times are needed , making

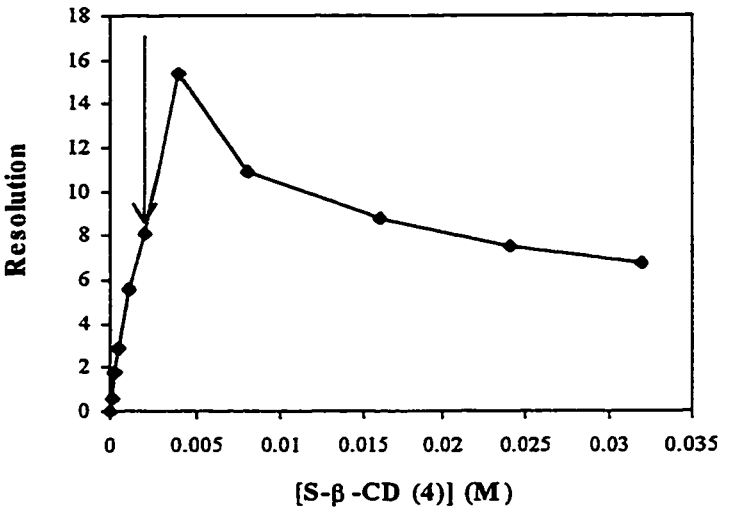

Figure 2.22 Resolution of homatropine enantiomers vs. SCD (4). Arrow indicates the optimum predicted by Wren-Rowe model. Conditions: 200 mM MES buffer, pH = 4.6, V = 10 kV, T = 20 °C, λ =214 nm, capillary 37/30 cm.

the ratio of resolution-to-time very small. This is shown in Fig. 2.23 as the local minimum. Due to the severe bandbroadening caused by electrodispersion the peak efficiency is at the lowest point (see Figure 2.24) near the Wren-Rowe optimum. Therefore it is of critical importance to minimize electrodispersion to obtain high efficiency in enantiomeric separations.

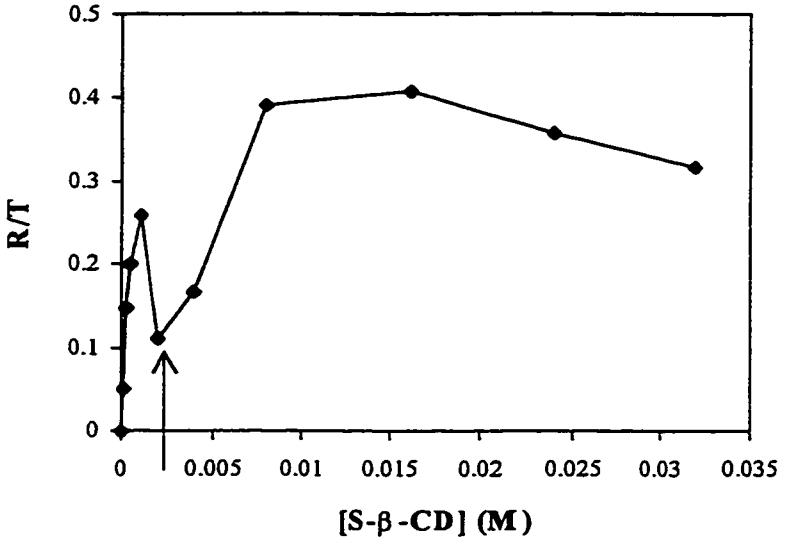

Figure 2.23 R/T as a function of SCD (4) concentration. Conditions: 200 mM MES buffer, pH = 4.6, V = 10 kV, T = 20 °C, λ =214 nm, capillary 37/30 cm.

Vigh et al have pointed out that using mobility matching buffer component is an effective way to minimize electrodispersion [25]. They also have shown that Jeffamine 900 is a good mobility matching ion for homatropine. Thus Jeffamine 900 was adopted in this work.

The apparent mobility of homatropine changes as the cyclodextrin concentration increases (Figure 2.11 and Table 2.7). It was found that the peak efficiency decreases as soon as cyclodextrin was added into the buffer system as shown in Figure 2.24 B. Under these conditions the peak starts fronting. At low CD concentrations the net homatropine mobility is positive, and so Jeffamine 900 provides mobility matching under these

A.

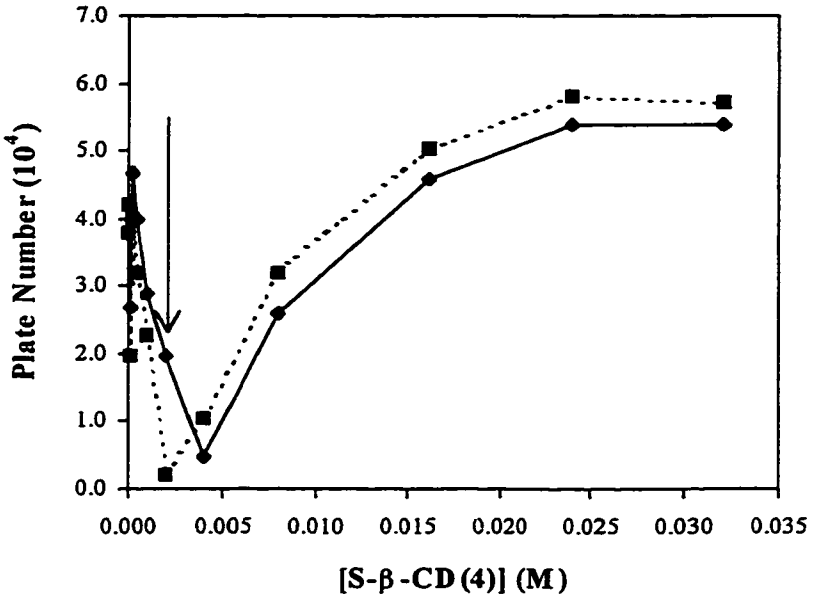

B

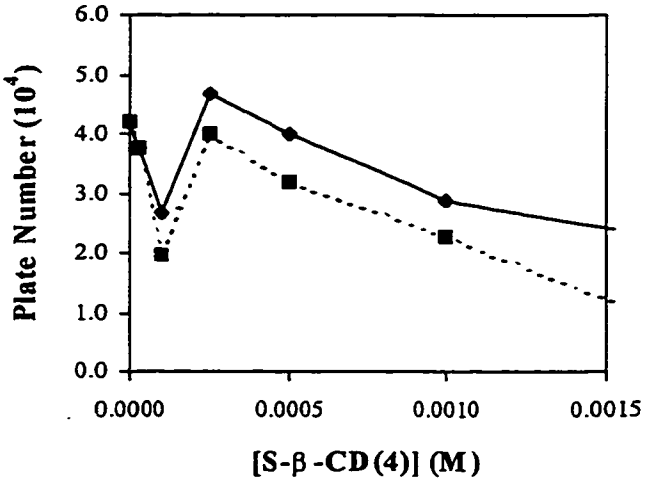

Figure 2.24 Peak efficiency as a function of tetra-sulfated CD concentration. The arrow indicates the optimum concentration predicted by Wren-Rowe model. A is the plate number versus tetra-sulfated β-cyclodextrin concentration over the concentration range of 0 to 32 mM. B is the enlarged plot at low concentrations

up to 1.5 mM. The solid line is the first enantiomer of homatropine and the dotted line is the second enantiomer of homatropine.

conditions. At a cyclodextrin concentration of 0.25 mM, the net mobility of the enantiomer is the same as Jeffamine 900, and the homatropine peak is symmetrical. At this time the peaks achieved the highest efficiency in the positive net mobility portion. When cyclodextrin concentration was increased higher than 0.25 mM, the peak efficiency starts dropping again. Therefore the mobility matching with Jeffamine 900 is only effective for a very narrow concentration range.

If we look at the high CD concentration part in Figure 2.24 A, the efficiency is much higher than what it was at low CD concentrations. At high CD concentrations, the net homatropine mobility is negative. Therefore Jeffamine 900 can not provide mobility matching anymore. The sulfated β-CD is the only anion that exists in the buffer in large quantity. Furthermore, since the sulfated CD is much larger than the solute, the complex mobility should be defined by the sulfated CD. Thus the sulfated CD will have a similar mobility as the solute-CD complex mobility. Under these conditions the sulfated β-CD itself provides mobility matching. Not only does this provide very high efficiency, but also the resolution and efficiency remains relatively constant over a wide range (see Fig. 2.23 and 2.24A), making the optimization of separation conditions easy.

2.4.4 SELECTIVITY CHANGING BETWEEN TETRA- AND 13-SULFATED β-CYCLODEXTRINS

Figure 2.25 shows the mobility of propranolol enantiomers as a function of the concentration of both tetra- and 13-sulfated β-cyclodextrins. The solid markers represent S-propranolol and hollow markers represent R-propranolol. The top two mobility lines are obtained with 13-sulfated β-cyclodextrins and the bottom two mobility lines are obtained with tetra-sulfated β-cyclodextrins.

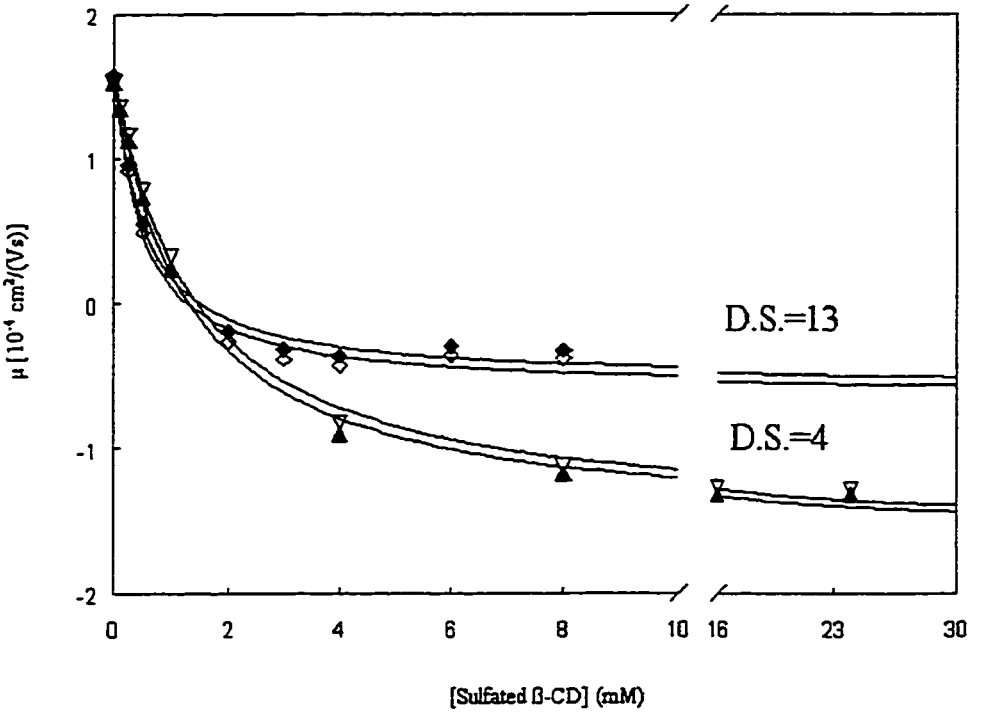

Figure 2.25 Propranolol mobility versus sulfated β-CD concentration. Solid symbols represent S-enantiomer of propranolol, hollow marks for R-enantiomers.

It can be seen in Figure 2.25 that, when tetra-sulfated β-cyclodextrin was used, the R enantiomer complexed with this CD stronger than the S enantiomer, shown as a more negative mobility. Whereas S enantiomer has a stronger affinity for 13-sulfated β-cyclodextrin than R enantiomer and has a more negative mobility when 13-sulfated β-cyclodextrin was used. This reversal of migration order indicates a different selectivity between tetra-sulfated cyclodextrin and 13-sulfated cyclodextrin. This proves again the chiral separation mechanisms of these two cyclodextrins are different.

Therefore there are two ways of controlling selectivity in sulfated β-cyclodextrin mediated CE separations. The first one is to take advantage of the intrinsic charge on these cyclodextrins. When oppositely charged solutes are to be separated, the cyclodextrins can cause a reversal of the migration direction as well as the migration order. For instance, the apparent mobility of homatropine is positive at low tetra-sulfated β-cyclodextrin concentrations. Thus the one enantiomer that has stronger affinity for the charged CD will be retarded more than the one that does not complex as strongly, and will come out later than the other one. However at high tetra-sulfated β-cyclodextrin concentrations the apparent mobility of the enantiomers are negative. The one that has higher affinity for the charged CD will have higher negative mobility and come out of the anode end of capillary faster than the other one. Therefore, there is a reversal in migration order at low and high charged cyclodextrin concentrations.

Another approach to switch the migration order, i.e. the selectivity, is to use a different cyclodextrin with similar substitution groups but different substitution numbers as we have seen with tetra- and 13-sulfated β-cyclodextrins.

The ability to control the selectivity of enantiomers is important especially when trace enantiomeric impurity is to be tested, where the trace component should always come out first to avoid the interference from the tailing of the large peak.

Unfortunately enantiomerically pure homatropine is not available. Thus, the same comparison can not be performed on homatropine.

2.5 SUMMARY

A systematic study of enantiomeric separations with tetra- and 13-sulfated β-cyclodextrin was performed. The electrostatic interaction contributes to the stability of the complex as it was found that the stability constants increased as the charge on the cyclodextrin increased. However, higher charges on cyclodextrins do not ensure better enantio-resolving power. The Wren-Rowe model was found to be effective at predicting optimal CD-concentrations for tetra-sulfated β-CD but not for the 13-sulfated β-CD. Sulfated β-CD provides mobility matching at high concentrations, minimizing the electrodispersion. The selectivity of tetra- and 13-sulfated cyclodextrins was found different and can be used to reverse the migration order of enantiomers, which can be useful in testing the purity of enantiomerically pure substances.

2.6 REFERENCES

1. Chankvetadze, B.; Endresz, G.; Blaschke, G. *Chem. Soc. Rev.* 1996, 142, 141.
2. Tait, R. J.; Thompson, D. O.; Stella, V. J.; Stobaugh, J. F. *Anal. Chem.* 1994, 66, 4013.

3. Terabe, S.; Ozaki, H.; Otsuka, K.; Ando, T. *J. Chromatogr.* 1985, 332, 211.

4. Stalcup, A. M.; Gahm, K. H. *Anal. Chem.* 1996, 68, 1360-1368.

5. Tanaka, Y.; Yanagawa, M.; Terabe, S. *J. High Resol. Chromatogr.* 1996, 19, 421.

6. Pak, C.; Marriott, P. J.; Carpenter, P. D.; Amiet, R. G. *J. Chromatogr. A*, 1998, 793, 357.

7. Rawjee, Y. Y.; Williams, R. L.; Vigh, Gy. *J. Chromatogr. A*, 1993, 652, 233.

8. *CRC Handbook of Chemistry and Physics*, 76th Edition, CRC press, New York, 1995-1996.

9. Florey, K. (Editor), "*Analytical Profiles of Drug Substances*", Vol. 16, Academic Press, London, 1987, p. 245.

10. Valtcheva, L.; Mohammad, J.; Pettersson, G.; Hjerten, S. *J. Chromatogr.* 1993, 638, 263-267.

11. Penn, S. G.; Bergstrom, E. T.; Knights, I.; Liu, G.; Ruddick, A.; Goodall, D. M. *J. Phys. Chem.* 1995, 99, 3875.

12. Cantwell, F. F. *"Analytical Separations: Gas Chromatography, Liquid Chromatography, Supercritical Fluid Chromatography, and Electrophoresis"*, Coursenotes, 1992.

13. Lucy, C. A.; Brown, R.; Yeung, K. K.-C. *J. Chromatogr. A* 1996, 745, 9-15.

14. Williams, B. A.; Vigh, Gy. *Anal. Chem.* 1996, 68, 1174-1180.

15. *Aldrich Catalogue*, Aldrich Chemical Company, 1994.

16. Budavari, S., Editor, *The Merck Index*, 11th Edition, Merck & Co., Inc., Rahway, 1989.

17. Penn, S. G.; Bergström, E. T.; Goodall, D. M. *Anal. Chem.* 1994, 66, 2866-2873.

18. Cai, H.; Vigh, Gy. *J. Microcolumn Separations* 1998, 10(3), 293.

20. Bowser, M. T.; Chen, D. D. Y. *Anal. Chem.* 1998, 70, 3261.

21. Wren, S. A. C.; Rowe, R. C. *J. Chromatogr.* 1992, 603, 235-241.

22. Cai, H.; Nguyen, T. V.; Vigh, Gy. *Anal. Chem.* 1998, 70, 580-589.

23. Bunke, A.; Jira, T. *J. Chromatogr.* 1998, 798, 275-280.

24. Surapaneni, S.; Ruterbories, K.; Lindstrom, T. *J. Chromatogr. A*, 1997, 761, 249-257.

25. Williams, R. L.; Childs, B.; Dose, E. V.; Guiochon, G.; Vigh, Gy. *J. Chromatogr. A*, 1997, 781, 107.

CHAPTER 3 MOBILITY CONSERVATION MODEL

3.1 INTRODUCTION

It is generally accepted that when a cyclodextrin and a solute form a host-guest inclusion complex in a separation system, the charge of this complex will be the sum of the cyclodextrin charge and the solute charge. This complex will then migrate in an electric field at a mobility (μ_{cpx}) determined by the net charge and the volume of the complex as expressed by equation (3.1):

$$\mu_{cpx} \propto \frac{Z_{solute} + Z_{CD}}{V^{constant}} \qquad (3.1)$$

where Z_{solute} and Z_{CD} are the absolute charges on the solute and derivatized cyclodextrin respectively, and V is the volume of the complex.

However, as observed in Figure 2.14 the mobility of the 13-sulfated cyclodextrin-homatropine complex plateaued out at a positive mobility, even though the net charge of the complex should be –12! This observation challenges the idea dictated by equation 3.1. This counter-intuitive observation prompted us to pursue a further understanding of the complex mobility. From the data obtained for different solutes with tetra- and 13-sulfated β-cyclodextrins in our laboratory a correlation between the free solute mobility and the complex mobility was found. Similar phenomena were also observed by other laboratories. Based on these results a mobility conservation model is proposed.

3.2 EXPERIMENTAL

3.2.1 APPARATUS AND PROCEDURES

All the experiments were carried out on a Beckman P/ACE 2100 system capillary electrophoresis instrument (Fullerton, CA, USA). The capillary is a polyacrylamide coated neutral capillary (eCap, Beckman) with an internal diameter of 50 μm and total length of 37 cm. The detection window was 7 cm from the end of capillary. Absorbance of solutes was measured at 214 nm. A voltage of 10 kV was used for all the mobility measurements. This voltage was chosen to be the highest concentration within the linear range of the Ohm's law (see Chapter 1, section 1.2.2.4). The capillary cartridge was temperature controlled at 20 °C.

3.2.2 REAGENTS

Sulfated β-cyclodextrins (SCD) with the degree of substitution (D.S.) of 4 and 13 were purchased from Cerestar (Hammond, IN, USA). Buffer components MES (morpholino-ethanesulfonic acid monohydrate) and Jeffamine 900 (poly(propylene glycol-b-ethylene glycol-b-propylene glycol) bis(2-aminopropyl ether)) were obtained from Sigma-Aldrich Canada Ltd. (Oakville, Ontario). Mesityl oxide (98%) was used as the neutral EOF marker, and was obtained from Aldrich. 1,5-Naphthalenedisulfonic acid disodium salt (NDS) (95%) homatropine (±), propranolol (DL) (99%) and (R, +) (98%), 4-(aminomethyl)benzene sulfonamide, benzylamine, benzyltrimethylammonium, diphenhydramine, histidine, imidazole, 1-methylimidazole, 2-methylimidazole, 4-methylimidazole, 2-ethylimidazole, 2-propylimidazole, and 1-butylimidazole were

obtained from Sigma-Aldrich Canada as well. All chemical reagents were used as received.

The chemical structures and pKa's of analytes are as follows (pKa values are obtained from reference [1] except where specified):

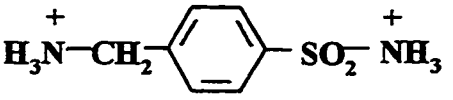

4-(aminomethyl) benzene sulfonamide (AB), $pK_{a1} = 8.52$, $pK_{a2} = 10.08$.

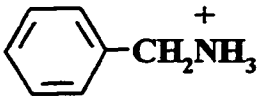

Benzylamine (BA), $pK_a = 9.33$

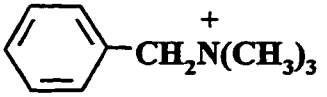

benzyltrimethylammonium (BT), permanently monocharged.

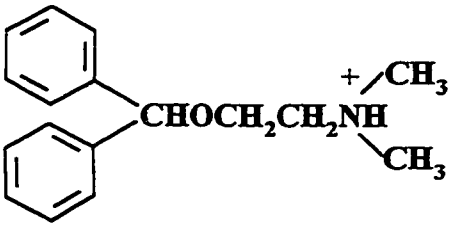

Diphenhydramine (DP), $pK_a = 9.1$.

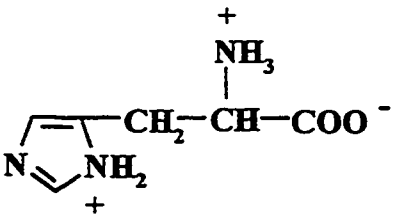

Histidine (HI), $pK_{a1} = 1.82$, $pK_{a2} = 6.0$, $pK_{a3} = 9.17$ [2].

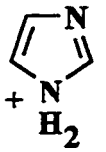

Imidazole (IM), $pK_a = 6.95$.

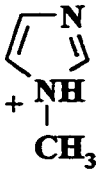

1-methylimidazole (1-MI), $pK_a = 6.95$.

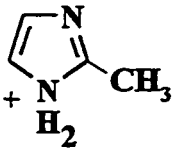

2-methylimidazole (2-MI), $pK_a = 7.85$.

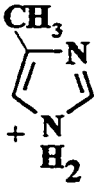

4-methylimidazole (4-MI), $pK_a = 7.52$.

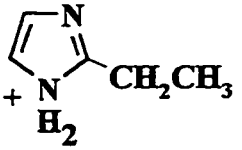

2-ethylimidazole (2-EI), $pK_a = 8.00$.

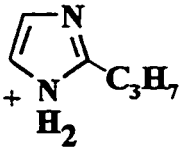

2-propylimidazole (2-PI), $pK_a \approx 8.0$ (estimated from 2-ethylimidazole).

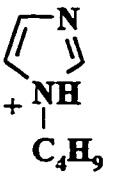

4-butylimidazole (4-BI), $pK_a \approx 7.5$ (estimated from 4-methylimidazole).

Figure 3.1 Chemical structures and pKa's of analytes.

3.2.3 PROCEDURES

A 400 mM MES stock solution was first made. This stock solution was then used to make the background electrolyte solution as follows: first, the appropriate amount of sulfated β-cyclodextrin (SCD) was weighed out and transferred into a 100 ml volumetric flask; then 50 ml of the 400 ml MES stock solution was added to this volumetric flask, and the volume was brought up to mark with distilled deionized water (Barnstead type D4700 NANOpure deionization system); finally, the pH of all solutions was adjusted to 4.6 with Jeffamine 900 or sulfuric acid (6M) and filtered through 0.45 μm syringe filters (Nalge Company, NY, USA).

All analyte solutions were made up in 200 mM MES buffer solution and adjusted to pH 4.6 using Jeffamine 900. A voltage of 10 kV was applied for all separations. A 3 s hydrodynamic injection (0.5 p.s.i.; 1 p.s.i. = 6894.76 Pa) was used to introduce samples onto the capillary. The capillary cartridge was maintained at 20 °C all the time. At the start of each day the capillary was flushed with deionized water for 10 min under high pressure (20 p.s.i.). The EOF in this neutral capillary was monitored using the 3-injection method (see section 2.2.5) to ensure the polyacrylamide coating was intact as indicated by small constant EOF values from day to day. After each run, the capillary was rinsed

(20 p.s.i.) with deionized water for 1.5 min and then with running buffer for 1.5 min. At the end of a day, the capillary was rinsed with 0.1 M HCl for 5 min, followed by deionized water for 10 min. Then the capillary was placed in a cassette box with both ends dipped in vials of deionized water and stored in a refrigerator in an upright position. Alternatively when this capillary is to be used again within 18 hours, the capillary may be kept in the instrument with both ends immersed in vials of deionized water.

3.2.4 DATA HANDLING

The aim of this chapter is to determine the relationship between the free solute mobility and the solute-cyclodextrin complex mobility. The free mobility (μ_{free}) is directly taken as the mobility measured in the absence of cyclodextrin (in 200 mM MES buffer alone). Electropherograms were then run for the same solute at increasing cyclodextrin concentrations. The observed mobility of the solute decreases as cyclodextrin concentration increases since greater portions of the solute are complexed by the negatively charged cyclodextrins. To compensate the complicate effects charged cyclodextrins induced in the buffer system, both Limited Range approach and NDS Correction approach were used to correct the observed mobilities besides the viscosity correction. The corrected mobilities were then fit into equation 1-14 to determine the 1:1 complex mobility (μ_{cpx}). For those solutes to which the nonlinear fits could not be applied, the lowest mobility points were used as complex mobilities.

3.3 RESULTS AND DISCUSSIONS

3.3.1 THIRTEEN-SULFATED β-CYCLODEXTRIN

3.3.1.1 BENZYLAMINE

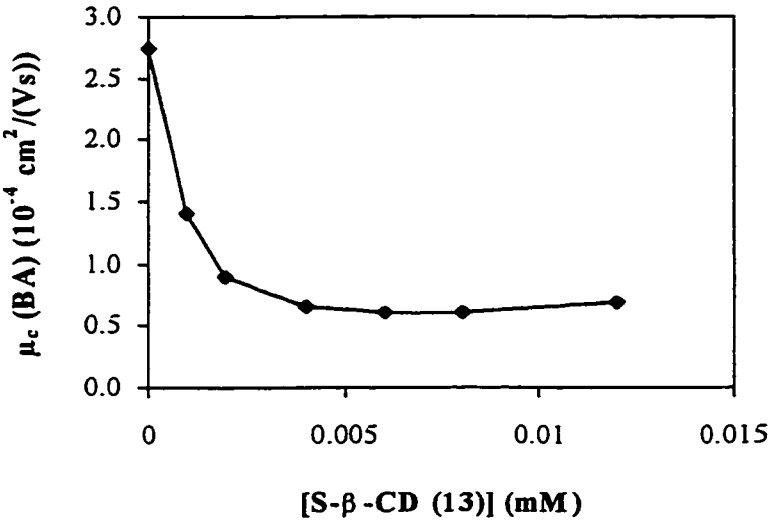

Figure 3.2 Benzylamine mobility as a function of 13-sulfated β-CD concentration. The line is simply connecting all data points. Conditions: 2.5 × 10^{-3} M benzylamine sample solution prepared in 200 mM MES buffer, pH = 4.6, V = 10 kV, T = 20 °C, λ =214, capillary 37/30 cm.

In Figure 3.2, the apparent mobility of benzylamine plateaued out as soon as cyclodextrin concentration reached 2.5 mM (the concentration of benzylamine is only 2.5 mM). This indicates very strong (almost irreversible) binding of benzylamine by 13-sulfated β-cyclodextrin. Penn et al. [3] have pointed out that it is the free CD concentration, not the total CD concentration, that should be used in all fits. Given the

Table 3.1 Mobility measurements of benzylamine with 13-sulfated β-CD[a].

[CD] (M)	t (min)	$\mu_a \times 10^4$ ($cm^2/(Vs)$)	t_V (min)	$\mu_c \times 10^4$ ($cm^2/(Vs)$)
0	6.77	2.733	7.52	2.733
0.001	13.44	1.376	7.67	1.404
0.002	21.29	0.869	7.74	0.894
0.004	29.76	0.622	7.82	0.646
0.006	32.18	0.575	7.87	0.602
0.008	32.48	0.570	7.98	0.604
0.012	29.40	0.629	8.19	0.685

a. Experimental conditions as in Figure 3.2. "t" is the migration time; "μ_a" is the apparent mobility (mobility without viscosity correction); "t_v" is time observed for the viscosity measurement as described in section 2.2.5; and "μ_c" is the corrected mobility (mobility with viscosity correction).

similarity in the concentration of benzylamine and SCD in Figure 3.2, it is not possible to accurately determine the free CD concentration. For this reason stable results of complex mobility and stability constant could not be obtained when nonlinear curve fitting was applied to benzylamine. Therefore the lowest mobility point (6 mM, 0.602×10^{-4} $cm^2/(Vs)$) was used as the complex mobility (μ_{cpx}) for benzylamine. The uncertainty associated with this estimate of the complex mobility is ~0.41×10^{-4} $cm^2/(Vs)$, as discussed below (or in Section 3.3.1.2).

In Figure 3.2 a positive drift in the benzylamine mobility is observed at high cyclodextrin concentrations. This drift is not expected from the Wren-Rowe model

(Section 1.3.1 and reference [4]), which predicts that the observed mobility should be constant after complete complexation is achieved. This positive drift turned out to be a common feature for all of the solutes studied with 13-sulfated β-cyclodextrin, as will be shown in Section 3.3.1.2 and 3.3.1.3. The cause of this drift was explored in Section 2.3.2, along with a discussion of how correction was made for this drift.

3.3.1.2 BENZYLTRIMETHYLAMMONIUM

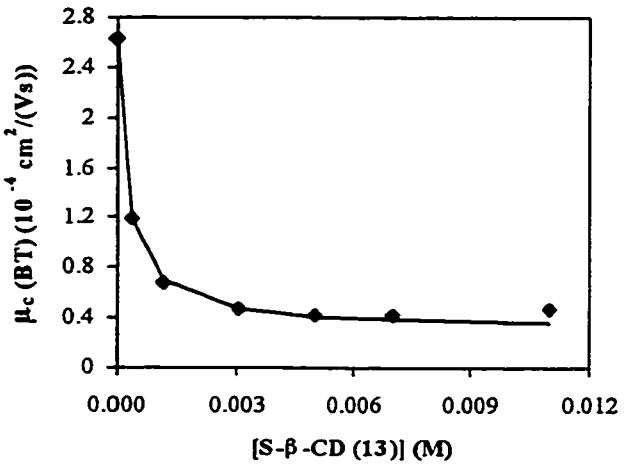

Figure 3.3 Benzyltrimethylammonium mobility as a function of 13-sulfated β-CD concentration. The line is constructed according to Equation 1-14 using the statistical results listed in Table 3.3 (Limited Range approach). Conditions: 1.0 × 10^{-3} M benzyltrimethylammonium sample solution prepared in 200mM MES buffer, pH = 4.6, V = 10 kV, T = 20 °C, λ =214, capillary 37/30 cm.

Table 3.2 Mobility measurements of benzyltrimethylammonium with 13-sulfated β-CD[a].

[CD] (M)	t (min)	$\mu_a \times 10^4$ ($cm^2/(Vs)$)	t_V (min)	$\mu_c \times 10^4$ ($cm^2/(Vs)$)	$\mu_{NDS} \times 10^4$ ($cm^2/(Vs)$)
0	7.04	2.628	7.52	2.628	2.628
0.001	15.81	1.170	7.67	1.193	1.464
0.002	28.16	0.657	7.74	0.676	1.024
0.004	41.44	0.446	7.82	0.464	0.798
0.006	46.31	0.399	7.87	0.418	—
0.008	47.32	0.391	7.98	0.415	0.714
0.012	43.7	0.423	8.19	0.461	0.724

a. Conditions are as in Figure 3.3. Meanings of symbols are as in Table 3.1. μ_{NDS} is the mobility corrected with naphthalene disulfonic acid mobilities (see text on NDS Correction approach for explanation). μ_{NDS} is not available for 6 mM.

The positive drift of observed mobility comes up again for benzyltrimethyl-ammonium, as shown in Figure 3.3. This drifting was corrected with two correction approaches, Limited Range and NDS Correction, as described in detail in Section 2.3.2.

Figure 3.4 showed the result obtained by NDS Correction approach. The points in Figure 3.4 are the experimental data corrected for the drift in mobility observed for NDS (last column in Table 3.2). By using NDS Correction approach the positive drifting phenomenon was diminished. The line in Figure 3.4 is the fit to the Wren-Rowe model (equation 1-14) (Section 1.3.1 and reference [4]).

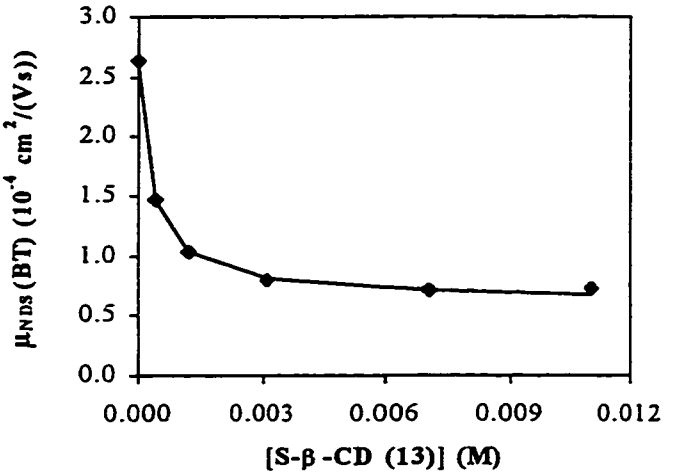

Figure 3.4 Benzyltrimethylammonium mobility as a function of 13-sulfated β-CD concentration. The line is constructed according to Equation 1-14 using the statistical results listed in Table 3.4 (NDS Correction approach). Conditions: 1.0 × 10^{-3} M benzyltrimethylammonium sample solution prepared in 200mM MES buffer, pH = 4.6, V = 10 kV, T = 20 °C, λ =214, capillary 37/30 cm.

The statistical results for benzyltrimethylammonium from both approaches are listed in Table 3.3 below.

Table 3.3 Curve fitting statistics for benzyltrimethylammonium with 13-sulfated β-CD.

1:1 BINDING		
	Limited Range	**NDS Correction**
μ_A*	2.628	2.628
μ_{ACD}*	0.31 ± 0.01	0.65 ± 0.01
K (M^{-1})	(4.3 ± 0.1) × 10^3	(3.5 ± 0.1) × 10^3
R^2	0.9999	0.9996

Fitting Equation	$y = (2.628 + \mu_{ACD}K[CD])/ (1 + K[CD])$	
1:1 +1:2 BINDING		
	Limited Range	**NDS Correction**
μ_A*	2.628	2.628
μ_{ACD}*	0.31 ± 0.01	0.571 ± 0.002
K_1 (M^{-1})	$(4.3 \pm 0.2) \times 10^3$	$(32.0 \pm 0.1) \times 10^2$
$\mu_{A(CD)2}$*	0 ± 60	0.58 ± 0.01
K_2 (M^{-1})	0 ± 60	-63 ± 6
R^2	0.9999	0.999999
Fitting Equation	$y = 2.628 + \frac{(\mu_{ACD} - 2.628)K_1[CD] + (\mu_{A(CD)_2} - 2.628)K_1K_2[CD]^2}{1 + K_1[CD] + K_1K_2[CD]^2}$	

*unit: 10^{-4} $cm^2/(Vs)$.

The statistical results in Table 3.3 show that both approaches give very good fitting. All fits in Table 3.3 display correlation coefficients (R^2) greater than 0.999. The fits which allow for both 1:1 and 1:2 solute-cyclodextrin binding (1:1 + 1:2 fits) give even better R^2s. However, the stability constants for the second complexation (0 in Limited Range approach, -63 in NDS Correction approach) do not have any physical meanings. Thus 1:2 binding was ignored in this case.

3.3.1.3 OTHER SOLUTES

All the solutes mobility behaviors are summarized in Figure 3.5. It turned out that all the other solutes behave like benzyltrimethylammonium (BT). Therefore, the same treatments (Limited Range and NDS Correction) were performed on these solutes. The statistical results are summarized in Table 3.4 to 3.15.

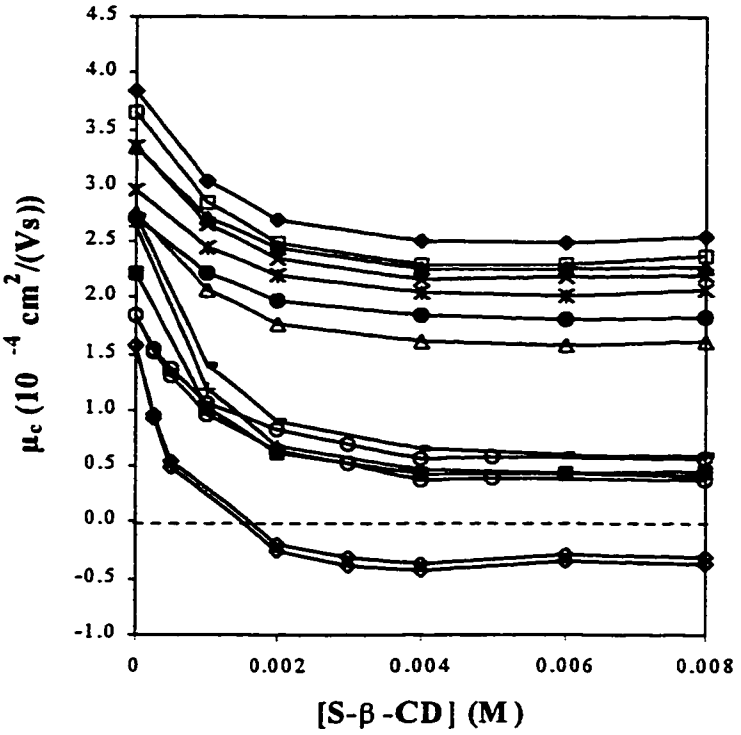

Figure 3.5 Mobilities of twelve analytes as a function of 13-sulfated β-CD concentration. The lines are simply connecting all data points. From top to bottom: 1 mM imidazole (◆), 1 mM 1-methylimidazole (□),1 mM 2-methylimidazole (▲),1 mM 4-methylimidazole (×),1 mM 2-ethylimidazole (✱),1 mM 2-propylimidazole (●),1 mM 1-butylimidazole (Δ), 2.5 mM benzylamine (-),1 mM benzyltrimethylammonium (+),1 mM histidine (■), 2×10^{-4} M homatropine (±) (○), and 1.5×10^{-4} M propranolol (R, S) (◊).

Table 3.4 Curve fitting statistics for histidine with 13-sulfated β-CD.

1:1 BINDING		
	Limited Range	**NDS Correction**
μ_A*	2.213	2.213
μ_{ACD}*	0.33 ± 0.01	0.71 ± 0.03
K (M^{-1})	$(4.7 \pm 0.2) \times 10^3$	$(4.4 \pm 0.5) \times 10^3$
R^2	0.9998	0.9965
Fitting Equation	$y = (2.213 + \mu_{ACD}K[CD])/ (1 + K[CD])$	
1:1 +1:2 BINDING		
	Limited Range	**NDS Correction**
μ_A*	2.213	2.213
μ_{ACD}*	0.33 ± 0.02	0.62 ± 0.03
K_1 (M^{-1})	$(4.7 \pm 0.3) \times 10^3$	$(3.7 \pm 0.3) \times 10^3$
$\mu_{A(CD)2}$*	0 ± 72	0.6 ± 0.1
K_2 (M^{-1})	0 ± 72	$(-7 \pm 4) \times 10^1$
R^2	0.9998	0.9995
Fitting Equation	$y = 2.213 + \frac{(\mu_{ACD} - 2.213)K_1[CD] + (\mu_{A(CD)_2} - 2.213)K_1K_2[CD]^2}{1 + K_1[CD] + K_1K_2[CD]^2}$	

*unit: 10^{-4} $cm^2/(Vs)$.

Table 3.5 Curve fitting statistics for imidazole with 13-sulfated β-CD.

1:1 BINDING		
	Limited Range	**NDS Correction**
μ_A*	3.830	3.830
μ_{ACD}*	2.37 ± 0.02	2.80 ± 0.04
K (M^{-1})	$(2.8 \pm 0.2) \times 10^3$	$(2.6 \pm 0.6) \times 10^3$
R^2	0.9993	0.9859
Fitting Equation	$y = (3.830 + \mu_{ACD}K[CD])/ (1 + K[CD])$	

1:1 +1:2 BINDING		
	Limited Range	**NDS Correction**
μ_A*	3.830	3.830
μ_{ACD}*	2.249 ± 0.005	2.58 ± 0.04
K_1 (M^{-1})	$(23.0 \pm 0.1) \times 10^2$	$(1.6 \pm 0.1) \times 10^3$
$\mu_{A(CD)2}$*	-0.1 ± 5	1 ± 3
K_2 (M^{-1})	-9 ± 20	-16 ± 35
R^2	1	0.9997
Fitting Equation	$y = 3830 + \frac{(\mu_{ACD} - 3.830)K_1[CD] + (\mu_{A(CD)_2} - 3.830)K_1K_2[CD]^2}{1 + K_1[CD] + K_1K_2[CD]^2}$	

*unit: 10^{-4} $cm^2/(Vs)$.

Table 3.6 Curve fitting statistics for 1-methylimidazole with 13-sulfated β-CD.

1:1 BINDING		
	Limited Range	**NDS Correction**
μ_A*	3.642	3.642
μ_{ACD}*	2.16 ± 0.02	2.61 ± 0.04
K (M^{-1})	$(2.7 \pm 0.2) \times 10^3$	$(2.7 \pm 0.6) \times 10^3$
R^2	0.9989	0.9825
Fitting Equation	$y = (3.642 + \mu_{ACD}K[CD])/(1 + K[CD])$	
1:1 +1:2 BINDING		
	Limited Range	**NDS Correction**
μ_A*	3.642	3.642
μ_{ACD}*	2.01 ± 0.01	2.37 ± 0.07
K_1 (M^{-1})	$(21.6 \pm 0.1) \times 10^2$	$(1.6 \pm 0.2) \times 10^3$
$\mu_{A(CD)2}$*	-0.02 ± 3	-2 ± 50
K_2 (M^{-1})	-13 ± 20	-6 ± 60
R^2	0.999999	0.9990

Fitting Equation	$y = 3.642 + \frac{(\mu_{ACD} - 3.642)K_1[CD] + (\mu_{A(CD)_2} - 3.642)K_1K_2[CD]^2}{1 + K_1[CD] + K_1K_2[CD]^2}$

*unit: 10^{-4} $cm^2/(Vs)$.

Table 3.7 Curve fitting statistics for 2-methylimidazole with 13-sulfated β-CD.

1:1 BINDING		
	Limited Range	**NDS Correction**
μ_A*	3.345	3.345
μ_{ACD}*	2.14 ± 0.03	2.53 ± 0.05
K (M^{-1})	$(2.4 \pm 0.2) \times 10^3$	$(1.8 \pm 0.5) \times 10^3$
R^2	0.9978	0.9737
Fitting Equation	$y = (3.345 + \mu_{ACD}K[CD])/(1 + K[CD])$	
1:1 +1:2 BINDING		
	Limited Range	**NDS Correction**
μ_A*	3.345	3.345
μ_{ACD}*	2.0 ± 0.1	2.23 ± 0.09
K_1 (M^{-1})	$(1.9 \pm 0.4) \times 10^3$	$(0.9 \pm 0.2) \times 10^3$
$\mu_{A(CD)2}$*	0 ± 80	0.5 ± 8
K_2 (M^{-1})	-14 ± 500	-14 ± 50
R^2	0.9994	0.9989
Fitting Equation	$y = 3.345 + \frac{(\mu_{ACD} - 3.345)K_1[CD] + (\mu_{A(CD)_2} - 3.345)K_1K_2[CD]^2}{1 + K_1[CD] + K_1K_2[CD]^2}$	

*unit: 10^{-4} $cm^2/(Vs)$.

Table 3.8 Curve fitting statistics for 4-methylimidazole with 13-sulfated β-CD.

1:1 BINDING		
	Limited Range	**NDS Correction**
μ_A*	3.333	3.333
μ_{ACD}*	2.04 ± 0.03	2.45 ± 0.04
K (M^{-1})	$(2.4 \pm 0.3) \times 10^3$	$(1.9 \pm 0.5) \times 10^3$
R^2	0.9976	0.9778
Fitting Equation	$y = (3.333 + \mu_{ACD}K[CD])/ (1 + K[CD])$	
1:1 +1:2 BINDING		
	Limited Range	**NDS Correction**
μ_A*	3.333	3.333
μ_{ACD}*	1.9 ± 0.1	2.2 ± 0.1
K_1 (M^{-1})	$(1.8 \pm 0.3) \times 10^3$	$(1.0 \pm 0.2) \times 10^3$
$\mu_{A(CD)2}$*	0 ± 50	7 ± 60
K_2 (M^{-1})	-17 ± 400	6 ± 80
R^2	0.9995	0.9984
Fitting Equation	$y = 3.333 + \frac{(\mu_{ACD} - 3.333)K_1[CD] + (\mu_{A(CD)_2} - 3.333)K_1K_2[CD]^2}{1 + K_1[CD] + K_1K_2[CD]^2}$	

*unit: 10^{-4} $cm^2/(Vs)$.

Table 3.9 Curve fitting statistics for 2-ethylimidazole with 13-sulfated β-CD.

1:1 BINDING		
	Limited Range	**NDS Correction**
μ_A*	2.965	2.965
μ_{ACD}*	1.90 ± 0.01	2.28 ± 0.03
K (M^{-1})	$(19.6 \pm 0.7) \times 10^2$	$(1.1 \pm 0.2) \times 10^3$
R^2	0.9997	0.9890
Fitting Equation	$y = (2.965 + \mu_{ACD}K[CD])/ (1 + K[CD])$	

1:1 +1:2 BINDING		
	Limited Range	**NDS Correction**
μ_A*	2.965	2.965
μ_{ACD}*	1.8 ± 0.2	2.10 ± 0.08
K_1 (M^{-1})	$(1.8 \pm 0.3) \times 10^3$	$(0.7 \pm 0.2) \times 10^3$
$\mu_{A(CD)2}$*	-1 ± 500	-1 ± 100
K_2 (M^{-1})	-3 ± 500	-5 ± 100
R^2	0.9999	0.9981
Fitting Equation	$y = 2.965 + \frac{(\mu_{ACD} - 2.965)K_1[CD] + (\mu_{A(CD)_2} - 2.965)K_1K_2[CD]^2}{1 + K_1[CD] + K_1K_2[CD]^2}$	

*unit: 10^{-4} $cm^2/(Vs)$.

Table 3.10 Curve fitting statistics for 2-propylimidazole with 13-sulfated β-CD.

1:1 BINDING		
	Limited Range	**NDS Correction**
μ_A*	2.709	2.709
μ_{ACD}*	1.70 ± 0.01	2.06 ± 0.03
K (M^{-1})	$(20.5 \pm 0.8) \times 10^2$	$(1.1 \pm 0.2) \times 10^3$
R^2	0.9997	0.9946
Fitting Equation	$y = (2.709 + \mu_{ACD}K[CD])/(1 + K[CD])$	
1:1 +1:2 BINDING		
	Limited Range	**NDS Correction**
μ_A*	2.709	2.709
μ_{ACD}*	1.70 ± 0.07	1.80 ± 0.01
K_1 (M^{-1})	$(2.0 \pm 0.3) \times 10^3$	$(5.8 \pm 0.2) \times 10^3$
$\mu_{A(CD)2}$*	0 ± 0.01	-2 ± 10
K_2 (M^{-1})	-0.01 ± 7	-5 ± 10
R^2	0.9997	0.99997

Fitting Equation	$y = 2.709 + \frac{(\mu_{ACD} - 2.709)K_1[CD] + (\mu_{A(CD)_2} - 2.709)K_1K_2[CD]^2}{1 + K_1[CD] + K_1K_2[CD]^2}$

*unit: 10^{-4} $cm^2/(Vs)$.

Table 3.11 Curve fitting statistics for 2-butylimidazole with 13-sulfated β-CD.

1:1 BINDING		
	Limited Range	**NDS Correction**
μ_A*	2.745	2.709
μ_{ACD}*	1.48 ± 0.01	1.84 ± 0.03
K (M^{-1})	$(2.7 \pm 0.1) \times 10^3$	$(1.8 \pm 0.3) \times 10^3$
R^2	0.9995	0.9924
Fitting Equation	$y = (2.745 + \mu_{ACD}K[CD])/(1 + K[CD])$	
1:1 +1:2 BINDING		
	Limited Range	**NDS Correction**
μ_A*	2.745	2.745
μ_{ACD}*	1.39 ± 0.02	1.68 ± 0.02
K_1 (M^{-1})	$(23.3 \pm 0.3) \times 10^2$	$(12.0 \pm 0.6) \times 10^2$
$\mu_{A(CD)2}$*	0.1 ± 8	-0.5 ± 10
K_2 (M^{-1})	-11 ± 70	-7 ± 30
R^2	0.999997	0.9999
Fitting Equation	$y = 2.745 + \frac{(\mu_{ACD} - 2.745)K_1[CD] + (\mu_{A(CD)_2} - 2.745)K_1K_2[CD]^2}{1 + K_1[CD] + K_1K_2[CD]^2}$	

*unit: 10^{-4} $cm^2/(Vs)$.

Table 3.12 Curve fitting statistics for the first eluting peak of homatropine with 13-sulfated β-CD.

1:1 BINDING		
	Limited Range	**NDS Correction**
μ_A*	1.829	1.829
μ_{ACD}*	0.26 ± 0.03	0.68 ± 0.08
K (M^{-1})	$(9.6 \pm 0.6) \times 10^2$	$(8 \pm 2) \times 10^3$
R^2	0.9985	0.9776
Fitting Equation	$y = (1.829 + \mu_{ACD}K[CD])/ (1 + K[CD])$	
1:1 +1:2 BINDING		
	Limited Range	**NDS Correction**
μ_A*	1.829	1.829
μ_{ACD}*	0.26 ± 0.04	0.3 ± 1
K_1 (M^{-1})	$(9.6 \pm 0.8) \times 10^2$	$(5 \pm 3) \times 10^3$
$\mu_{A(CD)2}$*	0 ± 0.8	-0.6 ± 1
K_2 (M^{-1})	0 ± 0.8	-155 ± 1000
R^2	0.9985	0.9806
Fitting Equation	$y = 1.829 + \frac{(\mu_{ACD} - 1.829)K_1[CD] + (\mu_{A(CD)_2} - 1.829)K_1K_2[CD]^2}{1 + K_1[CD] + K_1K_2[CD]^2}$	

*unit: 10^{-4} $cm^2/(Vs)$.

Table 3.13 Curve fitting statistics for the second eluting peak of homatropine with 13-sulfated β-CD.

1:1 BINDING		
	Limited Range	**NDS Correction**
μ_A*	1.829	1.829
μ_{ACD}*	0.01 ± 0.03	0.44 ± 0.08
K (M^{-1})	$(9.8 \pm 0.5) \times 10^2$	$(8 \pm 1) \times 10^2$
R^2	0.9991	0.9844
Fitting Equation	$y = (1.829 + \mu_{ACD}K[CD])/ (1 + K[CD])$	
1:1 +1:2 BINDING		
	Limited Range	**NDS Correction**
μ_A*	1.829	1.829
μ_{ACD}*	0.01 ± 0.04	-0.05 ± 0.4
K_1 (M^{-1})	$(9.8 \pm 0.6) \times 10^2$	$(5 \pm 2) \times 10^2$
$\mu_{A(CD)2}$*	0 ± 70	0.2 ± 2
K_2 (M^{-1})	0 ± 70	$(-1 \pm 6) \times 10^2$
R^2	0.9991	0.9887
Fitting Equation	$y = 1.829 + \frac{(\mu_{ACD} - 1.829)K_1[CD] + (\mu_{A(CD)_2} - 1.829)K_1K_2[CD]^2}{1 + K_1[CD] + K_1K_2[CD]^2}$	

*unit: 10^{-4} $cm^2/(Vs)$.

Table 3.14 Curve fitting statistics for R-propranolol with 13-sulfated β-CD.

1:1 BINDING		
	Limited Range	**NDS Correction**
μ_A*	1.572	1.572
μ_{ACD}*	-0.67 ± 0.03	-0.17 ± 0.04
K (M^{-1})	$(18.0 \pm 0.8) \times 10^2$	$(2.1 \pm 0.2) \times 10^2$
R^2	0.9993	0.9954

Fitting Equation	$y = (1.572 + \mu_{ACD}K[CD])/ (1 + K[CD])$	
1:1 +1:2 BINDING		
	Limited Range	**NDS Correction**
μ_A*	1.572	1.572
μ_{ACD}*	-0.67 ± 0.04	-0.3 ± 0.4
K_1 (M^{-1})	$(1.8 \pm 0.1) \times 10^3$	$(1.8 \pm 0.4) \times 10^3$
$\mu_{A(CD)2}$*	0 ± 100	3 ± 500
K_2 (M^{-1})	0 ± 100	6 ± 800
R^2	0.9993	0.9968
Fitting Equation	$y = 1.572 + \frac{(\mu_{ACD} - 1.572)K_1[CD] + (\mu_{A(CD)_2} - 1.572)K_1K_2[CD]^2}{1 + K_1[CD] + K_1K_2[CD]^2}$	

*unit: 10^{-4} $cm^2/(Vs)$.

Table 3.15 Curve fitting statistics for S-propranolol with 13-sulfated β-CD.

1:1 BINDING		
	Limited Range	**NDS Correction**
μ_A*	1.572	1.572
μ_{ACD}*	-0.75 ± 0.03	-0.23 ± 0.05
K (M^{-1})	$(17.9 \pm 0.9) \times 10^2$	$(2.2 \pm 0.2) \times 10^3$
R^2	0.9991	0.9951
Fitting Equation	$y = (1.572 + \mu_{ACD}K[CD])/ (1 + K[CD])$	
1:1 +1:2 BINDING		
	Limited Range	**NDS Correction**

μ_A*	1.572	1.572
μ_{ACD}*	-0.75 ± 0.04	-0.4 ± 0.2
K_1 (M^{-1})	$(1.9 \pm 0.1) \times 10^3$	$(1.8 \pm 0.3) \times 10^3$
$\mu_{A(CD)2}$*	0 ± 100	3 ± 200
K_2 (M^{-1})	0 ± 100	8 ± 600
R^2	0.9991	0.9972
Fitting Equation	$y = 1.572 + \frac{(\mu_{ACD} - 1.572)K_1[CD] + (\mu_{A(CD)_2} - 1.572)K_1K_2[CD]^2}{1 + K_1[CD] + K_1K_2[CD]^2}$	

*unit: 10^{-4} $cm^2/(Vs)$.

Regardless of the approach used, all results favored 1:1 stoichiometry. The complex mobilities and stability constants obtained for 1:2 binding are either not physically meaningful or are very small compared with 1:1 complex stability constants. Thus the 1:2 binding stoichiometry can be considered negligible. Therefore it can be concluded that 1:1 binding stoichiometry is the predominant complexation form of solutes with 13-charged β-cyclodextrin.

Introducing the NDS Correction has different impacts on the stability constants and the complex mobility. Changes in stability constants strongly depend on individual compounds. For instance, in the case of 2-ethylimidazole (Table 3.10) and 2-propylimidazole (Table 3.11), NDS Correction causes a ~50% drop in the stability constants. Whereas for some other solutes, such as imidazole (Table 3.6) the difference between Limited Ranged NDS Correction is minor. Therefore, care must be taken when one attempts to use quantitatively the stability constants when charged cyclodextrins are involved in the complexation process.

On the other hand a consistent difference in complex mobility is observed between the two different approaches. The NDS Correction method always gives higher (more positive) results than the Limited Range method. This bias ranges from about 0.3 $\times 10^{-4}$ $cm^2/(Vs)$ to 0.5 $\times 10^{-4}$ $cm^2/(Vs)$ for all solutes used with 0.4 $\times 10^{-4}$ $cm^2/(Vs)$ as the most common value. This fact indicates that the difference is a systematic bias and is not solute-dependent. Therefore, as discussed in Section 2.3.2, the comparison of these two approaches gives a reliable estimation of the uncertainty of the complex mobility.

Table 3.16 Free and complex mobility data for the twelve solutes in Figure 3.5 (complex mobilities are statistical results from Limited Range approach except benzylamine).

Solute	μ_{free} ($cm^2/(Vs)$)	μ_{cpx} ($cm^2/(Vs)$)
Imidazole (IM)	3.830	2.4 ± 0.4
1-Methyl-IM	3.642	2.2 ± 0.4
2-Methyl-IM	3.345	2.1 ± 0.4
4-Methyl-IM	3.333	2.0 ± 0.4
2-Ethyl-IM	2.965	1.9 ± 0.4
2-Propyl-IM	2.709	1.7 ± 0.4
1-Butyl-IM	2.745	1.5 ± 0.4
Benzylamine	2.733	0.6 ± 0.4
Benzyltrimethylammonium	2.628	0.3 ± 0.3
Histidine	2.213	0.3 ± 0.4
Homatropine	1.829	0.3 ± 0.4
	1.829	0.0± 0.4
Propranolol	1.572	-0.7 ± 0.5
	1.572	-0.8 ± 0.5

In Table 3.16 the complex mobilities obtained by Limited Range approach and the differences between the two approaches are listed. Since non-linear curve fitting could not be performed on benzylamine, the lowest mobility point in Figure 3.2 was used for complex mobility, and the average of all the other uncertainties was used for its uncertainty.

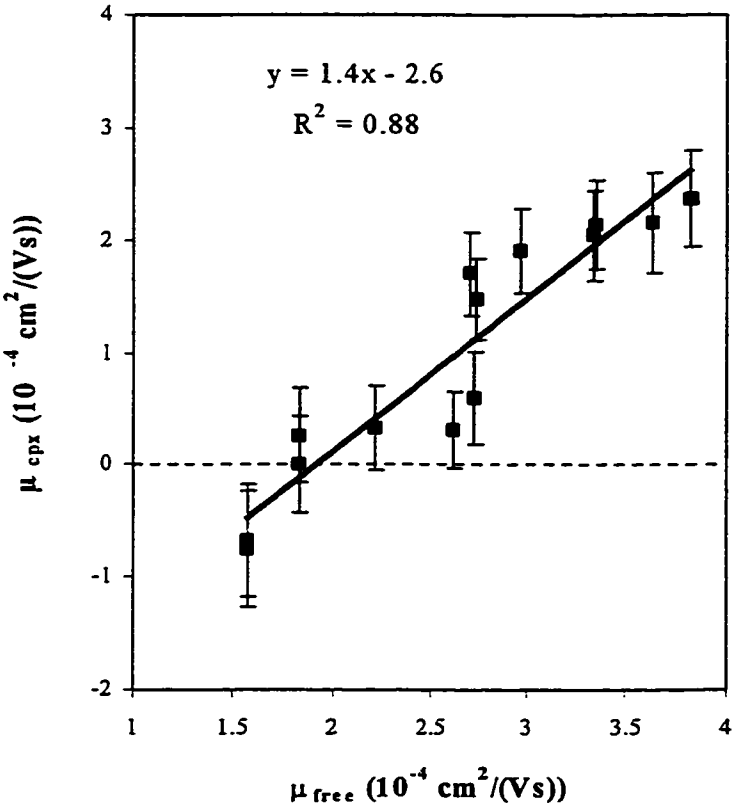

Figure 3.6 Solute-13-sulfated β-cyclodextrin complex mobilities (Limited Range approach) as a function of free solute mobilities. The error bars are the differences between the complex mobilities obtained by Limited Range and NDS Correction approaches. Experimental conditions are as shown in figure 3.2, 3.3 and 3.5.

The complex mobilities obtained by NDS Correction approach and the differences between the two approaches are listed in Table 3.17.

Table 3.17 Free and complex mobility data for the twelve solutes in Figure 3.5 (complex mobilities are statistical results from NDS Correction approach except benzylamine).

Solute	μ_{free} ($cm^2/(Vs)$)	μ_{cpx} ($cm^2/(Vs)$)
Imidazole (IM)	3.83	2.8 ± 0.4
1-Methyl-IM	3.642	2.6 ± 0.4
2-Methyl-IM	3.345	2.5 ± 0.4
4-Methyl-IM	3.333	2.4 ± 0.4
2-Ethyl-IM	2.965	2.3 ± 0.4
2-Propyl-IM	2.709	2.1 ± 0.4
1-Butyl-IM	2.745	1.8 ± 0.4
Benzylamine	2.733	0.6 ± 0.4
Benzyltrimethylammonium	2.628	0.6 ± 0.3
Histidine	2.213	0.7 ± 0.4
Homatropine	1.829	0.7 ± 0.4
	1.829	0.4 ± 0.4
Propranolol	1.572	-0.2 ± 0.5
	1.572	-0.2 ± 0.5

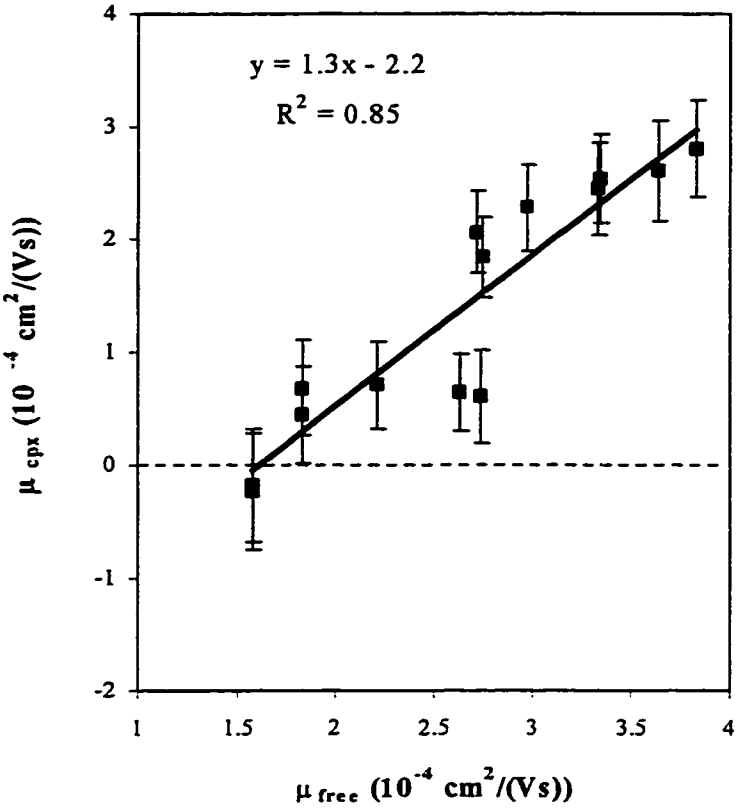

Figure 3.7 Solute-13-sulfated β-cyclodextrin complex mobilities (NDS Correction approach) as a function of free solute mobilities. The error bars are the differences between the complex mobilities obtained by Limited Range and NDS Correction approaches. Experimental conditions are as shown in figure 3.2, 3.3 and 3.5.

Figure 3.6 and 3.7 clearly show a linear relationship between free solute mobilities and solute-cyclodextrin complex mobilities. This is a very counter-intuitive observation. Since all solutes are monocharged, all the complexes have the same net charge. In addition cyclodextrins are much larger than the solutes used, the volume of

the complex would mainly be determined by the volume of cyclodextrin. Thus the complexes should have about the same volumes. Now all the complexes have about the same net charge and same volume, according to equation 3.1, all the solutes should have about the same complex mobilities! However, as we can see from Figure 3.8 and 3.9, the complex mobilities spread over a wide mobility range. No matter which correction approach was used we always get good correlation coefficients (R^2s). The uncertainties in complex mobilities are small compared with total complex mobility range. The slopes of these two straight lines are very similar, showing that different approaches do not affect the correlation. As can be expected, the intercept by NDS Correction is higher than that by Limited Range by ~ 0.47×10^{-4} $cm^2/(Vs)$. In our mobility conservation model (Section 3.3.4), the intercept is related to free cyclodextrin mobility. So if we could know the free cyclodextrin mobility, we would be able to identify which approach is more appropriate. Unfortunately, due to the lack of a proper method to measure free charged cyclodextrin mobility, the identification can not be done.

Note that more solutes have positive complex mobilities with 13-sulfated β-cyclodextrin than with tetra-sulfated β-cyclodextrin (Figure 3.15) even though the net charge is more negative in the former case.

Also can be seen from this figure is that the scattering between enantiomers (homatropine enantiomers and propranolol enantiomers, the last two pairs of data points in Figure 3.6 and 3.7) is much smaller than the difference between different solutes.

3.3.2 MOBILITY MEASUREMENTS WITH TETRA-SULFATED β-CYCLODEXTRIN

3.3.2.1 DIPHENHYDRAMINE

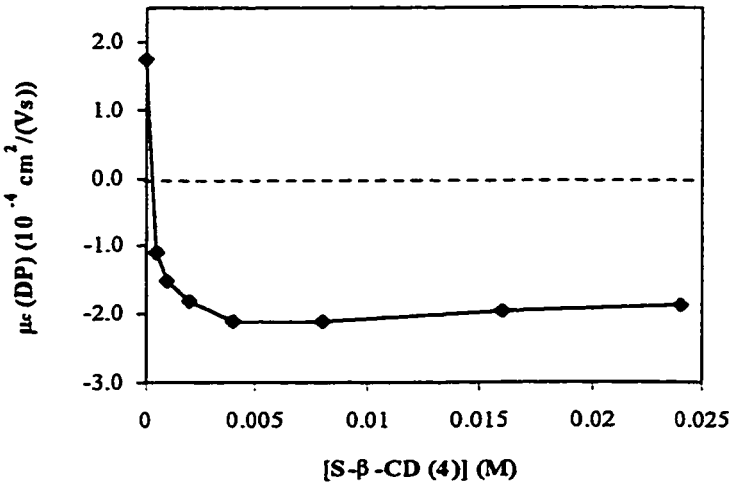

Figure 3.8 Diphenhydramine mobility as a function of tetra-sulfated β-CD concentration. The line is simply connecting all data points. Conditions: 1.0×10^{-3} M diphenhydramine sample solution prepared in 200 mM MES buffer, pH = 4.6, V = 10 kV, T = 20 °C, λ =214, capillary 37/30 cm.

In Figure 3.8 it is evident that diphenhydramine has a very strong affinity toward tetra-sulfated β-cyclodextrin. The mobility of diphenhydramine drops dramatically as soon as cyclodextrin is added and plateaus out soon after cyclodextrin concentration reaches 1 mM (the concentration of diphenhydramine was 1 mM). This behavior is very similar to that observed in Figure 3.2 for benzylamine with the 13-sulfated cyclodextrin. Stable results for the complex mobility and stability constant could not be obtained from

Table 3.18 Mobility measurements of Diphenhydramine with tetra-sulfated β-CD[a].

[CD] (M)	t (min)	$\mu_a \times 10^4$ ($cm^2/(Vs)$)	t_V (min)	$\mu_c \times 10^4$ ($cm^2/(Vs)$)
0	10.69	1.731	7.42	1.731
0.0005	17.1	-1.082	7.57	-1.104
0.001	12.5	-1.480	7.61	-1.518
0.002	10.44	-1.772	7.65	-1.827
0.004	9.08	-2.037	7.66	-2.103
0.008	9.24	-2.002	7.80	-2.105
0.016	10.12	-1.828	8.00	-1.971
0.024	11.05	-1.674	8.30	-1.873

a. Experimental conditions are as in Figure 3.8. The meanings of the symbols are as in Table 3.1.

nonlinear curve fitting of the data in Figure 3.8 for the same reasons stated in Section 3.3.1.1. That is, the difficulty in accurately determining free CD concentrations. Therefore for diphenhydramine the lowest mobility data point in Figure 3.8 (-2.105×10^{-4} $cm^2/(Vs)$) was used as the complex mobility. The upward drifting in the observed mobility of diphenhydramine is similar to what we saw with solutes in 13-sulfated cyclodextrin, indicating similar effects exist in this system as well. Although we did not see this drifting with other solutes studied with tetra-sulfated cyclodextrin (Figure 3.9 – 3.11 and 3.12), we believe that if the effect exists for one solute, it must be there for all solutes since the buffer composition is exactly the same for all of the solutes. The other solutes studied herein are still far from being fully complexed. Thus, the downward decrease in mobility caused by increasing complexation overrides the upward drift caused by the SCD buffer. Therefore the drift was corrected (Limited Range and NDS

Correction) for all other solutes except imidazole and 1-methylimidazole (Figure 3.9 and 3.10). The reasons why these solutes were treated differently will be discussed in the next section.

3.3.2.2 IMIDAZOLE AND 1-METHYLIMIDAZOLE

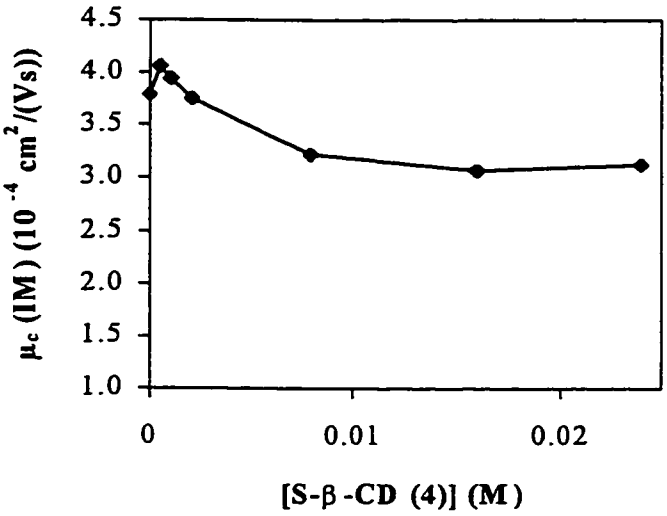

Figure 3.9 Imidazole mobility as a function of tetra-sulfated β-CD concentration. The line is simply connecting all data points. Conditions: 1.0×10^{-3} M imidazole sample solution prepared in 200 mM MES buffer, pH = 4.6, V = 10 kV, T = 20 °C, λ =214, capillary 37/30 cm.

Table 3.19 Mobility measurements of imidazole with tetra-sulfated β-CD[a]

[CD] (M)	t (min)	$\mu_a \times 10^4$ ($cm^2/(Vs)$)	t_V (min)	$\mu_c \times 10^4$ ($cm^2/(Vs)$)
0	4.88	3.791	7.42	3.791
0.0005	4.65	3.978	7.57	4.059
0.001	4.81	3.846	7.61	3.945
0.002	5.07	3.649	7.65	3.762
0.008	6.03	3.068	7.80	3.225
0.016	6.49	2.851	8.00	3.073
0.024	6.64	2.786	8.30	3.117

a. Experimental conditions are as in Figure 3.9. The meanings of the symbols are as in Table 3.1.

In Figure 3.9 the imidazole mobility shows an initial increase and then gradually decreases as the cyclodextrin concentration increases. The same phenomenon was also observed for 1-methylimidazole (Figure 3.10). Repetitive experiments were done and this phenomenon was found to be reproducible. The reason for this increase in mobility is not yet known. Note that this phenomenon was not observed with 13-sulfated β-cyclodextrin.

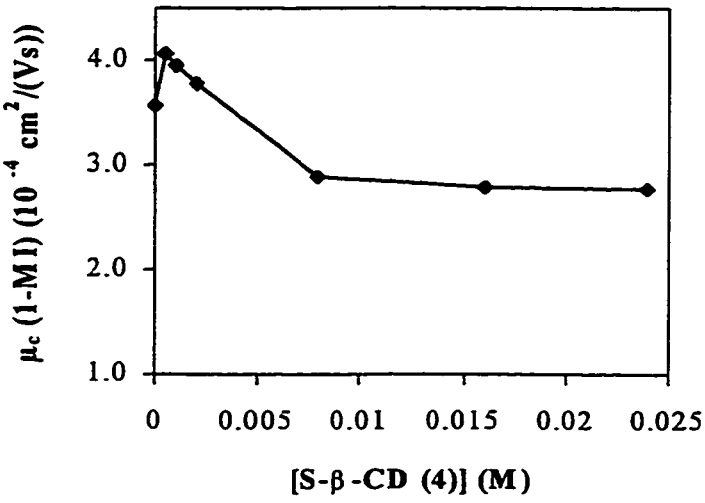

Figure 3.10 1-Methylimidazole mobility as a function of tetra-sulfated β-CD concentration. Conditions: 1.0×10^{-3} M 1-methylimidazole sample solution prepared in 200 mM MES buffer, pH = 4.6, V = 10 kV, T = 20 °C, λ =214, capillary 37/30 cm.

Table 3.20 Mobility measurements of 1-Methylimidazole with tetra-sulfated β-CD[a].

[CD] (M)	t (min)	$\mu_a \times 10^4$ ($cm^2/(Vs)$)	t_V (min)	$\mu_c \times 10^4$ ($cm^2/(Vs)$)
0	5.14	3.599	7.34	3.560
0.0005	4.65	3.978	7.57	4.059
0.001	4.81	3.846	7.61	3.945
0.002	5.07	3.649	7.65	3.762
0.008	6.54	2.829	7.58	2.890
0.016	6.99	2.647	7.82	2.789
0.024	7.28	2.541	8.08	2.767

a. Experimental conditions are as in Figure 3.10. The meanings of the symbols are as in Table 3.1.

Nonlinear curve fitting could not be performed because of this bump in the curves. However, considering the small size of imidazole and 1-methylimidazole, it is unlikely that they form higher complexes than the 1:1. At high cyclodextrin concentrations the mobility curves plateaued out. The plateau mobilities in Figure 3.9 and Figure 3.10 are used as imidazole's and 1-methylimidazole's complex mobilities, respectively.

3.3.2.2 BENZYLAMINE

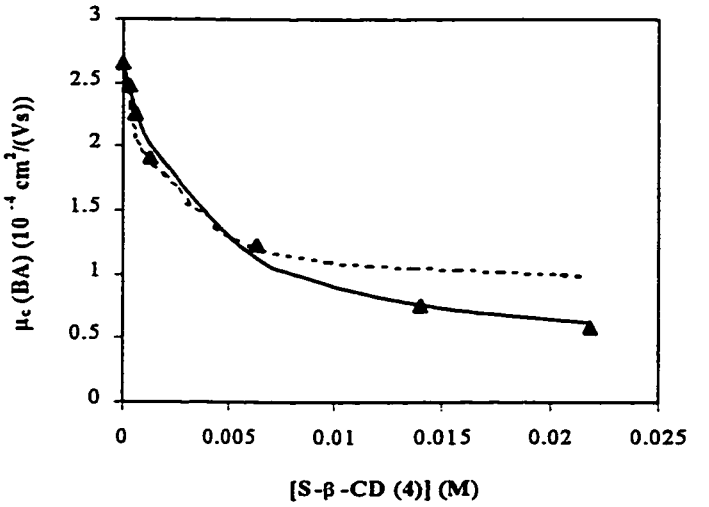

Figure 3.11 Benzylamine mobility as a function of tetra-sulfated β-CD concentration. The solid line is constructed according to equation (1-14) (1:1 stoichiometry) and using the statistical results without correction (Table 3.22). The dotted line is constructed using data with Limited Range. Conditions: 2.5 × 10^{-3} M benzylamine sample solution prepared in 200 mM MES buffer, pH = 4.6, V = 10 kV, T = 20 °C, λ =214, capillary 37/30 cm.

Table 3.21 Mobility measurements of benzylamine with tetra-sulfated β-CD[a]

[CD] (M)	t (min)	$\mu_a \times 10^4$ ($cm^2/(Vs)$)	t_V (min)	$\mu_c \times 10^4$ ($cm^2/(Vs)$)
0	6.98	2.650	7.42	2.650
0.0005	7.63	2.425	7.57	2.474
0.001	8.39	2.205	7.61	2.261
0.002	10.01	1.848	7.65	1.905
0.008	15.85	1.167	7.8	1.227
0.016	26.18	0.707	8	0.762
0.024	35.8	0.517	8.3	0.578

a. Experimental conditions are as in Figure 3.11. The meanings of the symbols are as in Table 3.1.

As a result of the scatter in the benzylamine mobility data, when the last two data were omitted (Limited Range approach), unreasonably high complex mobility and high stability constant were obtained. This can be seen as the dotted line in Figure 3.11. Therefore only the NDS Correction approach was used to treat the benzylamine data. The difference between the uncorrected approach and the NDS Correction was used as an estimate of the uncertainty associated with the complex mobility.

As described in Section 2.3.2, naphthalene disulfonic acid (NDS) was used to measure the effects of sulfated β-cyclodextrin on the observed mobilities. The NDS mobility was measured in a series of buffers with increasing tetra-sulfated β-cyclodextrin concentrations (Figure 2.7 and Table 2.2).

Table 3.22 Curve fitting statistics for benzylamine with tetra-sulfated β-CD.

1:1 BINDING		
	No Correction	**NDS Correction**
μ_A*	2.650	2.650
μ_{ACD}*	0.33 ± 0.09	0.3 ± 0.2
K (M^{-1})	$(3.1 \pm 0.4) \times 10^2$	$(2.2 \pm 0.5) \times 10^2$
R^2	0.9945	0.9892
Fitting Equation	$y = (2.650 + \mu_{ACD}K[CD])/ (1 + K[CD])$	
1:1 +1:2 BINDING		
	No Correction	**NDS Correction**
μ_A*	2.650	2.650
μ_{ACD}*	0.3 ± 0.1	0.3 ± 0.3
K_1 (M^{-1})	$(3.1 \pm 0.4) \times 10^2$	$(2.1 \pm 0.7) \times 10^2$
$\mu_{A(CD)2}$*	0 ± 0.0009	$0 \pm 4 \times 10^{-8}$
K_2 (M^{-1})	0 ± 0.0009	-2 ± 3
R^2	0.9945	0.9892
Fitting Equation	$y = 2.650 + \frac{(\mu_{ACD} - 2.650)K_1[CD] + (\mu_{A(CD)_2} - 2.650)K_1K_2[CD]^2}{1 + K_1[CD] + K_1K_2[CD]^2}$	

*unit: 10^{-4} $cm^2/(Vs)$.

In the fitting result for benzylamine we see that the 1:1 complex mobility and the stability constant for 1:1 binding are very similar for both the 1:1 binding model and the 1:1+1:2 model. Also, the complex mobility and stability constant for 1:2 binding are nearly zero. This shows that 1:1 binding is the predominant type of interaction between benzylamine and tetra-sulfated β-cyclodextrin.

3.3.2.3 OTHER SOLUTES

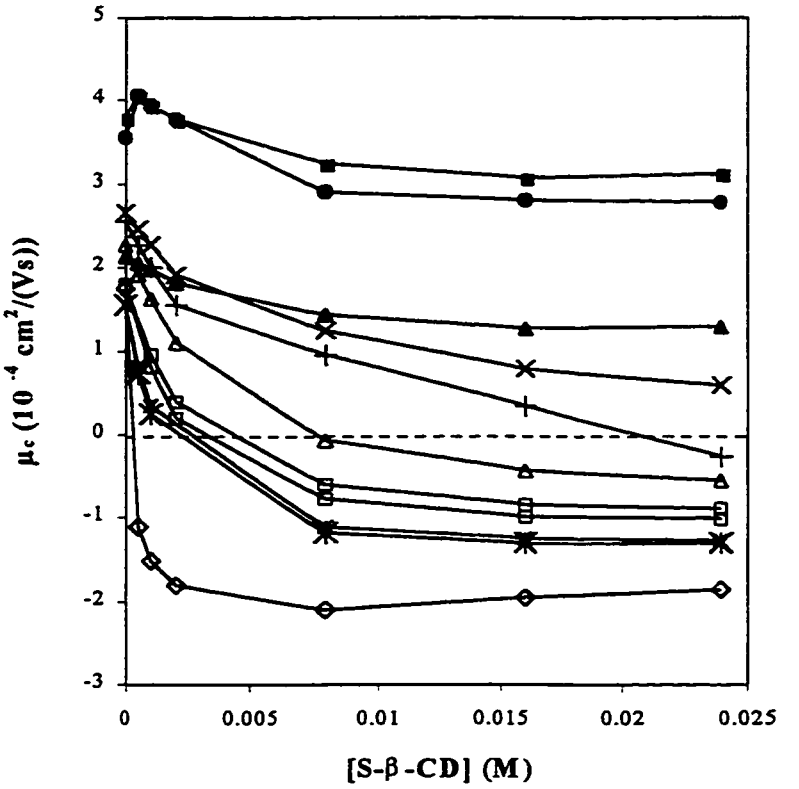

Figure 3.12 Mobilities of nine analytes as a function of tetra-sulfated β-CD concentration. From top to bottom: imidazole (■), 1-methylimidazole (●), histidine (▲), benzylamine (×), benzyltrimethylammonium (+), 4-(aminomethyl) benzene sulfonamide (Δ), homatropine enantiomers(□), propranolol enantiomers (∗), and diphenhydramine (◊).

Diphenhydramine, imidazole, 1-methylimidazole and benzylamine have been discussed in Sections 3.3.2.1, 3.3.2.2, 3.3.2.2 and 3.3.2.3, respectively. The statistical results for all other solutes studied are listed in Table 3.25 to 3.31. These solutes were

treated as described in Section 3.3.2.3 for benzylamine except that Limited Range approach was also applied as well as NDS Correction.

Table 3.23 Curve fitting statistics for 4-(aminomethyl)benzene sulfonamide with tetra-sulfated β-CD

1:1 BINDING		
	Limited Range	**NDS Correction**
μ_A*	2.267	2.267
μ_{ACD}*	-1.2 ± 0.1	-0.89 ± 0.05
K (M^{-1})	$(2.8 \pm 0.2) \times 10^2$	$(3.0 \pm 0.2) \times 10^2$
R^2	0.9989	0.9990
Fitting Equation	$y = (2.267 + \mu_{ACD}K[CD])/ (1 + K[CD])$	
1:1 +1:2 BINDING		
	Limited Range	**NDS Correction**
μ_A*	2.267	2.267
μ_{ACD}*	-1.2 ± 0.1	-0.89 ± 0.08
K_1 (M^{-1})	$(2.8 \pm 0.3) \times 10^2$	$(3.0 \pm 0.2) \times 10^2$
$\mu_{A(CD)2}$*	0 ± 1400	0 ± 15
K_2 (M^{-1})	0 ± 1400	0 ± 2
R^2	0.9989	0.9990
Fitting Equation	$y = 2.267 + \frac{(\mu_{ACD} - 2.267)K_1[CD] + (\mu_{A(CD)_2} - 2.267)K_1K_2[CD]^2}{1 + K_1[CD] + K_1K_2[CD]^2}$	

*unit: 10^{-4} $cm^2/(Vs)$.

The fit statistics according to Equation 1-14 (1:1 binding) and Equation 1-38 (1:2 binding) give similar 1:1 complex mobility and stability constants, but zero 1:2 complex mobility and stability constants. This indicates that 1:1 binding is dominant.

Table 3.24 Curve fitting statistics for benzyltrimethylammonium with tetra-sulfated β-CD.

1:1 BINDING		
	Limited Range	**NDS Correction**
μ_A*	2.552	2.552
μ_{ACD}*	-1.07 ± 0.07	-0.68 ± 0.06
K (M^{-1})	219 ± 8	(2.4 ± 0.1) × 10^2
R^2	0.9997	0.9990
Fitting Equation	$y = (2.552 + \mu_{ACD}K[CD])/(1 + K[CD])$	
1:1 +1:2 BINDING		
	Limited Range	**NDS Correction**
μ_A*	2.552	2.552
μ_{ACD}*	-0.9 ± 4	-0.6 ± 17
K_1 (M^{-1})	(2 ± 2) × 10^2	(0.2 ± 1) × 10^3
$\mu_{A(CD)2}$*	-0.0004 ± 3	0.4 ± 300
K_2 (M^{-1})	(0.8 ± 2) × 10^2	-4 ± 1200
R^2	0.99998	0.9991
Fitting Equation	$y = 2.552 + \frac{(\mu_{ACD} - 2.552)K_1[CD] + (\mu_{A(CD)_2} - 2.552)K_1K_2[CD]^2}{1 + K_1[CD] + K_1K_2[CD]^2}$	

*unit: 10^{-4} $cm^2/(Vs)$.

NDS Correction gives a negative secondary stability constant (K_2) for benzyltrimethylammonium, whereas Limited Range gives a reasonable value of 80. However, considering the very high uncertainties associated with all the parameters of 1:2 binding from Limited Range, the 1:2 binding is excluded. Therefore the parameters determined for 1:1 binding of benzyltrimethylammonium will be used in all further discussion.

Table 3.25 Curve fitting statistics for histidine with tetra-sulfated β-CD.

1:1 BINDING		
	Limited Range	**NDS Correction**
μ_A*	2.117	2.117
μ_{ACD}*	0.9 ± 0.1	1.1 ± 0.1
K (M^{-1})	$(1.9 \pm 0.3) \times 10^2$	$(1.8 \pm 0.6) \times 10^2$
R^2	0.9958	0.9788
Fitting Equation	$y = (2.117 + \mu_{ACD}K[CD])/ (1 + K[CD])$	
1:1 +1:2 BINDING		
	Limited Range	**NDS Correction**
μ_A*	2.117	2.117
μ_{ACD}*	0.9 ± 2230	0.5 ± 0.8
K_1 (M^{-1})	$(2 \pm 3000) \times 10^2$	$(1.0 \pm 0.9) \times 10^2$
$\mu_{A(CD)2}$*	$-0.03 \pm 1 \times 10^5$	1.1 ± 0.2
K_2 (M^{-1})	$-3 \pm 4 \times 10^5$	$(-1.1 \pm 0.4) \times 10^2$
R^2	0.9958	0.9991
Fitting Equation	$y = 2.117 + \frac{(\mu_{ACD} - 2.117)K_1[CD] + (\mu_{A(CD)_2} - 2.117)K_1K_2[CD]^2}{1 + K_1[CD] + K_1K_2[CD]^2}$	

*unit: 10^{-4} $cm^2/(Vs)$.

A negative K_2 observed with 1:2 binding is physically impossible. Therefore only 1:1 binding between histidine and tetra-sulfated β-cyclodextrin is considered. The use of Limited Ranges yields much better correlation. However, regardless of the quality of fit, both the EOF and NDS correction procedures yield comparable complex mobilities and stability constants for histidine.

Table 3.26 Curve fitting statistics for the first eluting peak of homatropine with tetra-sulfated β-CD.

1:1 BINDING		
	Limited Range	**NDS Correction**
μ_A*	1.779	1.779
μ_{ACD}*	-1.39 ± 0.05	-1.08 ± 0.06
K (M^{-1})	$(3.8 \pm 0.2) \times 10^2$	$(4.4 \pm 0.4) \times 10^2$
R^2	0.9996	0.9978
Fitting Equation	$y = (1.779 + \mu_{ACD}K[CD])/ (1 + K[CD])$	
1:1 +1:2 BINDING		
	Limited Range	**NDS Correction**
μ_A*	1.779	1.779
μ_{ACD}*	-2 ± 5	-1 ± 5
K_1 (M^{-1})	$(3 \pm 4) \times 10^2$	$(5 \pm 9) \times 10^2$
$\mu_{A(CD)2}$*	$(-2 \pm 800) \times 10^2$	0.3 ± 600
K_2 (M^{-1})	-2 ± 600	-2 ± 700
R^2	0.9998	0.9979
Fitting Equation	$y = 1.779 + \frac{(\mu_{ACD} - 1.779)K_1[CD] + (\mu_{A(CD)_2} - 1.779)K_1K_2[CD]^2}{1 + K_1[CD] + K_1K_2[CD]^2}$	

*unit: $10^{-4}\,cm^2/(Vs)$.

The large uncertainties associated with fitting the first homatropine peak to 1:1+1:2 binding make this model unreasonable. Both the EOF and NDS corrections yield reasonable fits of the data to the 1:1 binding model. Again, the parameters obtained using these two correction approaches are comparable.

Table 3.27 Curve fitting statistics for the second eluting peak of homatropine with tetra-sulfated β-CD.

1:1 BINDING		
	Limited Range	**NDS Correction**
μ_A*	1.779	1.779
μ_{ACD}*	-1.53 ± 0.06	-1.17 ± 0.05
K (M^{-1})	$(4.5 \pm 0.2) \times 10^2$	$(5.6 \pm 0.4) \times 10^2$
R^2	0.9994	0.9984
Fitting Equation	$y = (1.779 + \mu_{ACD}K[CD])/ (1 + K[CD])$	
1:1 +1:2 BINDING		
	Limited Range	**NDS Correction**
μ_A*	1.779	1.779
μ_{ACD}*	-0.2 ± 1	-1.2 ± 0.2
K_1 (M^{-1})	$(6 \pm 4) \times 10^2$	$(5 \pm 1) \times 10^2$
$\mu_{A(CD)2}$*	-1.3 ± 0.2	0 ± 2
K_2 (M^{-1})	$(3 \pm 2) \times 10^2$	1 ± 8
R^2	0.9999	0.9984
Fitting Equation	$y = 1.779 + \frac{(\mu_{ACD} - 1.779)K_1[CD] + (\mu_{A(CD)_2} - 1.779)K_1K_2[CD]^2}{1 + K_1[CD] + K_1K_2[CD]^2}$	

*unit: 10^{-4} $cm^2/(Vs)$.

In Table 3.29, both Limited Range and NDS Correction yield comparable 1:1 binding parameters. For 1:1+1:2 binding, however, Limited Range gives a reasonable value ($300 \pm 200\ M^{-1}$) for the secondary complexation stability constant while the very small value (1) from NDS Correction argues against 1:2 binding. The enantiomers of the same solute must have the same binding behavior. Since 1:2 binding was excluded in the case of the first eluting enantiomer of homatropine (Table 3.28), it is also ignored for the second enantiomer.

Table 3.28 Curve fitting statistics for the S-enantiomer of propranolol with tetra-sulfated β-CD.

1:1 BINDING		
	Limited Range	**NDS Correction**
μ_A*	1.535	1.535
μ_{ACD}*	-1.72 ± 0.07	-1.36 ± 0.02
K (M^{-1})	$(6.1 \pm 0.4) \times 10^2$	$(8.3 \pm 0.4) \times 10^2$
R^2	0.9987	0.9995
Fitting Equation	$y = (1.535 + \mu_{ACD}K[CD])/ (1 + K[CD])$	
1:1 +1:2 BINDING		
	Limited Range	**NDS Correction**
μ_A*	1.535	1.535
μ_{ACD}*	-2 ± 1	-1 ± 4
K_1 (M^{-1})	$(5 \pm 1) \times 10^2$	$(0.8 \pm 1) \times 10^3$
$\mu_{A(CD)2}$*	$(-0.2 \pm 2) \times 10^2$	-0.001 ± 3300
K_2 (M^{-1})	-4 ± 400	-0.4 ± 1000
R^2	0.9998	0.9995
Fitting Equation	$y = 1.535 + \frac{(\mu_{ACD} - 1.535)K_1[CD] + (\mu_{A(CD)_2} - 1.535)K_1K_2[CD]^2}{1 + K_1[CD] + K_1K_2[CD]^2}$	

*unit: 10^{-4} $cm^2/(Vs)$.

Both Limited Range and NDS Correction approaches yield good fits for 1:1 binding and give comparable stability constants and complex mobilities. The negative values obtained for 1:2 binding stability constants excluded the possibility of 1:2 binding.

Table 3.29 Curve fitting statistics for the R-propranolol with tetra-sulfated β-CD.

1:1 BINDING		
	Limited Range	**NDS Correction**
μ_A*	1.535	1.535
μ_{ACD}*	-1.74 ± 0.06	-1.39 ± 0.02
K (M^{-1})	$(6.7 \pm 0.4) \times 10^2$	$(9.3 \pm 0.4) \times 10^2$
R^2	0.9988	0.9994
Fitting Equation	$y = (1.535 + \mu_{ACD}K[CD])/ (1 + K[CD])$	
1:1 +1:2 BINDING		
	Limited Range	**NDS Correction**
μ_A*	1.535	1.535
μ_{ACD}*	-2 ± 1	-1 ± 2
K_1 (M^{-1})	$(5 \pm 1) \times 10^2$	$(9 \pm 8) \times 10^2$
$\mu_{A(CD)2}$*	5 ± 200	1 ± 6500
K_2 (M^{-1})	9 ± 300	0.3 ± 800
R^2	0.9998	0.9994
Fitting Equation	$y = 1.535 + \frac{(\mu_{ACD} - 1.535)K_1[CD] + (\mu_{A(CD)_2} - 1.535)K_1K_2[CD]^2}{1 + K_1[CD] + K_1K_2[CD]^2}$	

*unit: 10^{-4} $cm^2/(Vs)$.

For the R enantiomer of propranolol, the stability constants for 1:2 binding (K_2) are positive. However the small values of 9 M^{-1} and 0.3 M^{-1} (NDS) for 1:2 binding compared with the stability constants for 1:1 binding of 500 M^{-1} (EOF) and 900 M^{-1} (NDS) are negligible. Thus only 1:1 binding will be considered in further studies.

For all the solutes examined here the complex mobilities and stability constants obtained for 1:2 binding are either not physically meaningful or are very small compared with 1:1 complex stability constants. Thus the 1:2 binding stoichiometry can be considered negligible. We can conclude that 1:1 binding is the dominant complex form in tetra-sulfated cyclodextrin mediated buffers. The complex mobilities and stability constants obtained for 1:1 binding using the EOF and NDS correction approaches are comparable. In the discussion that follows, results obtained using each correction approach are shown. The difference between the EOF and NDS correction approaches is taken as the uncertainty.

The free solute mobilities and complex mobilities for all nine solutes are summarized in Table 3.30 and 3.31 below. The complex mobilities of imidazole, 1-methylimidazole, and diphenhydramine are directly taken as the plateau mobility from their mobility curve, and the average of the uncertainties obtained for other solutes are used for their uncertainties. Since Limited Range could not apply to benzylamine, the complex mobility from nonlinear curve fitting without correction was used in Table 3.30 and Figure 3.13. For all the other solutes complex mobilities are obtained by nonlinear curve fitting as specified.

Table 3.30 Free and complex mobility data with tetra-sulfated β-CD (Limited Range approach).

Solute	μ_{free} ($cm^2/(Vs)$)	μ_{cpx} ($cm^2/(Vs)$)
Imidazole	3.791	3.1 ± 0.3
Methylimidazole	3.599	2.8 ± 0.3
Benzylamine	2.650	0.3 ± 0.0
benzyltrimethylammonium	2.552	-1.1 ± 0.4
4-(aminomethyl)benzene sulfonamide	2.267	-1.2 ± 0.3
Histidine	2.117	0.9 ± 0.2
Homatropine	1.779	-1.4 ± 0.3
	1.779	-1.5 ± 0.4
Diphenhydramine	1.731	-2.1 ± 0.3
Propranolol	1.535 (S)	-1.7 ± 0.4
	1.535 (R)	-1.7 ± 0.4

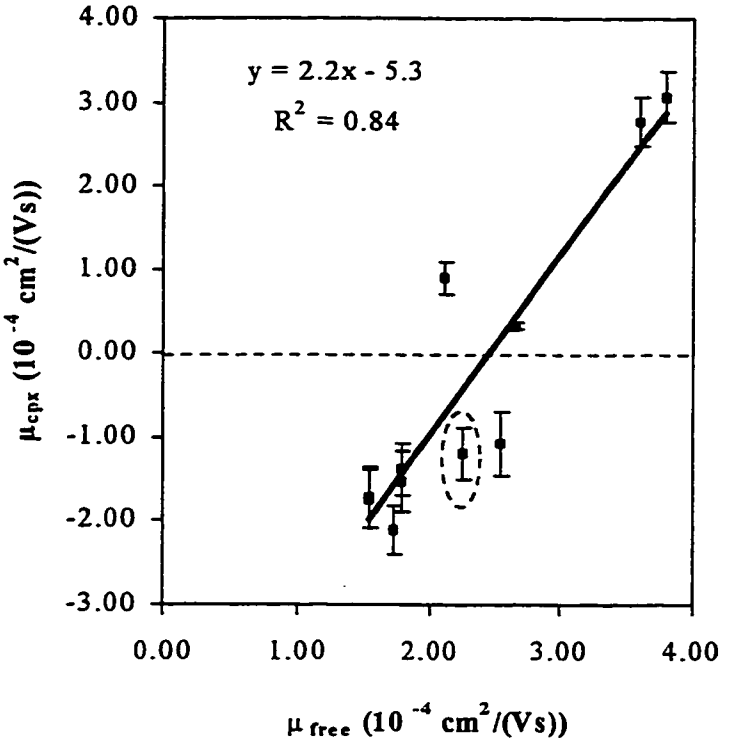

Figure 3.13 Solute-tetra-sulfated β-CD complex mobilities (Limited Range approach) as a function of free solute mobilities. The error bars are the differences between the complex mobilities obtained by Limited Range and NDS Correction approaches. Experimental conditions are as shown in Figure 3.10 to 3.15. The data point in the dotted oval is 4-(aminomethyl)benzene sulfonamide.

Table 3.31 Free and complex mobility data with tetra-sulfated β-CD (NDS Correction approach).

Solute	μ_{free} ($cm^2/(Vs)$)	μ_{cpx} ($cm^2/(Vs)$)
Imidazole	3.791	3.1 ± 0.3
Methylimidazole	3.599	2.8 ± 0.3
Benzylamine	2.650	0.3 ± 0.0
benzyltrimethylammonium	2.552	-0.7 ± 0.4
4-(aminomethyl)benzene sulfonamide	2.267	-0.9± 0.3
Histidine	2.117	1.1 ± 0.2
Homatropine	1.779	-1.1 ± 0.3
	1.779	-1.2 ± 0.4
Diphenhydramine	1.731	-2.1 ± 0.3
Propranolol	1.535 (S)	-1.4 ± 0.4
	1.535 (R)	-1.4 ± 0.4

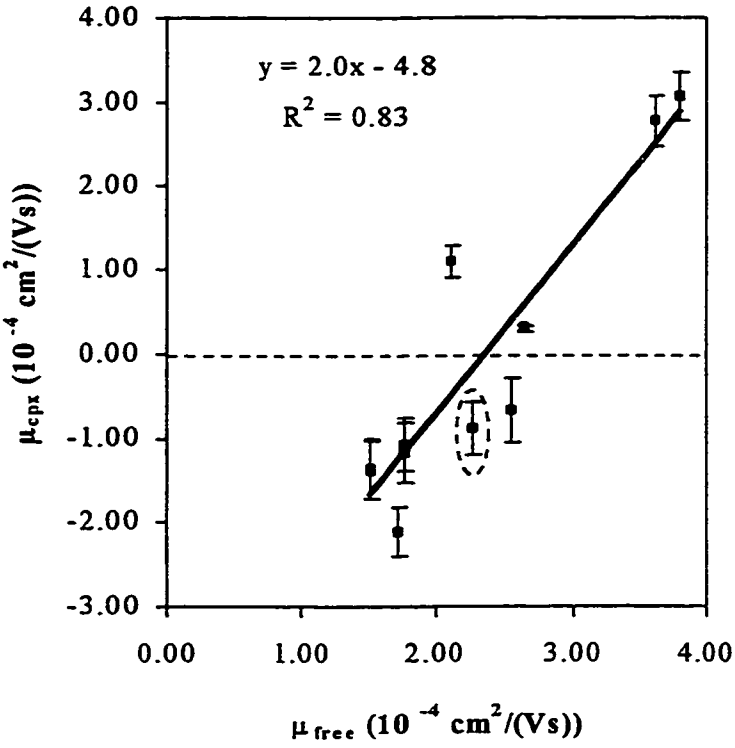

Figure 3.14 Solute-tetra-sulfated β-CD complex mobilities (NDS Correction approach) as a function of free solute mobilities. The error bars are the differences between the complex mobilities obtained by Limited Range and NDS Correction approaches. Experimental conditions are as shown in Figure 3.8 to 3.12. The data point in the dotted oval is 4-(aminomethyl)benzene sulfonamide.

As was seen with 13-sulfated β-CD in Figure 3.6 and 3.7, a linear relationship can be found between the solute-tetra-sulfated β-CD complex mobility and the free solute mobility. Different mobility correction approaches give similar slopes and slightly different intercepts. Note the data point in the dotted oval in Figure 3.13 and 3.14 is 4-(aminomethyl)benzene sulfonamide (AB), which is a di-cation at pH 4.6. Surprisingly,

the free mobility of 4-(aminomethyl)benzene sulfonamide is not faster than other monocharged cations even though its molecular weight is not much bigger than the other solutes. And the complex mobility of 4-(aminomethyl)benzene sulfonamide fits in the linear fitting line quite well.

The significance of Figures 3.13 and 3.14, along with Figure 3.6 and 3.7, will be discussed in Section 3.3.4.

3.3.3 MOBILITY MEASUREMENTS WITH NEUTRAL β-CYCLODEXTRIN

A correlation similar to those observed in Section 3.3.1 and 3.3.2 is found in data from the literature **[5]**. Britz-McKibbin and Chen studied the migration behavior of a group of deoxyribonucleotides (dNPs) at various concentrations of β-cyclodextrin. They then determined the analyte-cyclodextrin complex mobilities based on the Wren-Rowe model (Equation 1-14) using viscosity-corrected mobilities. The above obtained complex mobilities are plotted in Figure 3.15 against the free solute mobilities of these deoxyribonucleotides.

Again, a linear relationship is found between the data points in Figure 3.15. The weighted regression line has a slope of ~ 0.55 and an intercept of ~ $0.001 \times 10^{-3} cm^2/(Vs)$. The error bars are the standard deviations provided by the authors except the one for dCTP, which was estimated from dCDP. Although the weighted linear regression does not provide a correlation coefficient, a good correlation can be seen. All data points are statistically on the weighted regression line.

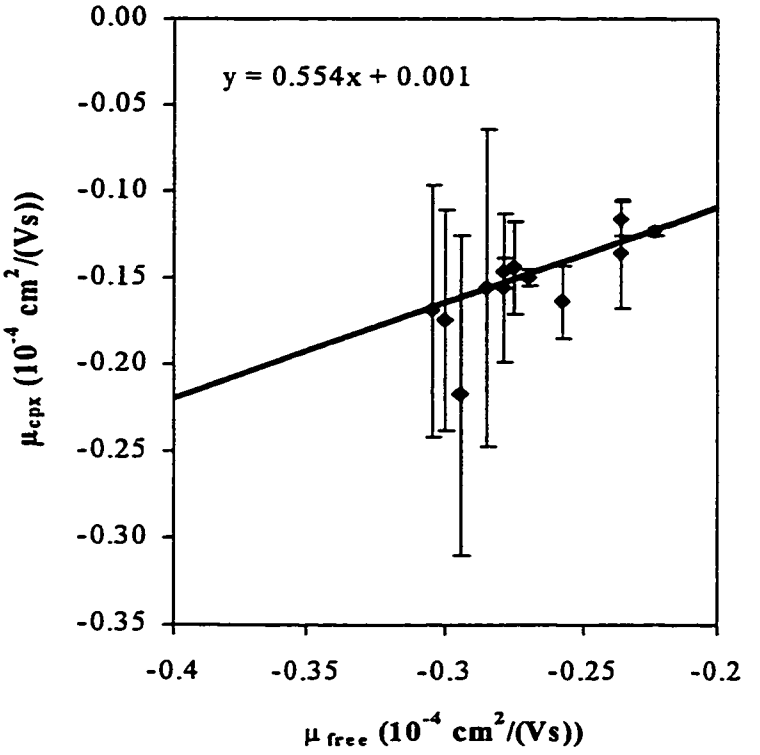

Figure 3.15 Deoxyribonucleotides-β-CD complex mobilities as a function of free deoxyribonucleotides mobilities. The error bars indicate standard deviations associated with each data point. The line is the weighted regression line. Conditions: 5.0×10^{-5} M deoxyribonucleotide sample solution, 160 mM borate buffer, pH = 9.0, electric field = 185 V/cm, T = 20 °C, λ =254 nm.

Our Mobility Conservation Model (Section 3.3.4) states that the intercept is related to the free cyclodextrin mobility. When neutral cyclodextrins are used, the free CD mobility, μ_{CD}, is zero. So the intercept should be zero. The weighted linear regression result (0.001×10^{-3}cm^2/(Vs)) in Figure 3.15 agrees very well with this expectation.

Table 3.32 Mobility measurement of deoxyribonucleotides with neutral β-CD[a].

Solute	$\mu_A \times 10^3$ ($cm^2/(Vs)$)	$\mu_{ACD} \times 10^3$ ($cm^2/(Vs)$)
dAMP	-0.2241 ± 0.0004	-0.123 ± 0.002
dGMP	-0.2359 ± 0.0004	-0.116 ± 0.010
dCMP	-0.2359 ± 0.0004	-0.136 ± 0.031
dUMP	-0.2572 ± 0.0004	-0.164 ± 0.021
dADP	-0.2701 ± 0.0005	-0.150 ± 0.005
dGDP	-0.2748 ± 0.0004	-0.144 ± 0.027
dATP	-0.2793 ± 0.0003	-0.147 ± 0.009
dGTP	-0.2793 ± 0.0003	-0.156 ± 0.043
dCDP	-0.2847 ± 0.0004	-0.217 ± 0.092
dCTP	-0.2941 ± 0.0004	-2.18[b] ± 0.092[c]
dUDP	-0.2994 ± 0.0004	-0.174 ± 0.064
dUTP	-0.3042 ± 0.0004	-0.169 ± 0.073

a. Experimental conditions are as in Figure 3.15.

b. Approximated value.

c. The standard deviation value is not available from the original paper.

This value is estimated from dCDP for they have similar μ_{ACD} values.

3.3.4 MOBILITY CONSERVATION MODEL

As mentioned in Section 3.1, people have intuitively thought that when solutes and cyclodextrins form complexes, they loose their individual electrophoretic properties. The complex mobility will then depend on the net charge and the total volume (mainly

determined by the much larger CD). However, the fact that some complexes have positive mobilities even if they are –3 or –12 charged shakes this belief.

Furthermore, the complex mobilities are found to vary over a range comparable to the free solute mobility range when charged CDs are used. They increase as the free solute mobility increases, and decrease when the free solute mobility decreases. Linear regressions revealed very good correlation between free solute mobilities and complex mobilities (Figures 3.6, 3.7 and 3.13-3.15).

Based on these observations a Mobility Conservation Model is proposed as follows.

The solutes and the cyclodextrins keep their individual electrophoretic properties even after they form complexes. The complex migration rate is not merely determined by the net charge and total volume of the complex. When positively charged solutes and negatively charged cyclodextrins are used, the uncomplexed solutes and cyclodextrins are drawn to different electrodes by electrostatic attractions, and thus move in opposite directions. Even when they are in a complex, they still try to move in the direction determined by their individual charges, forming two opposing forces on the complex. The migration direction of the complex depends on whether the solute or cyclodextrin moves faster.

We can write the concept in an equation as follows:

$$\mu_{cpx} = k\mu_A + f(\mu_{CD}) \qquad (3\text{-}2)$$

where k is a constant and the second term is a function of free cyclodextrin mobility. Obviously if we plot μ_{cpx} versus μ_A, k will be the slope and $f(\mu_{CD})$ the intercept.

The constant k is a quantity related to the solute properties. We do not know for sure what factors determine this constant. It does not seem to be directly related to the complex stability constants K. Since for neutral β-CD, tetra- and 13-sulfated β-CDs, 13-sulfated β-CD has the highest stability, yet the plot with tetra-sulfated β-CD has the highest k (and Table 3.35). The plot with neutral β-CD has the lowest k (Figure 3.18), so it is not simply inversely related either. Nonetheless, it can be seen that k is an important parameter determining the extent of separation. When k is large, the slope is steeper, even a small change in the free solute mobility can cause a big difference in the complex mobility, so the separation will be easy. Whereas when k is small, even a big difference in free solute mobility can not cause sufficient difference in the complex mobilities, thus the separation will be difficult. Therefore, the understanding of what determining k is of fundamental importance. Knowledge about k will also provide useful insight in rational design of chiral selectors.

The function $f(\mu_{CD})$ is related to the free cyclodextrin mobility. Since there is not any appropriate method to measure the mobilities of the two charged CDs we used, it is hard to know exactly what function is it.

A simplest case is considered here where $f(\mu_{CD}) = k\mu_{CD}$. In this case Equation 3-2 becomes

$$\mu_{cpx} = k\mu_A + k\mu_{CD} = k(\mu_A + \mu_{CD}) \qquad (3\text{-}3)$$

That is the free CD mobility and free solute mobility are related to the complex mobility through the same constant k. Now k does not only depend on solute properties, but also on cyclodextrin properties. Thus for different types of cyclodextrins, both the slope and the intercept of the linear regression lines should be different. For neutral cyclodextrins,

since μ_{CD} is zero, the intercept should be zero. The very small intercept (0.001×10^{-3} $cm^2/(Vs)$) in Figure 3.18 agrees with this expectation very well.

Equation 3-2 also states that when oppositely charged cyclodextrins and solutes are used the migration direction (positive for cathodic and negative for anodic) is determined by the relative magnitude of the free solute mobility and the free cyclodextrin mobility. The slope in the μ_{cpx} versus μ_A plot is the constant k. The intercept is the product of constant k and free CD mobility μ_{CD}. Then by dividing the intercept with the slope, we will obtain the mobility of the cyclodextrin.

A test was done on this postulate with Figure 3.8, 3.9, 3.16, and 3.17. The slopes and intercepts of these regression lines and the calculated free cyclodextrin mobilities are listed in Table 3.43 below. The uncertainties associated with the slopes and intercepts are obtained using the Microsoft Excel Linest function.

Table 3.33 Linear regression results in Figure 3.6, 3.7, 3.13 and 3.14 and the calculated free cyclodextrin mobilities.

CD Type	Figure	Slope	Intercept[a]	$\mu_{CD,cal}$[a]
13-Sulfated β-CD	3.8	1.4 ± 0.1	-2.6 ± 0.4	-1.9
	3.9	1.3 ± 0.2	-2.2 ± 0.4	-1.7
4-Sulfated β-CD	3.16	2.2 ± 0.3	-5.3 ± 0.8	-2.4
	3.17	2.0 ± 0.3	-4.8 ± 0.7	-2.4

a. Unit: $10^{-4} cm^2/(Vs)$.

The negative sign before calculated free cyclodextrin mobilities indicates that negatively charged cyclodextrins move in the anionic direction. Thus when the free solute mobility is greater than the absolute value of the cyclodextrin, the complex mobility will be positive (cationic); and when the absolute value of the cyclodextrin mobility is greater than the solute mobility, the complex mobility will be negative (anionic). Taking the calculated cyclodextrin mobilities back to Table 3.16, 3.17, 3.30 and 3.31, the prediction agrees with experimental data very well. There is some difficulty in predicting the migration direction of the data points that have very similar mobilities to cyclodextrin. For instance, the free mobility of homatropine is $1.829 \times 10^{-4}cm^2/(Vs)$, close to the mobility value of 13-sulfated cyclodextrin (1.92 and $1.61 \times 10^{-4}cm^2/(Vs)$). Using the cyclodextrin mobility to determine the migration direction of homatropine complex, it would be negative in Table 3.16, and be positive in Table 3.17. The experimental result is positive. For tetra-sulfated cyclodextrin, the free mobility of benzyltrimethylammonium ($2.552 \times 10^{-4}cm^2/(Vs)$) is close the calculated free CD mobility (2.46 and $2.37 \times 10^{-4}cm^2/(Vs)$), this method failed to tell the negative mobility of benzyltrimethylammonium. Histidine has abnormally high complex mobility, this method would predict it has negative complex mobility instead of the reality that it has positive mobility. Nonetheless, this method is successful in predicting the complex migration direction of all the other solutes.

In section 2.4.1.2.3 we have calculated the complex mobility for methyl mandelate and tetra-sulfated β-CD. Since methyl mandelate is neutral, it does not have any intrinsic mobility. So the complex mobility should be close to the free cyclodextrin mobility. The results obtained for mandelate are: -2.2 ± 0.9 (Limited Range) and $-3.5 \pm$

0.2 (NDS Correction) for the S enantiomer; -2.2 ± 0.7 (Limited Range) and –3.1 ± 2 (NDS Correction) for the R enantiomer. These values are very close to what calculated in Table 3.35 for tetra-sulfated β-CD.

However, although Equation 3-3 had some success in explaining experimental data, the conclusion is not to be drawn instantly. The determination of free cyclodextrin mobility is the key to study the second term in Equation 3-2. What we can say without doubt is that there is a linear relationship between the free solute mobilities and the solute-CD complex mobility.

3.4 REFERENCES

1. Perrin, D.D. *Dissociation Constants of Organic Bases*, Butterworths, London, 1965.
2. Lide, D.R., Editor in chief, *CRC Handbook of Chemistry and Physics 76th edition*, CRC press, 1996.
3. Penn, S. G.; Bergstrom, E. T.; Goodall, D. M. *Anal. Chem.* 1994, 66, 2866-2873.
4. Wren, S. A.; Rowe, R. C. *J. Chromatogr.* 1992, 603, 235-241.
5. Britz-McKibbin, P.; Chen, D.D.Y. *J. Chromatogr. A* 1997, 781, 23-34.

CHAPTER 4 FUTURE WORK

There are a number of areas for future work to be done on cyclodextrin mediated capillary electrophoresis. In this chapter I will detail a few ideas of what should be done.

4.1 CYCLODEXTRIN MOBILITY MEASUREMENT

Free positive solutes and negatively charged cyclodextrins migrate in opposite directions. The positive solutes move in the cathodic direction (positive), while the negative cyclodextrins move in the anodic direction (negative). From Equation 3-2 it is obvious that the migration of the solute-CD complex depends on both the free CD mobility and the free solute mobility. The free solute mobility can be obtained directly from experiments with buffers not containing cyclodextrins. Some further understanding of the relationship between the free solute mobility and the complex mobility was gained in this thesis (Section 3.4.3). The mobility of the complex can be determined as discussed in Chapters 2 and 3. The final information required is to fully understand the behavior of the intrinsic mobility of cyclodextrins. This would allow us to test the accuracy of the Mobility Conservation Model.

In the literature 3 types of anionic cyclodextrin derivatives (carboxymethyl β-cyclodextrin, sulfobutylether β-cyclodextrin, and sulfoethylether β-cyclodextrin) have been characterized by CE [1]. Indirect detection was used due to the weak UV absorbance of the cyclodextrins. Benzoate was added to the background electrolyte which was buffered at pH 6.0. The individual components of the CD mixtures were then separated electrophoretically. When an anionic CD is present in the buffer there must be a decrease in the localized benzoate concentration in order to maintain electroneutrality.

This decrease in benzoate concentration causes a decrease in the UV absorbance. The magnitude of this decrease is directly related to the concentration of charged CD. Similar method was also used by Luna et al to analyze sulfobutyl ether β-cyclodextrin mixtures [2].

Unfortunately our attempts to use this procedure in our buffer system were unsuccessful. Our buffer was very concentrated in order to minimize the ionic strength contribution from the cyclodextrins. Unfortunately, the high concentration of buffer ion in our system reduced the signal-to-noise achieved for the benzoate displacement. To further complicate the measurements our sulfated cyclodextrins are mixtures, and so no single component can fully represent the mobility of the whole mixture. We will probably have to average the different mobilities or, to use single isomer anionic cyclodextrins. Therefore, the characterization method will have to be altered to be closer to our experimental conditions to give us useful data; and a proper method has to be developed to obtain the correct free cyclodextrin mobilities.

4.2 IONIC STRENGTH EFFECT OF CHARGED CYCLODEXTRINS

Another consideration is that our CDs are multiply charged. The addition of such a CD to a buffer increases the ionic strength significantly. If we could calculate the ionic strength introduced by the cyclodextrins, the mobility in any ionic strength buffer will be given by [3]:

$$\mu = \mu_0 - Az\frac{\sqrt{I}}{1+2.4\sqrt{I}} \qquad (4\text{-}1)$$

where μ is the mobility of an ion under any ionic strength, μ_0 is the infinite dilution mobility of the ion, A is a constant, z is the charge on the solute, and I is the ionic strength of the buffer and is given by

$$I = \frac{1}{2}\sum_i z_i^2 c_i \qquad (4\text{-}2)$$

where z_i and c_i are the charge and concentration of each ion *i*.

Based on equation 4-1, the multiply charged CD ($z > 1$) used in our studies will be affected by the increase in ionic strength more strongly than the monocharged analyte ions ($z = 1$). Therefore while the free mobility of the solute stays relatively constant, the free mobility of the cyclodextrins would decrease as more and more cyclodextrin is added. Therefore the mobility ratio of the solute and the charged cyclodextrin will change as the cyclodextrin concentration goes up. The net result of this ionic strength effect is that the complex mobility would become more cathodic. This is indeed what was observed in Chapters 2 and 3. This ionic strength effect then may be part or all of the reason why we were seeing an upward drifting of the solute apparent mobility in Chapters 2 and 3.

Unfortunately the ionic strength can not be calculated for the charged cyclodextrins used in this work. This is because our CDs not only contain a mixture of different substitution numbers and patterns, but also contain significant concentrations of impurities such as formate (Gy. Vigh of Texas A&M, personal communication, February 1998). Thus it is impossible to accurately determine the charges and concentrations of each species. In our studies, we used high concentrations of zwitterionic buffer to keep

the ionic strength at a high level so that the addition of charged cyclodextrins would not have big impact on the ion mobilities in the system.

Some isomerically pure negative cyclodextrins became commercially available from Regis (Texas, USA) in 1998. These charged CDs are based on the work of Vigh et al.[4][5][6]. These CDs claim to have 100% purity and to be isomerically pure. These pure single-isomer cyclodextrins would make possible the study of CD-induced ionic strength effects and would make the cyclodextrin mobility determined in Section 5.1 more meaningful.

4.3 FURTHER STUDY OF ANOMALOUS SOLUTE MOBILITY BEHAVIORS

We have observed some odd solute mobility behavior in Chapter 3. Naphthalene disulfonic acid showed an increase in anodic mobility when low concentrations of either 13-sulfated CD (Figure 3.5) or tetra-sulfated CD (Figure 3.14) was added to the buffer solution. In contrast, imidazole and 1-methylimidazole increased in cathodic mobility at low tetra-sulfated CD concentrations. These increases in absolute ion mobilities can neither be explained by EOF effect, which should be negligible at low cyclodextrin concentrations, nor by ionic strength effect, which always causes a decrease in ionic mobilities. Since charged cyclodextrins are often used in low concentrations due to their high resolving power, an understanding of these odd behaviors at low CD concentrations is of special importance.

4.4 PARTIAL FILLING TECHNIQUE WITH 13-SULFATED β-CYCLODEXTRIN

The 13-sulfated cyclodextrin is UV absorbing. This makes detection of analytes difficult, especially when the concentration of cyclodextrin is high. Also the price of sulfated cyclodextrins is too high (US$300/100g) for them to be used as a buffer component for routine analysis, where tens of grams are required to make the series of solutions necessary to find out the optimum separation conditions.

One possibility that can solve this problem is partial filling technique. In this technique, cyclodextrins and analytes pass the detection widow at different times and only very small amount of cyclodextrins are needed.

Partial filling refers to a special way of doing electrophoretic separations in which only part of the capillary is filled with the buffer containing the resolving additive. The rest of the capillary is filled with additive-free buffer. Generally the solute has an opposite charge to that of the additive. After the solute is injected into the capillary, the solute and additive zones will migrate in opposite directions. They will meet in the middle of the capillary and interact while the solute is in the additive zone. After the solute leaves the additive zone, it moves toward the detector while the additive moves away from the detector.

The partial filling technique is most commonly used when the resolving additive interferes with detection. Tanaka et al. applied this technique coupled with mass-spectrometry to separate negative analytes using a positively charged cyclodextrin [7]. In this manner the partial filling technique prevented high concentrations of nonvolatile cyclodextrins from interfering with the mass spectrometry.

Preliminary results of partial filling technique using 13-sulfated cyclodextrin are presented in the following sections.

4.4.1 EXPERIMENTAL

4.4.1.1 APPARATUS AND PROCEDURES

All the experiments were carried out on a Beckman P/ACE 2100 capillary electrophoresis instrument (Fullerton, CA, USA). The capillary used is a polyacrylamide coated neutral capillary (eCap, Beckman) with an internal diameter of 50 □m and total length of 27cm (for homatropine) and 37 cm (for propranolol). The detection window was 7 cm from the end of capillary.

If an untreated capillary was used instead, there will be electroosmotic flow (EOF) existing in such capillary. The EOF will bring both the analyte and the cyclodextrin to the cathode since the magnitude of the flow is generally greater than the migration rate of all solutes. Therefore a neutral polyacrylamide coated capillary was used here to ensure the analyte and the cyclodextrin migrate in opposite directions, and thus pass through the detection window at different times.

Absorbance of solutes was measured at 214 nm. An electric field strength of 270 V/cm was used for all experiments. The capillary cartridge was thermostatted at 20 °C.

4.4.1.2 REAGENT

13-Sulfated β-cyclodextrin was purchased from Cerestar (Hammond, IN, USA). Buffer components MES (morpholino-ethanesulfonic acid monohydrate) and Jeffamine 900 (poly(propylene glycol-*b*-ethylene glycol-*b*-propylene glycol) bis(2-aminopropyl

ether)) were obtained from Sigma-Aldrich Canada Ltd. (Oakville, Ontario). Analytes homatropine (±) and propranolol (DL) (99%) were obtained from Sigma-Aldrich Canada as well. The structures of these solutes were shown previously (Figure 2.2). All reagents were used as received. All solutions were filtered through a 0.45 μm nylon syringe filter (Nalge Company, Rochester, NY, USA) before use.

4.4.2 PROCEDURES AND CALCULATIONS

4.4.2.1 PROCEDURES

The capillary was first rinsed under high pressure (20 p.s.i.) with 200 mM MES buffer (pH = 4.6) for 2 min. At this time the whole capillary is filled with this buffer (Figure 4.1a). Then, an identical buffer containing sulfated β-cyclodextrin was injected (0.5 p.s.i.) into the capillary for a certain period of time, forming a sulfated β-cyclodextrin buffer plug (Figure 4.1b). Next, this buffer plug was pushed under low pressure (0.5 p.s.i.) for 4 min (37 cm capillary) or 2 min (27 cm capillary) into the center of the capillary. The analyte solution (in 200 mM MES buffer) is now injected into the capillary (Figure 4.1c). A voltage of 10 kV (37 cm capillary) or 7.3 kV (27 cm capillary) is then applied across the capillary. The positively monocharged analyte and the negatively charged cyclodextrins migrate in opposite directions. They meet in the center of the capillary and interact. The enantiomers of the analyte get resolved during the time they are in the cyclodextrin buffer zone (Figure 4.1d). After the enantiomers

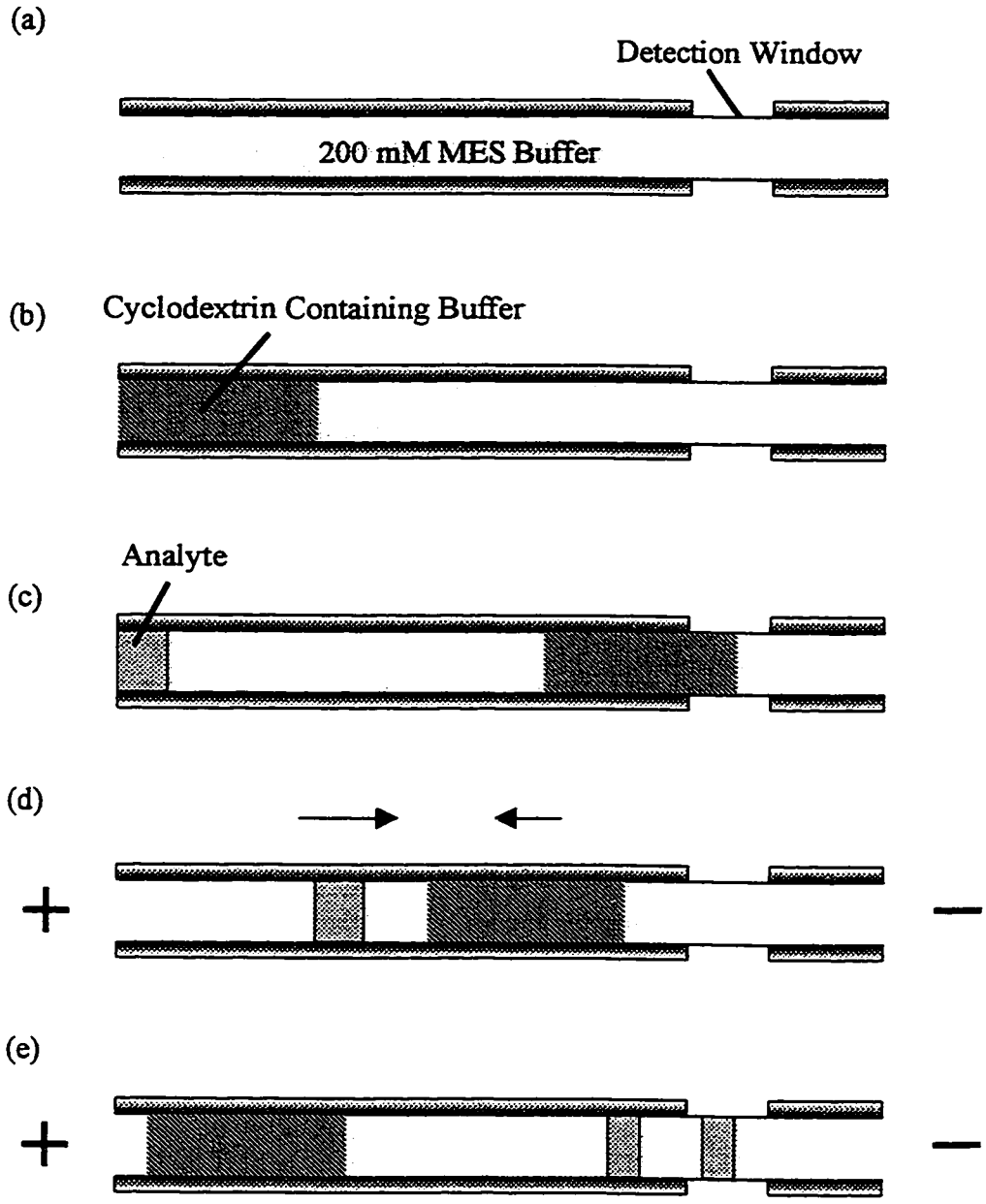

Figure 4.1 Schematic procedures of partial filling technique. See Section 4.4.2.1 for details.

migrate out of the cyclodextrin buffer zone, they will move towards the cathode at their native mobility and are detected. Meanwhile the cyclodextrin zone moves away from the detection window, and so does not interrupt the detection of the analyte.

4.4.2.2 CALCULATION OF CYCLODEXTRIN BUFFER PLUG LENGTHS

In Section 4.3.1, the length of cyclodextrin-containing buffer plug is controlled by the time of injection. However, time would change from instrument to instrument and be different for different capillaries. Therefore, it is desirable to use length units instead of time units to describe the plug.

To transfer time units to length units, the time (t_0) needed to push the buffer solution from the injection end of the capillary to the detector (l_0) was determined. The injection time (t) of the cyclodextrin-containing buffer is then compared with t_0 to determine the injection plug length (l_{plug}) as expressed in Equation 4-3.

$$l_{plug} = l_0 \, (t/t_0) \qquad (4\text{-}3)$$

This calculation ignores the viscosity difference between the cyclodextrin-containing buffer and the cyclodextrin-free buffer. However since the plugs are generally short relative to the total capillary length, the impact of the plug viscosity should be minimal.

4.4.3 RESULTS AND DISCUSSION

Two 13-sulfated cyclodextrin concentrations, 4 mM and 24 mM, were chosen to represent low concentrations and high concentrations of chiral selector, respectively. Experiments were performed according to the procedures described in Section 4.4.2.1.

The same concentration of 13-sulfated β-cyclodextrin solution was injected into the capillary for different periods of time. Electropherograms were then recorded during high voltage separation (Figure 4.1d).

4.4.3.1 RESULTS FOR HOMATROPINE WITH PARTIAL FILLING WITH 4 mM 13-SULFATED β-CYCLODEXTRIN

The electropherograms obtained for homatropine using 4 mM 13-sulfated cyclodextrin as resolving agent are shown in Figure 4.2. The CD-containing buffer was injected for 0s, 10s, 20s, 30s, 60s, and 90s. These times are converted to length according to Equation 4-3 and the results are listed in Table 4.1. The data in the first column is that obtained for pushing CD-free buffer under low pressure all the way to the detector (20 cm). This time was used to convert all other times to distance units.

Table 4.1 4 mM 13-sulfated β-CD-containing buffer plug length conversion.

t (s)	170.4	0	10	20	30	60	90
***l* (cm)**	20	0	1.2	2.3	3.5	7.0	10.6

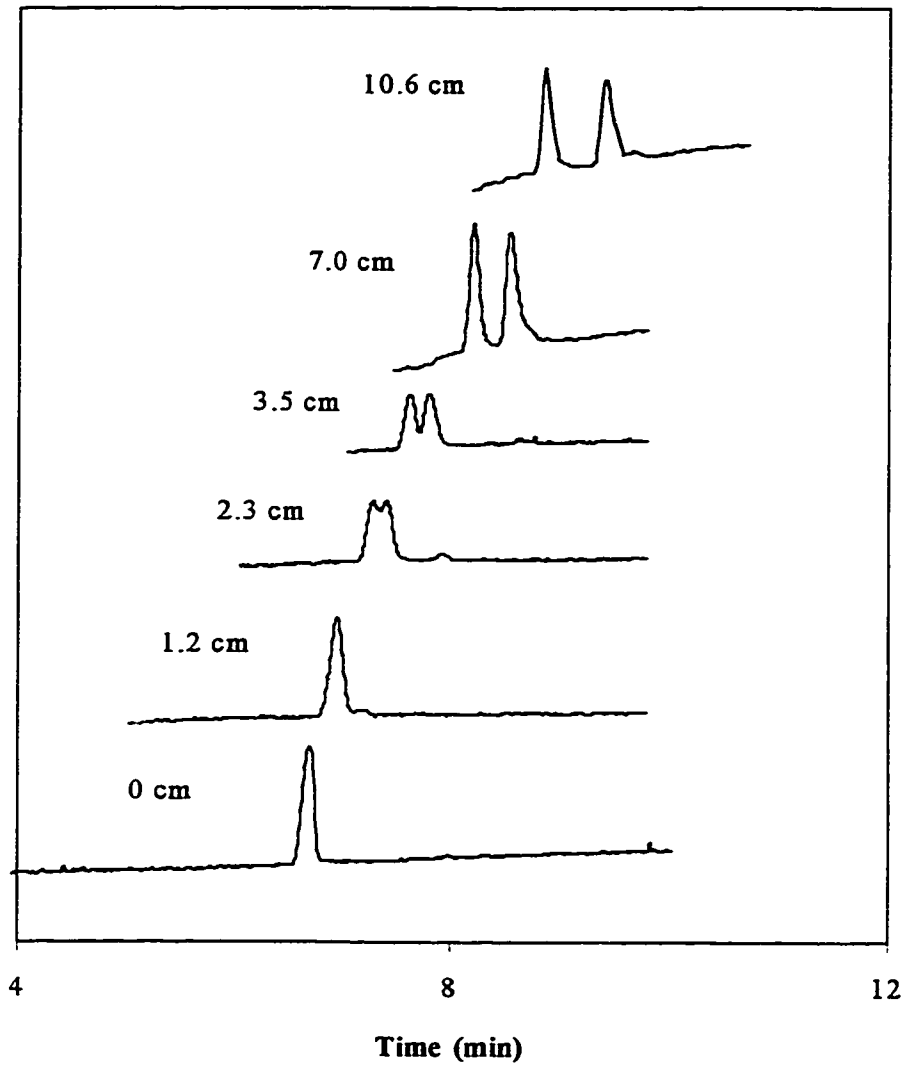

Figure 4.2 Electropherograms of homatropine with 4 mM 13-sulfated cyclodextrin. The number besides each electropherogram is the approximate cyclodextrin buffer plug length. Experimental conditions: $\lambda = 214$ nm, T = 20°C, capillary 27/20 cm, V = 7.3 kV, homatropine concentration = 2×10^{-4} M, all buffers are adjusted to pH 4.6.

A few observations can be drawn from Figure 4.2:

(a) The migration time of the analyte increases as the cyclodextrin buffer plug increases, i.e., as the interaction time getting longer. This is because the complexation with negatively charged cyclodextrin slows down the apparent positive mobility of the analyte.

(b) The resolution between the enantiomers improves as the interaction time increases.

(c) Baseline separation was achieved within 10 minutes. In contrast, 35 minutes were required for the separation using a capillary fully filled with 4 mM 13-sulfated β-cyclodextrin.

4.4.3.2 RESULTS OF HOMATROPINE WITH PARTIAL FILLING WITH 24 mM 13-SULFATED β-CYCLODEXTRIN

Partial filling with 24 mM 13-sufated β-CD was performed in the same manner as in Section 4.4.3.1 to separate homatropine. The CD-buffer plug lengths are converted in Table 4.2.

Table 4.2 24 mM 13-sulfated β-CD-containing buffer plug length conversion.

t (s)	170.4	0	5	10	15	20
***l* (cm)**	20	0	0.6	1.2	1.8	2.3

t (s)	30	40	50	60	90
***l* (cm)**	3.5	4.7	5.9	7.0	10.6

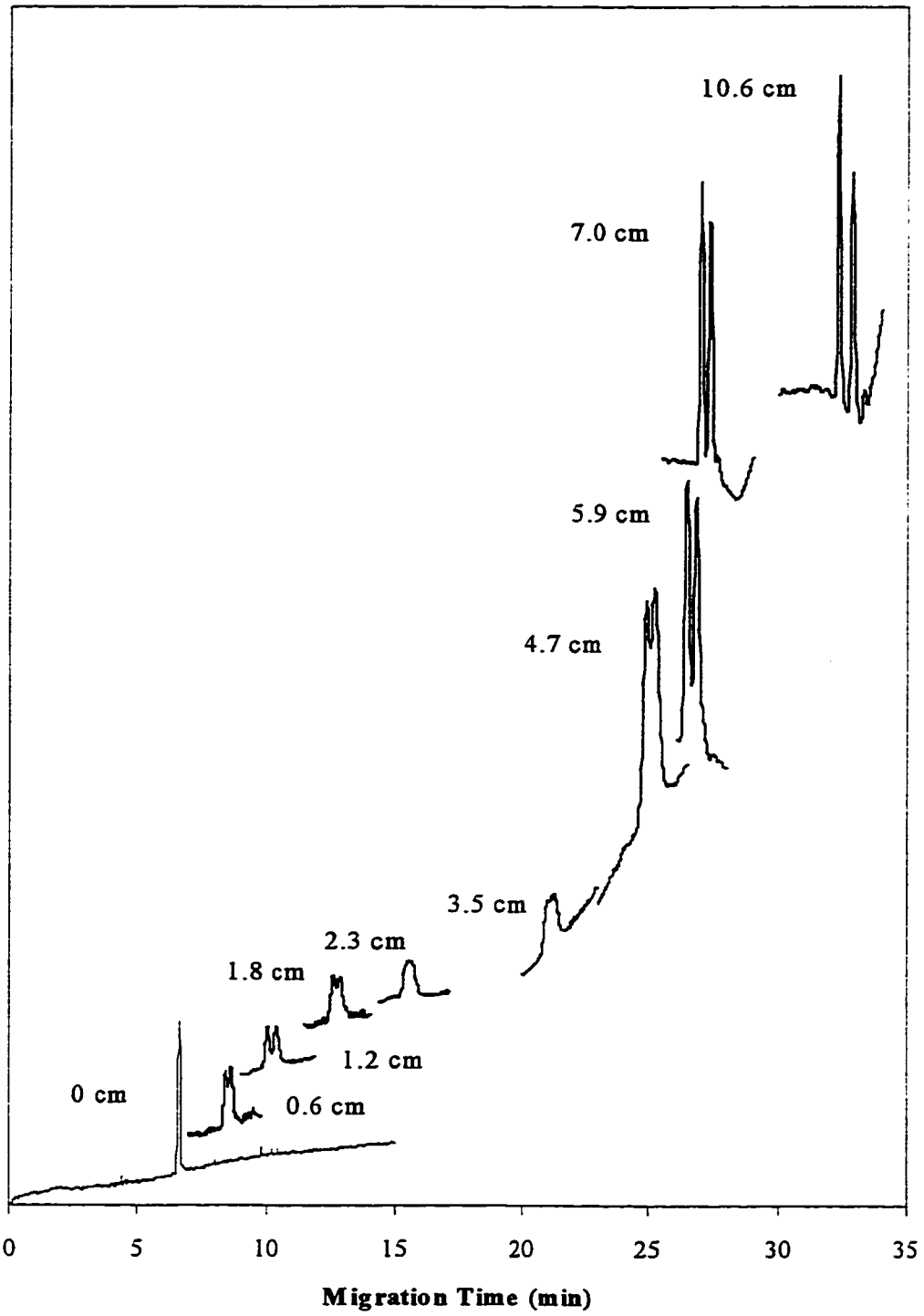

Figure 4.3 Partial filling electropherograms of homatropine with 24mM 13-sulfated cyclodextrin. The number besides each electropherogram is the

approximate cyclodextrin buffer plug length. Experimental conditions: λ = 214 nm, T = 20°C, capillary 27/20 cm, V = 7.3 kV, homatropine concentration = 2×10^{-4} M, all buffers are adjusted to pH 4.6.

The migration time of homatropine is longer with 24 mM 13-sulfated β-CD (~ 30 min at 10.6 cm cyclodextrin plug length) than with 4 mM 13-sulfated β-CD (~ 10 min at 10.6 cm cyclodextrin plug length). This longer migration time indicates a stronger influence of 24 mM cyclodextrin on the solute mobility than 4 mM cyclodextrin.

The resolution between enantiomers did not change monotonically as was observed with partial filling with 4 mM 13-sulfated cyclodextrin (Figure 4.2). The resolution first improved as the cyclodextrin buffer plug length increased from 0 cm to 1.2 cm, then decreased from 1.2 cm to 3.5 cm. However, after the cyclodextrin buffer plug length was increased to 4.7 cm, the resolution started to increase steadily.

This appears to be a reversal in enantiomeric selectivity. That is, enantiomer A migrates faster than enantiomer B at short cyclodextrin plug lengths, but is slower with long cyclodextrin plug lengths. Thus the mobility of A decreases as cyclodextrin plug length increases, while the mobility of B increases as cyclodextrin plug length increases. At one point these two mobilities reach the same value and the enantiomeric separation disappears. After this point, the difference in their mobilities keeps increasing but with B being faster and the resolution also improves steadily. Unfortunately enantiomeric pure single isomers of homatropine are not commercially available. As a result, we can not confirm any selectivity change (the switch in the migration order of the enantiomers) in Figure 4.3.

Another observation from Figure 4.3 is that the peak heights are different at short and long cyclodextrin buffer plug lengths. All the electropherograms are drawn to scale. The sample concentration is constant throughout. However, the peaks at short cyclodextrin buffer plug lengths are short and badly broadened, whereas the peaks at longer cyclodextrin plug lengths show a much higher signal to noise ratio. Also, the peaks at high cyclodextrin plug lengths have higher peak efficiencies than those at low cyclodextrin plug lengths even though the migration time is longer for the long cyclodextrin plug lengths.

4.4.3.3 RESULTS OF PROPRANOLOL WITH PARTIAL FILLING WITH 4 mM 13-SULFATED β-CYCLODEXTRIN

From Section 2.4.1.3 we know that the homatropine-13-sulfated β-cyclodextrin complex mobility is positive. Therefore, even after homatropine forms complex with the 13-sulfated CD, it still has positive mobility and moves towards the detector. Thus there was no worry about homatropine coming out of the cyclodextrin plug and being detected in Sections 4.4.3.1 and 4.4.3.2.

However, the apparent mobility of propranolol is negative even at 4 mM 13-sulfated β-cyclodextrin (Figure 2.15). That is, propranolol will move toward the anode (injection end) when it is in the cyclodextrin buffer plug at a negative mobility slower than that of the CD buffer plug. Therefore, if there is not enough time for propranolol to come out of the cyclodextrin plug it will be carried out of the capillary by the CD buffer plug and will not be detected. Therefore care must be taken in choosing CD buffer plug length and position in the capillary.

The conversion of CD buffer injection time to buffer plug lengths is done as described in Section 4.4.2.2 and results are listed in Table 4.3.

Table 4.3 4 mM 13-sulfated β-CD-containing buffer plug length conversion.

t (s)	436.2	0	20	30	60	90	120	150
l (cm)	30	0	1.4	2.1	4.1	6.2	8.2	10.3

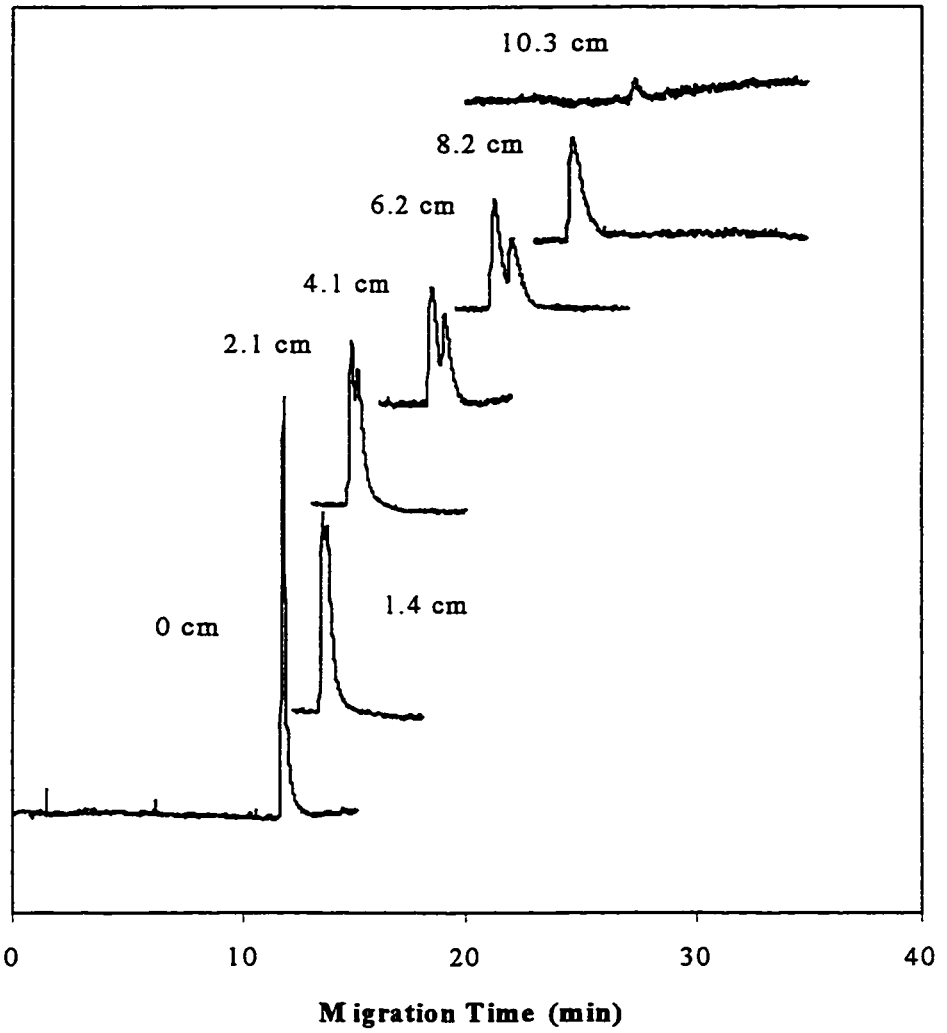

Figure 4.4 Electropherograms of propranolol with 4mM 13-sulfated cyclodextrin. The number besides each electropherogram is the approximate cyclodextrin

buffer plug length. Experimental conditions: $\lambda = 214$ nm, T = 20°C, capillary 37/30 cm, V = 10 kV, propranolol concentration = 1×10^{-4} M (R) and 0.5×10^{-4} M (S), all buffers are adjusted to pH 4.6.

The separation between propranolol enantiomers increases as longer CD buffer plugs are used. Unfortunately before baseline resolution was achieved the slower S-enantiomer has already swept out of the capillary and never reached the detector (see the electropherogram at 8.2 cm CD buffer plug). When the CD buffer plug length was increased to 10.3 cm, even the R-enantiomer was carried out the capillary (see the last electropherogram). This result is consistent with what we saw in Section 2.4.1.3 in that the difference in the apparent mobilities of propranolol enantiomers complexed with 13-sulfated β-cyclodextrin was smaller than that for homatropine. That is, when the capillary was completely filled with CD buffer, the resolution was poorer for propranolol than homatropine. With the partial filling technique, the resolution is again poorer for propranolol than for homatropine (Figure 4.2).

The migration times for the propranolol enantiomers were longer than those observed for the homatropine enantiomers in Figure 4.2. This is because the negative mobility of propranolol-13-sulfated β-CD complex causes propranolol to migrate away from the detector while it is in the cyclodextrin plug.

4.4.3.4 RESULTS OF PROPRANOLOL WITH PARTIAL FILLING WITH 24 mM 13-SULFATED β-CYCLODEXTRIN

Partial filling experiments were performed with 24 mM 13-sulfated β-cyclodextrin. However, due to the strong counter-migration of the propranolol-sulfate cyclodextrin, only very short plug lengths were studied.

Table 4.4 24 mM 13-sulfated β-CD-containing buffer plug length conversion.

t (s)	436.2	0	10	20	30
***l* (cm)**	30	0	0.7	1.4	2.1

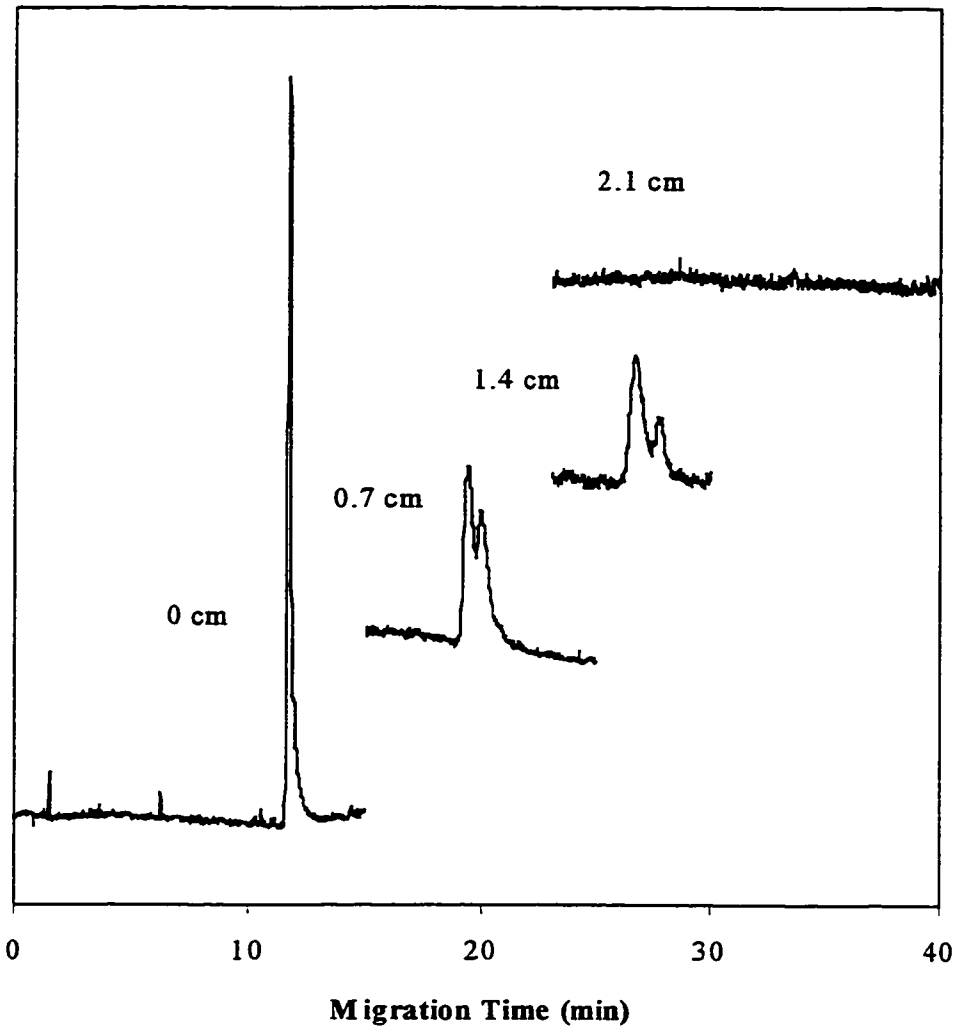

Figure 4.5 Electropherograms of propranolol with 24 mM 13-sulfated cyclodextrin. The number besides each electropherogram is the approximate cyclodextrin buffer plug length. Experimental conditions: $\lambda = 214$ nm, T = 20°C, capillary 37/30 cm, V = 10 kV, propranolol concentration = 1×10^{-4} M (R) and 0.5×10^{-4} M (S), all buffers are adjusted to pH 4.6.

Compared to the electropherograms in Figure 4.4, we can see a stronger interaction between propranolol and the 24 mM 13-sulfated cyclodextrin buffer than the interaction between propranolol and 4 mM cyclodextrin buffer. This is evident in the rapidly increasing migration times. Enantiomers were carried out of the capillary at a CD buffer plug length as short as 2.1 cm. As a result, the conditions that would be tried were limited and no baseline resolution was observed.

4.4.4 CONCLUSIONS

The results obtained show that the partial filling technique is applicable with charged cyclodextrin as chiral resolving agent. The advantages of this technique include low resolving agent consumption, short optimization time, labor saving, and the avoidance of the disturbance of the absorbance from resolving agent. The ability to resolve a specific solute is very solute dependent. The success of this technique depends on proper choice of the chiral resolving agent and the solute pair. When a resolving agent has high resolving power in the fully filled technique, it would also have high resolving power in the partial filling technique. The reverse is also true. Thus this technique can be used for screening suitable resolving agents for a particular analysis. However, the results are just preliminary, further and more extensive study is needed to better understand and efficiently apply this technique.

4.5 REFERENCES

1. Chankvetadze, B.; Endresz, G.; Blaschke, G. *J. Chromatogr. A*, 1995, 704, 234.
2. Luna, E. A.; Bornancini, E. R. N.; Tait, R. J.; Thompson, D. O.; Stobaugh, J. F.; Rajewski, R. A.; Stella, V. J. *J. Pharm. Biomed. Anal.* 1996, 15, 63.
3. Li, D.; Fu, S.; Lucy, C. A. *Anal. Chem.*, submitted.
4. Vincent, J. B.; Sokolowski, A. D.; Nguyen, T. V.; Vigh, Gy. *Anal. Chem.* 1997, 69, 4226.
5. Vincent, J. B.; Kirby, D. M.; Nguyen, T. V.; Vigh, Gy. *Anal. Chem.* 1997, 69, 4419.
6. Cai, H.; Nguyen, T. V.; Vigh, Gy. *Anal. Chem.* 1997, 69, 4226
7. Tanaka, Y.; Kishimoto, Y.; Terabe, S. *J. Chromatogr. A*, 1998, 802, 83.

BIBLIOGRAPHY

Ahmadzadeh, H.; Arriaga, E.; Stathakis, C.; Dovichi, N. J.; Righetti, P. G., Poster Presentation, HPCE'98, 1998, Orlando, Florida, USA.

Aldrich Catalogue, Aldrich Chemical Company, 1994.

Bender, M. L.; Komiyama, M. *"Cyclodextrin Chemistry"*, Springer-Verlag, New York, 1978.

Bowser, M. T.; Chen, D. D. Y. *Anal. Chem.*, 1998, 70, 3261.

Britz-McKibbin, P.; Chen, D.D.Y. *J. Chromatogr. A* 1997, 781, 23-34.

Budavari, S., Editor, *The Merck Index*, 11th Edition, Merck & Co., Inc., Rahway, 1989.

Bunke, A.; Jira, T. *J. Chromatogr.* 1998, 798, 275-280.

Cai, H.; Nguyen, T. V.; Vigh, Gy. *Anal. Chem.* 1997, 69, 4226

Cai, H.; Nguyen, T. V.; Vigh, Gy. *Anal. Chem.* 1998, 70, 580-589.

Cai, H.; Vigh, Gy. *J. Microcolumn Separations* 1998, 10(3), 293.

Cantwell, F. F. "Analytical Separations: Gas Chromatography, Liquid Chromatography, Supercritical Fluid Chromatography, and Electrophoresis", Coursenotes, 1992.

Chankvetadze, B.; Endresz, G.; Blaschke, G. *Chem. Soc. Rev.* 1996, 142, 141-153.

Chankvetadze, B.; Endresz, G.; Blaschke, G. *J. Chromatogr. A*, 1995, 704, 234.

Copper, C. L.; Davis, J. B.; Cole, R. O.; Sepaniak, M. J. *Electrophoresis* 1994, 15, 785.

CRC Handbook of Chemistry and Physics, 76th Edition, CRC press, New York, 1995-1996.

Florey, K. (Editor), "*Analytical Profiles of Drug Substances*", Vol. 16, Academic Press, London, 1987, p. 245.

Gasper, M. P.; Berthod, A.; Nair, U. B.; Armstrong, D. W. *Anal. Chem.* 1996, 68, 2501.

Gassmann, E.; Kuo, J. E.; Zare, R. N. *Science*, 1985, 230, 813-814.

Groom, C. A.; Luong, J. H. T. *Electrophoresis* 1997, 18, 1166.

Gübitz, G.; Schmid, M. G. *J. Chromatogr. A*, 1997, 792, 179-225.

Heiger, D. N. *"High Performance Capillary Electrophoresis – An Introduction"*, , Hewlett-Packard Company, Germany, 1992.

Li, D.; Fu, S.; Lucy, C. A. *Anal. Chem.*, submitted.

Li, S.; Purdy, W. C. *Anal. Chem.* 1992, 64, 1405.

Lide, D.R., Editor in chief, *CRC Handbook of Chemistry and Physics 76th edition*, CRC press, 1996.

Lin, B.; Zhu, X.; Epperlein, U.; Schwierskott, M.; Schlunk, R.; Koppenhoefer, B. *J. High. Resol. Chromatogr.* 1998, 21, 215.

Lucy, C. A.; Brown, R.; Yeung, K. K.-C. *J. Chromatogr. A* 1996, 745, 9-15.

Luna, E. A.; Bornancini, E. R. N.; Tait, R. J.; Thompson, D. O.; Stobaugh, J. F.; Rajewski, R. A.; Stella, V. J. *J. Pharm. Biomed. Anal.* 1996, 15, 63.

Lurie, I. S.; Klein, R. F. X. *Anal. Chem.* 1994, 66, 4019.

Miura, M.; Funazo, K.; Tanaka, M. *Analytica Chimica Acta* 1997, 357, 177.

Nakatani, M.; Shibukawa, A.; Nakagawa, T. Electrophoresis 1995, 16, 1451-1456.

O'Keeffe, F.; Shamsi, S. A.; Darcy, R.; Schwinté, P.; Warner, I. M. *Anal. Chem.* 1997, 69, 4773.

Pak, C.; Marriott, P. J.; Carpenter, P. D.; Amiet, R. G. J. Chromatogr. A, 1998, 793, 357.

Penn, S. G.; Bergström, E. T.; Goodall, D. M. *Anal. Chem.* 1994, 66, 2866-2873.

Penn, S. G.; Bergstrom, E. T.; Knights, I.; Liu, G.; Ruddick, A.; Goodall, D. M. *J. Phys. Chem.* 1995, 99, 3875.

Perrin, D.D. *Dissociation Constants of Organic Bases*, Butterworths, London, 1965.

Rawjee, Y. Y.; Staerk, D. U.; Vigh, Gy. *J. Chromatogr.* 1993, 635, 291-306.

Rawjee, Y. Y.; Williams, R. L.; Vigh, Gy. *J. Chromatogr. A*, 1993, 652, 233.

Rawjee, Y. Y.; Williams, R. L.; Vigh, Gy. *J. Chromatogr. A*, 1994, 680, 599-607.

Stalcup, A. M.; Gahm, K. H. *Anal. Chem.* 1996, 68, 1360-1368.

Surapaneni, S.; Ruterbories, K.; Lindstrom, T. J. Chromatogr. A, 1997, 761, 249-257.

Tait, R. J.; Thompson, D. O.; Stella, V. J.; Stobaugh, J. F. *Anal. Chem.* 1994, 66, 4013.

Tanaka, Y.; Kishimoto, Y.; Terabe, S. *J. Chromatogr. A*, 1998, 802, 83.

Tanaka, Y.; Yanagawa, M.; Terabe, S. *J. High Resol. Chromatogr.* 1996, 19, 421.

Terabe, S. *J. Chromatogr. A*, 1994, 666, 295-319.

Terabe, S.; Ozaki, H.; Otsuka, K.; Ando, T. *J. Chromatogr.* 1985, 332, 211.

Valtcheva, L.; Mohammad, J.; Pettersson, G.; Hjerten, S. *J. Chromatogr.* 1993, 638, 263-267.

Vincent, J. B.; Kirby, D. M.; Nguyen, T. V.; Vigh, Gy. *Anal. Chem.* 1997, 69, 4419.

Vincent, J. B.; Sokolowski, A. D.; Nguyen, T. V.; Vigh, Gy. *Anal. Chem.* 1997, 69, 4226.

Ward, T. J. *Anal. Chem.* 1994, 66, 633A.

Williams, B. A.; Vigh, Gy. *Anal. Chem.* 1996, 68, 1174-1180.

Williams, R. L.; Childs, B.; Dose, E. V.; Guiochon, G.; Vigh, Gy. *J. Chromatogr. A,* 1997, 781, 107.

Wren, S. A. C.; Rowe, R. C. *J. Chromatogr.* 1992, 603, 235-241.

Wren, S. A. *J. Chromatogr,* 1993, 636, 57-62.

Wren, S. A.; Rowe, R. C *J. Chromatogr.* 1993, 635, 113-118.

Wren, S. A.; Rowe, R. C. *J. Chromatogr.* 1992, 603, 235-241.

Yeung, K. K.-C.; Lucy, C. A. *Anal. Chem.* 1997, 69, 3435-3441.

IMAGE EVALUATION
TEST TARGET (QA-3)

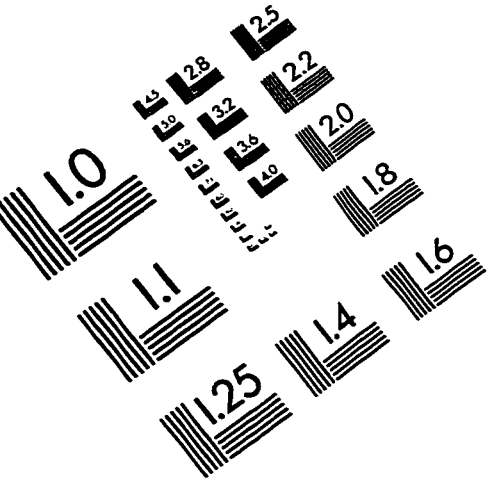

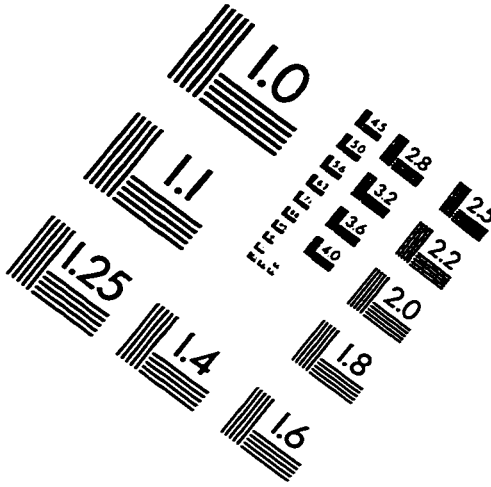

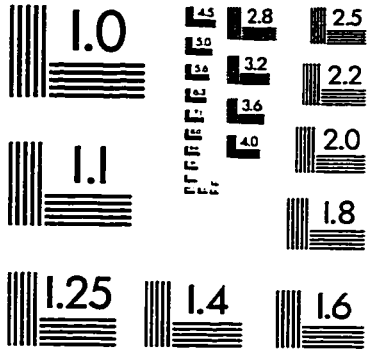

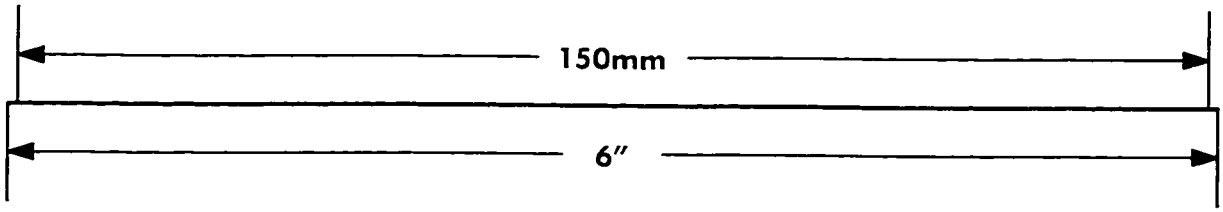

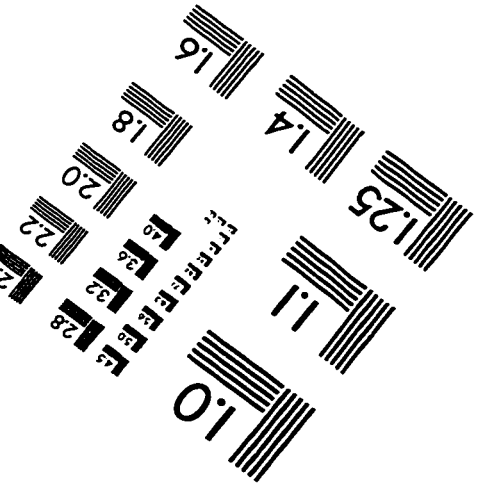

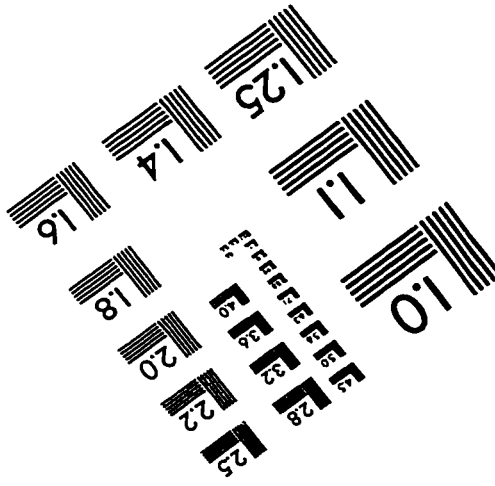

APPLIED IMAGE, Inc
1653 East Main Street
Rochester, NY 14609 USA
Phone: 716/482-0300
Fax: 716/288-5989

© 1993, Applied Image, Inc., All Rights Reserved